

Sparse Gaussian chain graphs with the spike-and-slab LASSO: Algorithms and asymptotics

Yunyi Shen^{*}, Claudia Solís-Lemus[†] and Sameer K. Deshpande[‡]

July 15, 2022

Abstract

The Gaussian chain graph model simultaneously parametrizes (i) the direct effects of p predictors on q correlated outcomes and (ii) the residual partial covariance between pair of outcomes. We introduce a new method for fitting sparse Gaussian chain graph models with spike-and-slab LASSO (SSL) priors. We develop an Expectation Conditional Maximization algorithm to obtain sparse estimates of the $p \times q$ matrix of direct effects and the $q \times q$ residual precision matrix. Our algorithm iteratively solves a sequence of penalized maximum likelihood problems with self-adaptive penalties that gradually filter out negligible regression coefficients and partial covariances. Because it adaptively penalizes model parameters, our method is seen to outperform fixed-penalty competitors on simulated data. We establish the posterior concentration rate for our model, buttressing our method’s excellent empirical performance with strong theoretical guarantees. We use our method to reanalyze a dataset from a study of the effects of diet and residence type on the composition of the gut microbiome of elderly adults.

^{*}Laboratory for Information & Decision Systems, Massachusetts Institute of Technology. The work was done while the author was at the University of Wisconsin–Madison.

[†]Wisconsin Institute for Discovery & Dept. of Plant Pathology, University of Wisconsin–Madison, Correspondence to: solislemus@wisc.edu

[‡]Dept. of Statistics, University of Wisconsin–Madison. Correspondence to: sameer.deshpande@wisc.edu

1 Introduction

1.1 Motivation

There are between 10 and 100 trillion microorganisms living within each person’s lower intestines. These bacteria, fungi, viruses and other microbes constitute the human gut *microbiome* (Guinane and Cotter, 2013). Recent research suggests that the composition of human gut microbiome can have a substantial effect on our health and well-being (Shreiner et al., 2015): microbes living in the gut play an integral role in our digestive and metabolic processes (Larsbrink et al., 2014; Belcheva et al., 2014); they can mediate our immune response to various diseases (Kamada and Núñez, 2014; Kim et al., 2017); and they can even influence disease pathogenesis and progression (Scher et al., 2013; Wang et al., 2011).

Additional emerging evidence suggests that the gut microbiome mediates the effects of lifestyle factors such as diet and medication use on human health (Singh et al., 2017; Battson et al., 2018; Hills Jr et al., 2019). That is, such lifestyle factors may first affect the composition of the gut microbiome, which in turn influences health outcomes. In fact, lifestyle factors and medication use can impact the composition of the microbiome in direct and indirect ways. For instance, many antibiotics target and kill certain microbial species, thereby directly affecting the abundances of the targeted species. However, by killing the targeted species, the antibiotics may reduce the overall competition for nutrients, thereby allowing non-targeted species to proliferate. In other words, by directly reducing the abundance of certain targeted microbes, antibiotics may indirectly increase the abundance of other non-targeted species. Our goal in this paper is to estimate such direct and indirect effects.

1.2 Sparse chain graph models

At a high level, the statistical challenge is to estimate the functional relationship between a vector of predictors $\mathbf{x} \in \mathbb{R}^p$ and vector of responses $\mathbf{y} \in \mathbb{R}^q$. In our application, we re-analyze a dataset from Claesson et al. (2012) containing $n = 178$ predictor-response pairs (\mathbf{x}, \mathbf{y}) where \mathbf{x} contains measures of $p = 11$ factors related to diet, medication use, and residence type, and \mathbf{y} contains the logit-transformed relative abundances of $q = 14$ different microbial taxa. Our goal is to uncover the direct and indirect effect of these factors on the abundance of each microbial taxon as well as any interactions between microbial taxa. The Gaussian chain graph model (Lauritzen and Wermuth, 1989; Frydenberg, 1990; Lauritzen and Richardson, 2002), which simultaneously parameterizes the direct effects of predictors

on responses and the residual dependence structure between response, is natural for these data. The model asserts that

$$\mathbf{y}|\Psi, \Omega, \mathbf{x} \sim \mathcal{N}(\Omega^{-1}\Psi^\top \mathbf{x}, \Omega^{-1}). \quad (1)$$

where Ψ is a $p \times q$ matrix and Ω is a symmetric, positive definite $q \times q$ matrix. As we detail in Section 2.1, the (j, k) entry of Ψ , $\psi_{j,k}$, quantifies the direct effect of the j^{th} predictor X_j on the k^{th} response Y_k . The (k, k') entry of Ω , $\omega_{k,k'}$, encodes the residual conditional covariance between outcomes Y_k and $Y_{k'}$ that remains after accounting for the direct effects of the predictors and all of the other response variables.

To fit the model in Equation (1), we must estimate $pq + q(q + 1)/2$ unknown parameters. When the total number of unknown parameters is comparable to or larger than the sample size n , it is common to assume that the matrices Ψ and Ω are sparse. If $\omega_{k,k'} = 0$, we can conclude that after adjusting for the covariates and all other outcomes, outcomes Y_k and $Y_{k'}$ are conditionally independent. If $\psi_{j,k} = 0$, we can conclude that X_j does not have a *direct* effect on the k^{th} outcome variable Y_k . Furthermore, when $\psi_{j,k} = 0$, any marginal correlation between X_j and Y_k is due solely to X_j 's *direct* effects on other outcomes $Y_{k'}$ that are themselves conditionally correlate with Y_k .

1.3 Our contributions

We introduce the chain graph spike-and-slab LASSO (cgSSL) procedure for fitting the model in Equation (1) in a sparse fashion. At a high level, we place separate spike-and-slab LASSO priors (Ročková and George, 2018) on the entries of Ψ and on the off-diagonal entries of Ω in Equation (1). We derive an efficient Expectation Conditional Maximization algorithm to compute the *maximum a posteriori* (MAP) estimates of Ψ and Ω . Our algorithm is equivalent to solving a series of maximum likelihood problems with *self-adaptive* penalties. On synthetic data, we demonstrate that our algorithm displays excellent support recovery and estimation performance. We further establish the posterior contraction rate for each of $\Psi, \Omega, \Psi\Omega^{-1}$, and $X\Psi\Omega^{-1}$. Our contraction results imply that our proposed cgSSL procedure consistently estimates these quantities and also provides an upper bound for the minimax optimal rate of estimating these quantities in the Frobenius norm. To the best of our knowledge, ours are the first posterior contraction results for fitting sparse Gaussian chain graph models with element-wise priors on Ψ and Ω .

Here is an outline for the rest of our paper. We review the Gaussian chain graph model and spike-and-slab LASSO in Section 2. We next introduce the cgSSL procedure in Section 3 and carefully derive our ECM algorithm for finding the MAP in Sections 3.2. We present our asymptotic results in Section 4 before demonstrating the excellent finite sample performance of the cgSSL on several synthetic datasets in Section 5. We apply the cgSSL to our motivating gut microbiome data in Section 6. We conclude in Section 7 by outlining several avenues for future development.

2 Background

2.1 The Gaussian chain graph model

Graphical models are a convenient way to represent the dependence structure between several variables. Specifically, we can represent each variable as a node in a graph and we can draw edges to indicate *conditional* dependence between variables. Absence of an edge between two nodes indicates the corresponding variables are *conditionally independent* given all of the other variables. In the context of our gut microbiome data, we can represent each predictor X_j with a node and each outcome Y_k with a node. We are primarily interested in detecting edges between predictors and outcomes and edges between outcomes. Figure 1a is a cartoon illustration of such a graphical model with $p = 3$ and $q = 4$. Note that we have not drawn any edges between the predictors as such edges are not typically of primary interest.

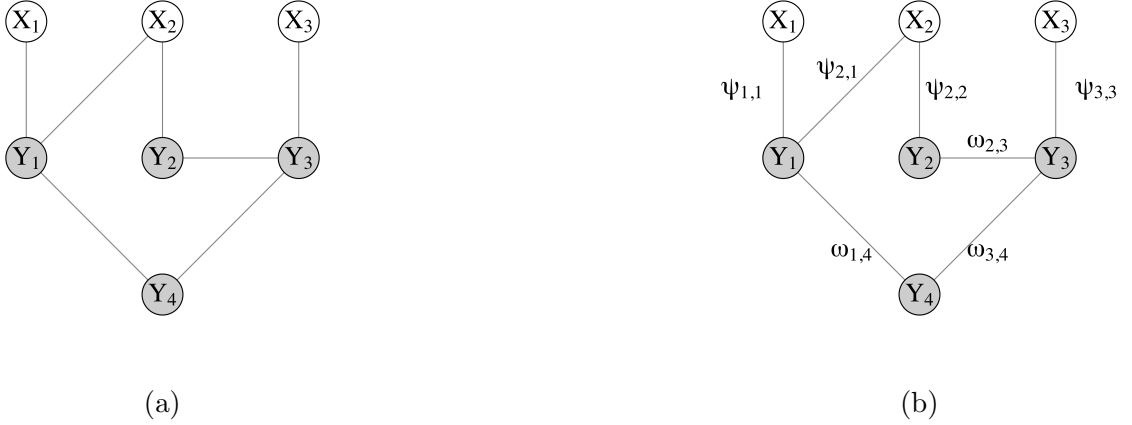


Figure 1: Cartoon illustrations of a general graphical model (a) and a Gaussian chain graph model (b) with $p = 3$ covariates and $q = 4$ outcomes. Edges in both graphs encode conditional dependence relationships. The edge labels in (b) correspond to the non-zero parameters in Equation (1).

Without additional modeling assumptions, estimating a discrete graph like that in Figure 1a from n pairs of data $(\mathbf{x}_1, \mathbf{y}_1), \dots, (\mathbf{x}_n, \mathbf{y}_n)$ is a challenging task. The Gaussian chain graph model in Equation (1) translates the discrete graph estimation problem into a much more tractable continuous parameter estimation problem. Specifically, the model introduces two matrices, Ψ and Ω and asserts that $\mathbf{y}|\Psi, \Omega, \mathbf{x} \sim \mathcal{N}(\Omega^{-1}\Psi^\top \mathbf{x}, \Omega^{-1})$. Under the Gaussian graph model, X_j and Y_k are conditionally independent if and only if $\psi_{j,k} = 0$. Furthermore, Y_k and $Y_{k'}$ are conditionally independent if and only if $\omega_{k,k'} = 0$. In other words, by first estimating Ψ and Ω and then examining their supports, we can recover the underlying graphical model. Figure 1b reproduces the cartoon from Figure 1a with edges labelled by the corresponding non-zero parameters in Equation (1).

In the Gaussian chain graph model, the direct effect of X_j on Y_k is defined as

$$\mathbb{E}[Y_k|X_j = x_j + 1, Y_{-k}, X_{-j}, \Psi, \Omega] - \mathbb{E}[Y_k|X_j = x_j, Y_{-k}, X_{-j}, \Psi, \Omega] = -\psi_{j,k}/\omega_{k,k}$$

That is, fixing the values of all of the other covariates and all of the other outcomes, an increase of one unit in X_j is associated with $-\psi_{j,k}/\omega_{k,k}$ unit increase in the expectation of Y_k . Notice that the direct effect of X_j on Y_k is defined conditionally on the values of all other outcome $Y_{k'}$. Because of this, the direct effect of X_j on Y_k is typically not equal to its

marginal effect, which is defined as

$$\mathbb{E}[Y_k|X_j = x_j + 1, X_{-j}, \Psi, \Omega] - \mathbb{E}[Y_k|X_j = x_j, X_{-j}, \Psi, \Omega] = \beta_{j,k},$$

where $\beta_{j,k}$ is the (j, k) entry of the matrix $B = \Psi\Omega^{-1}$. Notice that we can re-parametrize the Gaussian chain graph model in Equation (1) in terms of B

$$\mathbf{y}|B, \Omega, \mathbf{x} \sim \mathcal{N}(B^\top \mathbf{x}, \Omega^{-1}). \quad (2)$$

We will refer to this re-parametrized model as the marginal regression model. There is a considerable literature on fitting sparse marginal regression models and we refer the reader to [Deshpande et al. \(2019\)](#) and references therein for a review.

Generally speaking, under (1), the supports of Ψ and B will be different. Specifically, it is possible for X_j to have a marginal effect but no direct effect on Y_k . For instance, in Figure 1, although X_3 does not directly affect Y_2 , it may still be marginally correlated with Y_2 thanks to the conditional correlation between Y_2 and Y_3 . That is, changing the value of X_3 can change the value of Y_3 , which in turn changes the value of Y_2 . Consequently, if we fit a sparse marginal regression model, we cannot generally expect to recover sparse estimates of the matrix of direct effects.

2.2 Related works

Learning sparse chain graphs. [McCarter and Kim \(2014\)](#) proposing fitting sparse Gaussian chain graphical models by maximizing a penalized negative log-likelihood. They specifically proposed homogeneous L_1 penalties on the entries of Ψ and Ω and used cross-validation to set the penalty parameters for Ψ and Ω . [Shen and Solis-Lemus \(2021\)](#) developed a Bayesian version of that chain graphical LASSO and put a Gamma prior on the penalty parameters. In this way, they automatically learned the degree to which the entries $\psi_{j,k}$ and $\omega_{k,k'}$ are shrunk to zero. Although these paper differ in how they determine the appropriate amount of penalization, both [McCarter and Kim \(2014\)](#) and [Shen and Solis-Lemus \(2021\)](#) deploy a single fixed penalty on all of the entries in Ψ and a single fixed penalty on all entries in Ω . With such fixed penalties, larger parameter estimates are shrunk towards zero as aggressively as the smaller parameter estimates, which can introduce substantial estimation bias.

Spike-and-slab variable selection with the EM algorithm. Spike-and-slab priors are the workhorses of sparse Bayesian modeling. As introduced by [Mitchell and Beauchamp](#)

(1988), the spike-and-slab prior is mixture between a point mass at 0 (the “spike”) and a uniform distribution over a wide interval (the “slab”). George and McCulloch (1993) introduced a continuous relaxation of the original spike-and-slab prior, respectively replacing the point mass spike and uniform slab distributions with zero-mean Gaussians with extremely small and large variances. In this way, one may imagine generating all of the “essentially negligible” parameters in a model from the spike distribution and generating all of the “relevant” or “significant” parameters from the slab distribution. Despite their intuitive appeal, spike-and-slab priors usually produce extremely multimodal posterior distributions. In high dimensions, exploring these distributions with Markov chain Monte Carlo (MCMC) is computationally prohibitive.

In response, Ročková and George (2014) introduced EMVS, a fast EM algorithm targeting the *maximum a posteriori* (MAP) estimate of the regression parameters. They later extended EMVS, which used conditionally conjugate Gaussian spike and slab distributions, to use Laplacian spike and slab distributions in Ročková and George (2018). The resulting spike-and-slab LASSO (SSL) procedure demonstrated excellent empirical performance. At a high-level, the SSL algorithm solves a sequence of L_1 penalized regression problems with *self-adaptive* penalties. The adaptive penalty mixing is key to the empirical success of the SSL (George and Ročková, 2020; Bai et al., 2021), as it facilitates shrinking larger parameter estimates to zero less aggressively than smaller parameter estimates.

Since Ročková and George (2014), the general EM technique for maximizing spike-and-slab posteriors has been successfully applied to many problems. For instance, Bai et al. (2020) introduced a grouped version of the SSL that adaptively shrinks groups of parameter values towards zero. Tang et al. (2017, 2018) similarly deployed the SSL and its grouped variant to generalized linear models. Outside of the single-outcome regression context, continuous spike-and-slab priors have been used to estimate sparse Gaussian graphical models (Li et al., 2019; Gan et al., 2019a,b), sparse factor models Ročková and George (2016), and to bi-clustering Moran et al. (2021). Deshpande et al. (2019) introduce a multivariate SSL for estimating B and Ω in the marginal regression model in Equation (2). In each extension, the adaptive penalization performed by the EM algorithm resulted in support recovery and parameter estimation superior to that of fixed penalty methods.

The asymptotics of spike-and-slab variable selection. Beyond its excellent empirical performance, Ročková and George (2018)’s SSL enjoys strong theoretical support. Using general techniques proposed by Zhang and Zhang (2012) and Ghosal and van der Vaart

(2017), they proved that, under mild conditions, the posterior induced by the SSL prior in high-dimensional, single-outcome linear regression contracts at a near minimax-optimal rate as $n \rightarrow \infty$. Their contraction result implies that the MAP estimate returned by their EM algorithm is consistent and is, up to a log factor, rate-optimal. By directly applying Ghosal and van der Vaart (2017)’s general theory, Bai et al. (2020) extended these results to the group SSL posterior with an unknown variance.

In the context of Gaussian graphical models, Gan et al. (2019a) showed that the MAP estimator corresponding to placing spike-and-slab LASSO priors on the off-diagonal elements of a precision matrix is consistent. They did not, however, establish the contraction rate of the posterior. Ning et al. (2020) showed that the joint posterior distribution of (B, Ω) in the multivariate regression model in Equation (2) concentrates when using a group spike-and-slab prior with Laplace slab and point mass spike on B and a carefully selected prior on the eigendecomposition of Ω^{-1} . To the best of our knowledge, however, the asymptotic properties of the posterior formed by placing SSL priors on both the precision matrix Ω and regression coefficients Ψ in Equation (1) have not yet been established.

3 Introducing the cgSSL

3.1 The cgSSL prior

To quantify the prior belief that many entries in Ψ are essentially negligible, we model each $\psi_{j,k}$ as having been drawn either from a spike distribution, which is sharply concentrated around zero, or a slab distribution, which is much more diffuse. More specifically, we take the spike distribution to be $\text{Laplace}(\lambda_0)$ and the slab distribution to be $\text{Laplace}(\lambda_1)$, where $0 < \lambda_1 \ll \lambda_0$ are fixed positive constants. This way, the spike distribution is much more heavily concentrated around zero than is the slab. We further let $\theta \in [0, 1]$ be the prior probability that each $\psi_{j,k}$ is drawn from the slab and model the $\psi_{j,k}$ ’s as conditionally independent given θ . Thus, the prior density for Ψ , conditional on θ , is given by

$$\pi(\Psi|\theta) = \prod_{j=1}^p \prod_{k=1}^q \left(\frac{\theta\lambda_1}{2} e^{-\lambda_1|\psi_{j,k}|} + \frac{(1-\theta)\lambda_0}{2} e^{-\lambda_0|\psi_{j,k}|} \right). \quad (3)$$

Since Ω is symmetric, it is enough to specify a prior on the entries $\omega_{k,k'}$ where $k \leq k'$. To this end, we begin by placing an entirely analogous spike-and-slab prior on the off-diagonal

entries. That is, we model each $\omega_{k,k'}$ as being drawn from a $\text{Laplace}(\xi_1)$, with probability $\eta \in [0, 1]$, or a $\text{Laplace}(\xi_0)$, with probability $1 - \eta$, where $0 < \xi_1 \ll \xi_0$. We similarly model each $\omega_{k,k'}$ as conditionally independent given η and place independent $\text{Exp}(\xi_1)$ priors on the diagonal entries of Ω . We then truncate the resulting distribution of $\Omega|\theta$ to the cone of symmetric positive definite matrices, yielding the prior density

$$\pi(\Omega|\eta) \propto \left(\prod_{1 \leq k < k' \leq q} \left[\frac{\eta \xi_1}{2} e^{-\xi_1 |\omega_{k,k'}|} + \frac{(1-\eta) \xi_0}{2} e^{-\xi_0 |\omega_{k,k'}|} \right] \right) \times \left(\prod_{k=1}^q \xi e^{-\xi \omega_{k,k}} \right) \times \mathbb{1}(\Omega \succ 0) \quad (4)$$

Observe that $1 - \theta$ and $1 - \eta$ respectively quantify the proportion of entries in Ψ and Ω that are essentially negligible. To model our uncertainty about these proportions, we place Beta priors on each of θ and η . Specifically, we independently model $\theta \sim \text{Beta}(a_\theta, b_\theta)$ and $\eta \sim \text{Beta}(a_\eta, b_\eta)$, where $a_\theta, b_\theta, a_\eta, b_\eta > 0$ are fixed positive constants.

3.2 Targeting the MAP

Unfortunately the posterior distribution of $(\Psi, \theta, \Omega, \eta)|\mathbf{Y}$ is analytically intractable. Further, it is generally high-dimensional and rather multimodal, rendering stochastic search techniques like Markov Chain Monte Carlo computationally impractical. We instead follow [Ročková and George \(2018\)](#)'s example and focus on finding the *maximum a posteriori* (MAP) estimate of $(\Psi, \theta, \Omega, \eta)$. Throughout, we assume that the columns of X have been centered and scaled to have norm n .

To this end, we attempt to maximize the log posterior density

$$\begin{aligned}
\log \pi(\Psi, \theta, \Omega, \eta | \mathbf{Y}) = & -\frac{n}{2} \log |\Omega| - \frac{1}{2} \text{tr}((Y - X\Psi\Omega^{-1})\Omega(Y - X\Psi\Omega)^{\top}) \\
& + \sum_{j=1}^p \sum_{k=1}^q \log(\theta \lambda_1 e^{-\lambda_1 |\psi_{j,k}|} + (1-\theta) \lambda_0 e^{-\lambda_0 |\psi_{j,k}|}) \\
& + \sum_{k=1}^{q-1} \sum_{k' > k}^q \log(\eta \xi_1 e^{-\xi_1 |\omega_{k,k'}|} + (1-\eta) \xi_0 e^{-\xi_0 |\omega_{k,k'}|}) \\
& - \sum_{k=1}^q \xi_0 \omega_{k,k} + \log \mathbb{1}(\Omega \succ 0) \\
& + (a_{\theta} - 1) \log(\theta) + (b_{\theta} - 1) \log(1 - \theta) \\
& + (a_{\eta} - 1) \log(\eta) + (b_{\eta} - 1) \log(1 - \eta)
\end{aligned} \tag{5}$$

Optimizing the log posterior density directly is complicated by the non-concavity of $\log \pi(\Omega | \eta)$. Instead, following [Deshpande et al. \(2019\)](#), we iteratively optimize a surrogate objective using an EM-like algorithm.

To motivate this approach, observe that we can obtain the posterior density $\pi(\Omega | \eta)$ in Equation (4) by marginalizing an *augmented* prior

$$\pi(\Omega | \eta) = \int \pi(\Omega | \boldsymbol{\delta}) \pi(\boldsymbol{\delta} | \eta) d\boldsymbol{\delta}$$

where $\boldsymbol{\delta} = \{\delta_{k,k'} : 1 \leq k < k' \leq q\}$ is a collection of $q(q-1)/2$ i.i.d. Bernoulli(η) variables and

$$\pi(\Omega | \boldsymbol{\delta}) \propto \left(\prod_{1 \leq k < k' \leq q} (\xi_1 e^{-\xi_1 |\omega_{k,k'}|})^{\delta_{k,k'}} (\xi_0 e^{-\xi_0 |\omega_{k,k'}|})^{1-\delta_{k,k'}} \right) \times \left(\prod_{k=1}^q \xi e^{-\xi \omega_{k,k}} \right) \times \mathbb{1}(\Omega \succ 0).$$

In our augmented prior, $\delta_{k,k'}$ indicates whether $\omega_{k,k'}$ is drawn from the slab ($\delta_{k,k'} = 1$) or the spike ($\delta_{k,k'} = 0$).

The above marginalization immediately suggests an EM algorithm: rather than optimize $\log \pi(\Psi, \theta, \Omega, \eta | \mathbf{Y})$ directly, we can iteratively optimize a surrogate objective formed by marginalizing the augmented log posterior density. That is, starting from some initial guess $(\Psi^{(0)}, \theta^{(0)}, \Omega^{(0)}, \eta^{(0)})$, for $t > 1$, the t^{th} iteration of our algorithm consists of two steps. In the

first step, we compute the surrogate objective

$$F^{(t)}(\Psi, \theta, \Omega, \eta) = \mathbb{E}_{\boldsymbol{\delta}}[\log \pi(\Psi, \theta, \Omega, \eta, \boldsymbol{\delta} | \mathbf{y}) | \Psi = \Psi^{(t-1)}, \Omega = \Omega^{(t-1)}, \theta = \theta^{(t-1)}, \eta = \eta^{(t-1)}],$$

where the expectation is taken with respect to the conditional posterior distribution of the indicators $\boldsymbol{\delta}$ given the current value of $(\Psi, \theta, \Omega, \eta)$. Then in the second step, we maximize the surrogate objective and set $(\Psi^{(t)}, \theta^{(t)}, \Omega^{(t)}, \eta^{(t)}) = \arg \max F^{(t)}(\Psi, \theta, \Omega, \eta)$.

It turns out that, given Ω and η , the indicators $\delta_{k,k'}$ are conditionally independent Bernoulli random variables whose means are easy to evaluate, making it simple to compute a closed form expression for the surrogate objective $F^{(t)}$. Unfortunately, maximizing $F^{(t)}$ is still difficult. Consequently, similar to [Deshpande et al. \(2019\)](#), we carry out two conditional maximizations, first optimizing with respect to (Ψ, θ) while holding (Ω, η) fixed, and then optimizing with respect to (Ω, η) while holding (Ψ, θ) fixed. That is, in the second step of each iteration of our algorithm, we set

$$(\Psi^{(t)}, \theta^{(t)}) = \arg \max_{\Psi, \theta} F^{(t)}(\Psi, \theta, \Omega^{(t-1)}, \eta^{(t-1)}) \quad (6)$$

$$(\Omega^{(t)}, \eta^{(t)}) = \arg \max_{\Omega, \eta} F^{(t)}(\Psi^{(t)}, \theta^{(t)}, \Omega, \eta). \quad (7)$$

In summary, we propose finding the MAP estimate of $(\Psi, \theta, \Omega, \eta)$ using an Expectation Conditional Maximization (ECM; [Meng and Rubin, 1993](#)) algorithm.

When we fix the values of Ω and η , the surrogate objective $F^{(t)}$ is separable in Ψ and θ . That is, the objective function $F^{(t)}(\Psi, \theta, \Omega^{(t-1)}, \eta^{(t-1)})$ in Equation (6) can be written as the sum of a function of Ψ alone and a function of θ alone. This means that we can separately compute $\Psi^{(t)}$ and $\theta^{(t)}$ while fixing $(\Omega, \eta) = (\Omega^{(t-1)}, \eta^{(t-1)})$. The objective function in Equation (7) is similarly separable and we can separately compute $\Omega^{(t)}$ and $\eta^{(t)}$ while fixing $(\Psi, \theta) = (\Psi^{(t)}, \theta^{(t)})$. As we describe in Section S1 of the Supplementary Materials, computing $\theta^{(t)}$ and $\eta^{(t)}$ is relatively straightforward; we compute $\theta^{(t)}$ with a simple Newton algorithm and there is a closed form expression for $\eta^{(t)}$. The main computational challenge is computing $\Psi^{(t)}$ and $\Omega^{(t)}$. In the next subsection, we detail how updating Ψ and Ω reduces to solving penalized likelihood problems with *self-adaptive* penalties.

3.3 Adaptive penalty mixing

Before describing how we compute $\Psi^{(t)}$ and $\Omega^{(t)}$, we introduce two important functions:

$$p^*(x, \theta) = \frac{\theta \lambda_1 e^{-\lambda_1 |x|}}{\theta \lambda_1 e^{-\lambda_1 |x|} + (1 - \theta) \lambda_0 e^{-\lambda_0 |x|}}$$

$$q^*(x, \eta) = \frac{\eta \xi_1 e^{-\xi_1 |x|}}{\eta \xi_1 e^{-\xi_1 |x|} + (1 - \eta) \xi_0 e^{-\xi_0 |x|}}$$

For each $1 \leq j \leq p$ and $1 \leq k \leq q$, $p^*(\psi_{j,k}, \theta)$ is the conditional posterior probability that $\psi_{j,k}$ was drawn from the $\text{Laplace}(\lambda_1)$ slab distribution. Similarly, for $1 \leq k < k' \leq q$, $q^*(\omega_{k,k'}, \eta)$ is just the conditional posterior probability that $\omega_{k,k'}$ was drawn from the $\text{Laplace}(\xi_1)$ slab. That is, $q^*(\omega_{k,k'}, \eta) = \mathbb{E}[\delta_{k,k'} | \mathbf{Y}, \Psi, \Omega, \theta, \eta]$.

Updating Ψ . Fixing the value $\Omega = \Omega^{(t-1)}$, computing $\Psi^{(t)}$ is equivalent to solving the following penalized optimization problem

$$\Psi^{(t)} = \arg \max_{\Psi} \left\{ -\frac{1}{2} \text{tr} \left((Y\Omega - X\Psi)\Omega^{-1}(Y\Omega - X\Psi)^\top \right) + \sum_{jk} \text{pen}(\psi_{j,k}; \theta) \right\} \quad (8)$$

where

$$\text{pen}(\psi_{j,k}; \theta) = \log \left(\frac{\pi(\psi_{j,k} | \theta)}{\pi(0 | \theta)} \right) = -\lambda_1 |\psi_{j,k}| + \log \left(\frac{p^*(\psi_{j,k}, \theta)}{p^*(0, \theta)} \right).$$

Note that the first term in the objective of Equation (8) can be obtained by distributing a factor of Ω through the quadratic form that appears in the log-likelihood (see Equations (S5) and (S7) of the Supplementary Materials for details).

Following arguments similar to those in [Deshpande et al. \(2019\)](#), the Karush-Kuhn-Tucker (KKT) condition for (8) tells us that

$$\psi_{j,k}^{(t)} = n^{-1} \left[|z_{j,k}| - \lambda^*(\psi_{j,k}^{(t)}, \theta) \right]_+ \text{sign}(z_{j,k}), \quad (9)$$

where

$$\begin{aligned}
z_{jk} &= n\psi_{j,k}^{(t)} + X_j^\top \mathbf{r}_k + \sum_{k' \neq k} \frac{(\Omega^{-1})_{k,k'}}{(\Omega^{-1})_{k,k}} X_j^\top \mathbf{r}_{k'} \\
\mathbf{r}_{k'} &= (Y\Omega - X\Psi^{(t)})_{k'} \\
\lambda^*(\psi_{j,k}^{(t)}, \theta) &= \lambda_1 p^*(\psi_{j,k}^{(t)}, \theta) + \lambda_0 (1 - p^*(\psi_{j,k}^{(t)}, \theta)).
\end{aligned}$$

The KKT conditions suggest a natural coordinate-ascent strategy for computing $\Psi^{(t)}$: starting from some initial guess Ψ_0 , we cyclically update the entries $\psi_{j,k}$ by soft-thresholding $\psi_{j,k}$ at $\lambda_{j,k}^*$. During our cyclical coordinate ascent, whenever the current value of $\psi_{j,k}$ is very large, the corresponding value of $p^*(\psi_{j,k}, \theta)$ will be close to one, and the threshold λ^* will be close to the slab penalty λ_1 . On the other hand, when $\psi_{j,k}$ is very small, the corresponding p^* will be close to zero and the threshold λ^* will be close to the spike penalty λ_0 . Since $\lambda_1 \ll \lambda_0$, we are therefore able to apply a stronger penalty to the smaller entries of Ψ and a weaker penalty to the larger entries. As our cyclical coordinate ascent proceeds, we iteratively refine the thresholds λ^* , thereby adaptively shrinking our estimates of $\psi_{j,k}$.

Before proceeding, we note that the quantity $z_{j,k}$ depends not only on the inner product between the X_j , the j^{th} column of the design matrix, and the partial residual \mathbf{r}_k but also on the inner product between X_j and all other partial residuals $\mathbf{r}_{k'}$ for $k' \neq k$. Practically this means that in our cyclical coordinate ascent algorithm, our estimate of the direct effect of predictor X_j on outcome Y_k can depend on how well we have fit all other outcomes $Y_{k'}$. Moreover, the entries of Ω^{-1} determine the degree to which $\psi_{j,k}$ depends on the outcomes $Y_{k'}$ for $k' \neq k$. Specifically, if $(\Omega^{-1})_{k,k'} = 0$, then we are unable to leverage information contained in $Y_{k'}$ to inform our estimate of $\psi_{j,k}$.

Updating Ω . Fixing $\Psi = \Psi^{(t)}$ and letting $S = n^{-1}Y^\top Y$ and $M = n^{-1}(X\Psi)^\top X\Psi$, we can compute $\Omega^{(t)}$ by solving

$$\Omega^{(t)} = \arg \max_{\Omega \succ 0} \left\{ \frac{n}{2} (\log|\Omega| - \text{tr}(S\Omega) - \text{tr}(M\Omega^{-1})) - \sum_{k=1}^q \left[\xi \omega_{k,k} + \sum_{k' > k} \xi_{k,k'}^* |\omega_{k,k'}| \right] \right\} \quad (10)$$

where $\xi_{k,k'}^* = \xi_1 q^*(\omega_{k,k'}^{(t-1)}, \eta^{(t-1)}) + \xi_0 (1 - q^*(\omega_{k,k'}^{(t-1)}, \eta^{(t-1)}))$.

The objective in Equation (10) is extremely similar to the conventional graphical LASSO (GLASSO; Friedman et al., 2008) objective. However, there are two crucial differences. First,

because the conditional mean of Y depends on Ω in the Gaussian chain graph model (1), we have an additional term $\text{tr}(M\Omega^{-1})$ that is absent in the GLASSO objective. Second, and more substantively, the objective in Equation (10) contains *individualized* penalties $\xi_{k,k'}^*$ on the off-diagonal entries of Ω . Here, the penalty $\xi_{k,k'}^*$ will be large (resp. small) whenever the previous estimate of $\omega_{k,k'}^{(t-1)}$ is small (resp. large). In other words, as we run our ECM algorithm, we can refine the amount of penalization applied to each off-diagonal entry in Ω .

Although the objective in Equation (10) is somewhat different than the GLASSO objective, we can solve it by suitably modifying an existing GLASSO algorithm. Specifically, we solve the optimization problem in Equation (10) with a modified version of Hsieh et al. (2011)’s QUIC algorithm. Our solution repeatedly (i) forms a quadratic approximation of the objective, (ii) computes a suitable Newton direction, and (iii) follows that Newton direction for step size chosen with an Armijo rule. In Section S2.4 of the Supplementary Materials, we show that the optimization problem in Equation (10) has a unique solution and that our modification to QUIC converges to the unique solution.

3.4 Selecting the spike and slab penalties

The proposed ECM algorithm depends on two sets of hyperparameters. The first set, containing $a_\theta, b_\theta, a_\eta$, and b_η , encode our initial beliefs about the overall proportion of non-negligible entries in Ψ and Ω . We set $a_\theta = 1, b_\theta = pq, a_\eta = 1$, and $b_\eta = q$ similar to Deshpande et al. (2019). The second set of hyperparameters consists of the spike and slab penalties $\lambda_0, \lambda_1, \xi_0$ and ξ_1 . Rather than run cgSSL with a single set of these penalties, we use Deshpande et al. (2019)’s path-following *dynamic posterior exploration* (DPE) strategy to obtain the MAP estimates corresponding to several different choices of spike penalties.

Specifically, we fix the slab penalties λ_1 and ξ_1 and specify grids of increasing spike penalties $\mathcal{I}_\lambda = \{\lambda_0^{(1)} < \dots < \lambda_0^{(L)}\}$ and $\mathcal{I}_\xi = \{\xi_0^1 < \dots < \xi_0^{(L)}\}$. We then run cgSSL with warmstarts for each combination of spike penalties, yielding a set of posterior modes $\{(\Psi^{(s,t)}, \theta^{(s,t)}, \Omega^{(s,t)}, \eta^{(s,t)})\}$ indexed by the choices $(\lambda_0^{(s)}, \xi_0^{(t)})$. To warm start the estimation of the mode corresponding to $(\lambda_0^{(s)}, \xi_0^{(t)})$, we first compute the models found with $(\lambda_0^{s-1}, \xi_0^{(t-1)})$, $(\lambda_0^s, \xi_0^{(t-1)})$ and $(\lambda_0^{s-1}, \xi_0^{(t)})$. We evaluate the posterior density using $(\lambda_0, \xi_0) = (\lambda_0^{(s)}, \xi_0^{(t)})$ at each of the three previously computed modes and initialize at the mode with largest density.

Following this DPE strategy provides a snapshot of the many different cgSSL posteriors. However, it can be computationally intensive, as we must run our ECM algorithm to convergence for every pair of spike penalties. Deshpande et al. (2019) introduced a faster variant,

called dynamic *conditional* posterior exploration (DCPE), which we also implemented for the cgSSL. In DCPE, we first run our ECM algorithm with warm-starts over the ladder \mathcal{I}_λ while keeping $\Omega = I$ fixed. Then, fixing (Ψ, θ) at the final value from the first step, we run our ECM algorithm with warm-starts over the ladder \mathcal{I}_Ω . Finally, we run our ECM algorithm starting from the final estimates of the parameters obtained in the first two steps with $(\lambda_0, \xi_0) = (\lambda_0^{(L)}, \xi_L^{(0)})$. Generally speaking, DPE and DCPE trace different paths through the parameter space and typically return different final estimates.

When the spike and slab penalties are similar in size (i.e. $\lambda_1 \approx \lambda_0, \xi_1 \approx \xi_0$), we noticed that our ECM algorithm would sometimes return very dense estimates of Ψ and diagonal estimates of Ω with very large diagonal entries. Essentially, when the spike and slab distributions are not too different, our ECM algorithm has a tendency to overfit the response with a dense Ψ , leaving very little residual variation to be quantified with Ω . On further investigation, we found that we could detect such pathological behavior by examining the condition number of the matrix $Y\Omega - X\Psi$. To avoid propagating dense Ψ 's and diagonal Ω 's through the DPE and DCPE, we terminate our ECM early whenever the condition number of $Y\Omega - X\Psi$ exceeds $10n$. We then set the corresponding $\Psi^{(s)} = 0$ and $\Omega^{(t)} = I$ and continue the dynamic exploration from that point. While this is admittedly ad hoc heuristic, we have found that it works well in practice and note that Moran et al. (2019) utilized a similar strategy in the single-outcome high-dimensional linear regression setting with unknown variance.

The DPE and DCPE cgSSL procedures are implemented in the **mSSL** R (R Core Team, 2022) package, which is available at <https://github.com/YunyiShen/mSSL>. Note that this package contains a new implementation of Deshpande et al. (2019)'s mSSL procedure as well.

4 Asymptotic theory of cgSSL

If the Gaussian chain graph model in Equation (1) is well-specified – that is, if our data $(\mathbf{x}_i, \mathbf{y}_i)$ are truly generated according to the model – will the posterior distribution of Ψ and Ω collapse to a point-mass at the true data generating parameters as $n \rightarrow \infty$? Such a collapse would, among other things, imply the MAP estimate returned by the cgSSL procedure described in Section 3 is consistent, providing an asymptotic justification for its use. In this section, we answer the question affirmatively: under some mild assumptions and with some slight modifications, the cgSSL posterior *concentrates* around the truth. We

further establish the rate of concentration, which quantifies the speed at which the posterior distribution shrinks to the true data generating parameters. We begin by briefly reviewing our general proof strategy before precisely stating our assumptions and results. Proofs of our main results are available in Section S5 of the Supplementary Materials.

4.1 Proof strategy

To establish the posterior concentration rate for Ψ and Ω , we followed Ning et al. (2020) and Bai et al. (2020) and first showed that the posterior concentrates in log-affinity (see Section S5.3 in the Supplementary Materials for details). Posterior concentration of the individual parameters followed as a consequence. To show that the posterior concentrates in log-affinity, we appealed to general results about posterior concentration for independent but non-identically distributed observations. Specifically, we verified the three conditions of Theorem 8.23 of Ghosal and van der Vaart (2017). First, we confirmed that the cgSSL prior introduced in Section 3.1 places enough prior probability mass in small neighborhoods around every possible choice of (Ψ, Ω) . This was done by verifying that for each (Ψ, Ω) , the prior probability contained in a small Kullback-Leibler ball around (Ψ, Ω) can be lower bounded by a function of the ball’s radius (the so-called “KL-condition” in Lemma S2 of the Supplementary Materials). Then we studied a sequence of likelihood ratio tests defined on sieves of the parameter space that can correctly distinguish between parameter values that are sufficiently far away from each other in log-affinity. In particular, we bounded the error rate of such tests and then bounded the covering number of the sieves (Lemma S4 of the Supplementary Materials).

Ning et al. (2020) studied the sparse marginal regression model in Equation (2) instead of the sparse chain graph. Although these are somewhat different models, our overall proof strategy is quite similar to theirs. However, we pause here to highlight some important technical differences. First, Ning et al. (2020) placed a prior on Ω ’s eigendecomposition while we placed an arguably simpler and more natural element-wise prior on Ω . The second and more substantive difference is in how we bound the covering number of sieves of the underlying parameter space. Because Ning et al. (2020) specified exactly sparse priors on the elements of $B = \Psi\Omega^{-1}$, it was enough for them to carefully bound the covering number of exactly low-dimensional sets of the form $\mathcal{A} \times \{0\}^r$ where \mathcal{A} is some subset of a multi-dimensional Euclidean space and $r > 0$ is a positive integer. In contrast, because we specified absolutely continuous priors on the elements of Ψ , we had to cover “effectively low-dimensional” sets

of the form $\mathcal{A} \times [-\delta, \delta]^r$ for small $\delta > 0$. Our key lemma (Lemma S4 in the Supplementary Materials) provides sufficient conditions on δ for bounding the ϵ -packing number of such effectively low-dimensional sets using the ϵ' -packing number of \mathcal{A} for a carefully chosen $\epsilon' > 0$.

4.2 Contraction of cgSSL

In order to establish our posterior concentration results, we first assume that the data $(\mathbf{x}_1, \mathbf{y}_1), \dots, (\mathbf{x}_n, \mathbf{y}_n)$ were generated according to a Gaussian chain graph model with true parameter Ψ_0 and Ω_0 . We need to make additional assumptions about the spectra of Ψ_0 and Ω_0 and on the dimensions n, p and q .

A1 Ψ_0 and Ω_0 have bounded operator norm: that is, $\Psi_0 \in \mathcal{T}_0 = \{\Psi : |||\Psi|||_2 < a_1\}$ and $\Omega_0 \in \mathcal{H}_0\{\Omega : |||\Omega|||_2 \in [1/b_2, 1/b_1]\}$ where $|||\cdot|||$ is the operator norm and $a_1, b_1, b_2 > 0$ are fixed positive constants.

A2 Dimensionality: We assume that $\log(n) \lesssim \log(q)$; $\log(n) \lesssim \log(p)$; and

$$\max\{p, q, s_0^\Omega, s_0^\Psi\} \log(\max\{p, q\})/n \rightarrow 0,$$

where s_0^Ω and s_0^Ψ are the number of non-zero free parameters in Ω and Ψ respectively; and $a_n \lesssim b_n$ means for sufficient large n , there exists a constant C independent of n such that $a_n \leq Cb_n$

A3 Tuning the Ψ prior: We assume that $(1 - \theta)/\theta \sim (pq)^{2+a'}$ for some $a' > 0$; $\lambda_0 \sim \max\{n, pq\}^{2+b'}$ for some $b' > 1/2$; and $\lambda_1 \asymp 1/n$

A4 Tuning the Ω prior: We assume that that $(1 - \eta)/\eta \sim \max\{Q, pq\}^{2+a}$ for some $a > 0$, where $Q = q(q - 1)/2$; $\xi_0 \sim \max\{Q, pq, n\}^{4+b}$ for some $b > 0$; $\xi_1 \asymp 1/n$ and $\xi \asymp 1/\max\{Q, n\}$

Before stating our main result, we pause to highlight two key differences between the above assumptions and model introduced in Section 3.1. Although the prior in Section 3.1 restricts Ω to the positive-definite cone, Assumption 1 is slightly stronger as it bounds the smallest eigenvalue of Ω away from zero. The stronger assumption ensures that the entries of $X\Psi\Omega^{-1}$ do not diverge in our theoretical analysis. We additionally restricted our theoretical analysis to the setting where the proportion of non-negligible parameters, θ and η , are fixed and known (Assumption 4). We note that Ročková and George (2018) and Gan et al. (2019a)

make similar assumptions in their theoretical analyses.

Theorem 1 (Posterior contraction of cgSSL). *Under Assumptions A1–A4, there is a constant $M_1 > 0$, which does not depend on n , such that*

$$\sup_{\Psi \in \mathcal{T}_0, \Omega \in \mathcal{H}_0} \mathbb{E}_0 \Pi \left(\Psi : \|X(\Psi \Omega^{-1} - \Psi_0 \Omega_0^{-1})\|_F^2 \geq M_1 n \epsilon_n^2 |Y_1, \dots, Y_n\right) \rightarrow 0 \quad (11)$$

$$\sup_{\Psi \in \mathcal{T}_0, \Omega \in \mathcal{H}_0} \mathbb{E}_0 \Pi \left(\Omega : \|\Omega - \Omega_0\|_F^2 \geq M_1 \epsilon_n^2 |Y_1, \dots, Y_n\right) \rightarrow 0 \quad (12)$$

where $\epsilon_n = \sqrt{\max\{p, q, s_0^\Omega, s_0^\Psi\} \log(\max\{p, q\})/n}$. Note that $\epsilon_n \rightarrow 0$ as $n \rightarrow \infty$.

A key step in proving Theorem 1 is Lemma 1, which shows that the cgSSL posterior does not place too much probability on Ψ 's and Ω 's with too many large entries. In order to state this lemma, we denote the effective dimensions of Ψ and Ω by $|\nu(\Psi)|$ and $|\nu(\Omega)|$. The effective dimension of Ψ (resp. Ω) counts the number of entries (resp. off-diagonal entries in the lower-triangle) whose absolute value exceeds the intersection point of the spike and slab prior densities.

Lemma 1 (Dimension recovery of cgSSL). *For a sufficiently large number $C'_3 > 0$, we have:*

$$\sup_{\Psi \in \mathcal{T}_0, \Omega \in \mathcal{H}_0} \mathbb{E}_0 \Pi \left(\Psi : |\nu(\Psi)| > C'_3 s^* |Y_1, \dots, Y_n\right) \rightarrow 0 \quad (13)$$

$$\sup_{B \in \mathcal{T}_0, \Omega \in \mathcal{H}_0} \mathbb{E}_0 \Pi \left(\Omega : |\nu(\Omega)| > C'_3 s^* |Y_1, \dots, Y_n\right) \rightarrow 0 \quad (14)$$

where $s^* = \max\{p, q, s_0^\Omega, s_0^\Psi\}$.

Lemma 1 essentially guarantees that the cgSSL posterior does not grossly overestimate the number of predictor-response and response-response edges in the underlying graphical model.

Note that the result in Equation (11) shows that the vector containing the n evaluations of the regression function (i.e. the vector $X\Psi\Omega^{-1}$), converges to the vector containing the evaluations of the true regression function $\Omega_0^{-1}\Psi_0^\top \mathbf{x}$. Importantly, apart from Assumption A2 about the dimensions of X , we did not make any additional assumptions about the design matrix. The contraction rates for Ψ and $\Psi\Omega^{-1}$, however, depend critically on X . To state these results, denote the restricted eigenvalue of a matrix A as

$$\phi^2(s) = \inf_{A \in \mathbb{R}^{p \times q} : 0 \leq |\nu(A)| \leq s} \left\{ \frac{\|XA\|_F^2}{n\|A\|_F^2} \right\}.$$

Corollary 1 (Recovery of regression coefficients in cgSSL). *Under Assumptions A1–A4, there is some constant $M' > 0$, which does not depend on n , such that*

$$\sup_{\Psi \in \mathcal{T}_0, \Omega \in \mathcal{H}_0} \mathbb{E}_0 \Pi \left(\|\Psi \Omega^{-1} - \Psi_0 \Omega_0^{-1}\|_F^2 \geq \frac{M' \epsilon_n^2}{\phi^2(s_0^\Psi + C'_3 s^*)} \right) \rightarrow 0 \quad (15)$$

$$\sup_{\Psi \in \mathcal{T}_0, \Omega \in \mathcal{H}_0} \mathbb{E}_0 \Pi \left(\|\Psi - \Psi_0\|_F^2 \geq \frac{M' \epsilon_n^2}{\min\{\phi^2(s_0^\Psi + C'_3 s^*), 1\}} \right) \rightarrow 0. \quad (16)$$

Corollary 1 shows that the posterior distribution of $\Psi \Omega^{-1}$ can contract at a faster or slower rate than the posterior distributions of $X \Psi \Omega^{-1}$ and Ω , depending on the design matrix. In particular, when X is poorly conditioned, we might expect the rate to be slower. In contrast, the term $\min\{\phi^2(s_0^\Psi + C'_3 s^*), 1\}$ appearing in the denominator of the rate in Equation (16) implies that the posterior distribution of Ψ cannot concentrate at a faster rate than the posterior distributions of $\Psi \Omega^{-1}$ and Ω , regardless of the design matrix. To develop some intuition about this phenomenon, notice that we can decompose the difference $\Psi - \Psi_0$ as

$$\Psi - \Psi_0 = (\Psi \Omega^{-1} - \Psi_0 \Omega_0^{-1}) \Omega + (\Psi_0 \Omega_0^{-1} (\Omega - \Omega_0) \Omega^{-1}) \Omega.$$

Roughly speaking, the decomposition suggests that in order to estimate Ψ well, we must be able to estimate both Ω and $\Psi \Omega^{-1}$ well. In other words, estimating Ψ is at least as hard, statistically, as estimating Ω and $\Psi \Omega^{-1}$. Taken together, the two results in Corollary 1 suggest that while a carefully constructed design matrix can improve estimation of the matrix of *marginal* effects, $B = \Psi \Omega^{-1}$, it cannot generally improve estimation of the matrix of *direct* effects Ψ .

5 Synthetic experiments

We performed a simulation study to assess how well our two implementations of cgSSL (cgSSL-DPE and cgSSL-DCPE) (i) recover the supports of Ψ and Ω and (ii) estimate each matrix. We compared both implementations of cgSSL to several competitors: a fixed-penalty method (cgLASSO), which deploys a single penalty λ for the entries in Ψ and a single fixed penalty ξ for the entries in Ω ; Shen and Solis-Lemus (2021)’s CAR-LASSO procedure (CAR), which puts Laplace priors on Ψ and Ω entries and Gamma prior on the overall shrinkage strength; and Shen and Solis-Lemus (2021)’s adaptive CAR-LASSO (CAR-A), which puts individualized Laplace prior on free parameters of Ψ and Ω . Note that cgSSL and cgLASSO

perform optimization while **CAR** and **CAR-A** run MCMC. Further, we selected the penalties in **cgLASSO** with 10-fold cross-validation. Additionally, **cgLASSO** and **CAR** apply the same amount of shrinkage to every element of Ψ and the same amount of shrinkage to every element of Ω . **CAR-A**, on the other hand, applied individualized shrinkage.

We simulated several synthetic datasets of various dimensions and with different sparsity patterns in Ω (Figure 2). Across all of these choices of dimension and Ω , we found that **cgSSL-DPE** achieved somewhat lower sensitivity but much higher precision in estimating the supports of both Ψ and Ω than the competing methods. Taken together, these findings suggest that while **cgSSL-DPE** tended to return fewer non-zero parameter estimates than the other methods, we can be much more certain that those parameters are truly non-zero. Put another way, although the other methods can recover more of the truly non-zero signal, they do so at the expense of making many more false positive identifications in the supports of Ψ and Ω than **cgSSL-DPE**.

5.1 Simulation design

We simulated data with three different choices of dimensions $(n, p, q) = (100, 10, 10), (100, 20, 30)$, and $(400, 100, 30)$. For each choice of (n, p, q) , we considered five different choices of Ω : (i) an AR(1) model for Ω^{-1} so that Ω is tri-diagonal; (ii) an AR(2) model for Ω^{-1} so that $\omega_{k,k'} = 0$ whenever $|k - k'| > 2$; (iii) a block model in which Ω is block-diagonal with two dense $q/2 \times q/2$ diagonal blocks; (iv) a star graph where the off-diagonal entry $\omega_{k,k'} = 0$ unless k or k' is equal to 1; and a dense model with all off-diagonal elements $\omega_{k,k'} = 2$.

In the AR(1) model we set $(\Omega^{-1})_{k,k'} = 0.7^{|k-k'|}$ so that $\omega_{k,k'} = 0$ whenever $|k - k'| > 1$. In the AR(2) model, we set $\omega_{k,k} = 1, \omega_{k-1,k} = \omega_{k,k-1} = 0.5$, and $\omega_{k-2,k} = \omega_{k,k-2} = 0.25$. For the block model, we partitioned $\Sigma = \Omega^{-1}$ into 4 $q/2 \times q/2$ blocks and set all entries in the off-diagonal blocks of Σ to zero. We then set $\sigma_{k,k} = 1$ and $\sigma_{k,k'} = 0.5$ for $1 \leq k \neq k' \leq q/2$ and for $q/2 + 1 \leq k \neq k' \leq q$. For the star graph, we set $\omega_{k,k} = 1, \omega_{1,k} = \omega_{k,1} = 0.1$ for each $k = 2, \dots, q$, and set the remaining off-diagonal elements of Ω equal to zero.

These five specifications of Ω (top row of Figure 2) correspond to rather different underlying graphical structure among the response variables (bottom row of Figure 2). The AR(1) model, for instance, represents an extremely sparse but regular structure while the AR(2) model is somewhat less sparse. While the star model and AR(1) model contain the same number of edges, the underlying graphs have markedly different degree distributions. Compared to the AR(1), AR(2), and star models, the block model is considerably denser. We

included the full model, which corresponds to a dense Ω , to assess how well all of the methods perform in a misspecified regime.

In total, we considered 15 combinations of dimensions (n, p, q) and Ω . For each combination, we generated Ψ by randomly selecting 20% of entries to be non-zero. We drew the non-zero entries uniformly from a $\mathcal{U}(-2, 2)$ distribution. For each combination of (n, p, q) , Ω and Ψ , we generated 100 synthetic datasets from the Gaussian chain graph model (1). The entries of the design matrix X were independently drawn from a standard $\mathcal{N}(0, 1)$ distribution.

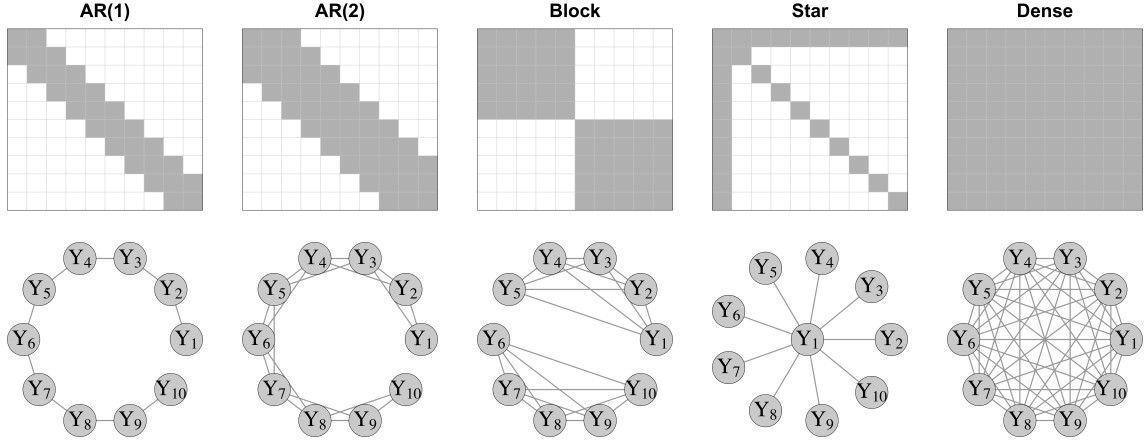


Figure 2: Visualization of the supports of Ω for $q = 10$ under each of the five specifications (top) and corresponding graph (bottom). In the top row, we have gray cells indicate non-zero entries in Ω and white cells indicate zeros

5.2 Results

To assess estimation performance, we computed the Frobenius norm between the estimated matrices and the true data generating matrices. To assess the support recovery performance, we counted the number of elements in each of Ψ and Ω that were (i) correctly estimated as non-zero (true positives; TP); (ii) correctly estimated as zero (true negatives; TN); (iii) incorrectly estimated as non-zero (false positives; FP); and (iv) incorrectly estimated as zero (false negatives; FN). We report the sensitivity ($TP/(TP + FN)$) and precision ($TP/(TP + FP)$). Generally speaking, we prefer methods with high sensitivity and high precision. High sensitivity indicates that the method has correctly estimated most of the true non-zero parameters as non-zero. High precision, on the other hand, indicates that most of the estimated non-zero parameters are truly non-zero. For brevity, we only report the average sensitivity, precision, and Frobenius errors for the $(n, p, q) = (100, 10, 10)$ setting in Table 1.

We observed qualitatively similar results for the other two settings of dimension and report average performance in those settings in Tables S2–S3 of the Supplementary Materials.

Table 1: Average (sd) sensitivity, precision, and Frobenius error for Ψ and Ω when $(n, p, q) = (100, 10, 10)$ for each specification of Ω across 100 simulated datasets. For each choice of Ω , the best performance is bold-faced.

Method	SEN	Ψ recovery		SEN	Ω recovery	
		PREC	FROB		PREC	FROB
<i>AR(1) model</i>						
cgLASSO	0.88 (0.08)	0.44 (0.15)	0.13 (0.16)	0.78 (0.37)	0.55 (0.31)	31.93 (22.08)
CAR	0.86 (0.06)	0.31 (0.03)	0.04 (0.01)	1 (0)	0.3 (0.03)	4.16 (1.18)
CAR-A	0.87 (0.06)	0.59 (0.07)	0.02 (0.01)	1 (0)	0.83 (0.1)	2.75 (1.59)
cgSSL-dcpe	0.64 (0.05)	0.8 (0.16)	0.08 (0.05)	0.94 (0.11)	0.96 (0.07)	6.32 (6.64)
cgSSL-dpe	0.65 (0.05)	0.99 (0.03)	0.04 (0.01)	1 (0)	0.97 (0.05)	2.49 (1.12)
<i>AR(2) model</i>						
cgLASSO	1 (0.02)	0.22 (0.06)	0.17 (0.09)	0.84 (0.29)	0.55 (0.17)	2.7 (1.66)
CAR	0.9 (0.06)	0.34 (0.04)	0.03 (0.01)	0.98 (0.03)	0.57 (0.06)	0.58 (0.21)
CAR-A	0.89 (0.05)	0.67 (0.08)	0.02 (0.01)	1 (0.02)	0.91 (0.06)	0.46 (0.32)
cgSSL-dcpe	0.96 (0.06)	0.43 (0.12)	0.45 (0.28)	0.24 (0.3)	0.63 (0.14)	5 (0.98)
cgSSL-dpe	0.73 (0.05)	1 (0.01)	0.02 (0.01)	1 (0)	0.86 (0.06)	0.38 (0.21)
<i>Block model</i>						
cgLASSO	0.95 (0.05)	0.39 (0.18)	0.13 (0.11)	0.73 (0.38)	0.78 (0.21)	5.15 (2.27)
CAR	0.89 (0.06)	0.31 (0.03)	0.03 (0.01)	0.95 (0.02)	0.61 (0.06)	1.89 (0.75)
CAR-A	0.87 (0.06)	0.57 (0.07)	0.03 (0.01)	0.86 (0.07)	0.93 (0.05)	2.97 (1.22)
cgSSL-dcpe	0.76 (0.06)	0.29 (0.02)	0.28 (0.02)	0.01 (0.03)	0.71 (0.39)	8.85 (0.2)
cgSSL-dpe	0.69 (0.07)	0.99 (0.02)	0.03 (0.01)	0.71 (0.06)	0.95 (0.05)	3.28 (1.17)
<i>Star model</i>						
cgLASSO	0.96 (0.04)	0.48 (0.14)	0.04 (0.02)	0.36 (0.41)	0.2 (0.18)	0.86 (0.35)
CAR	0.91 (0.05)	0.34 (0.03)	0.02 (0)	0.55 (0.18)	0.25 (0.08)	0.57 (0.29)
CAR-A	0.91 (0.04)	0.57 (0.06)	0.02 (0.01)	0.22 (0.14)	0.46 (0.24)	0.57 (0.26)
cgSSL-dcpe	0.83 (0.04)	0.96 (0.05)	0.01 (0)	0.05 (0.09)	0.9 (0.24)	0.22 (0.12)
cgSSL-dpe	0.79 (0.06)	0.99 (0.03)	0.01 (0.01)	0.09 (0.13)	0.71 (0.29)	0.29 (0.19)
<i>Dense model</i>						
cgLASSO	0.92 (0.04)	0.57 (0.07)	0.03 (0.01)	0.88 (0.32)	1 (0)	16.93 (32.74)
CAR	0.85 (0.06)	0.28 (0.03)	0.04 (0.01)	0.03 (0.02)	1 (0)	92.51 (1.74)
CAR-A	0.84 (0.06)	0.4 (0.04)	0.04 (0.01)	0 (0.01)	1 (0)	96.04 (1.21)
cgSSL-dcpe	0.82 (0.03)	0.84 (0.06)	0.02 (0)	0.01 (0.02)	1 (0)	99.93 (0.39)
cgSSL-dpe	0.72 (0.07)	0.93 (0.06)	0.03 (0.01)	0.05 (0.04)	1 (0)	99.99 (0.98)

In terms of identifying non-zero direct effects (i.e. estimating the support of Ψ), cgLASSO consistently achieves the highest sensitivity. On further inspection, we found that the penalties selected by 10-fold cross-validation tended to be quite small, meaning that cgLASSO returned many non-zero $\hat{\psi}_{j,k}$'s. As the precision results indicate, many of cgLASSO's "discoveries" were in fact false positives. The other fixed penalty method, CAR, similarly displayed somewhat high sensitivity and low precision. Interestingly, for several choices of Ω , the pre-

cisions of **cgLASSO** and **CAR** for recovering the support of Ψ were less than 0.5. Such low precisions indicate that most of the returned non-zero estimates were in fact false positives. In contrast, methods that deployed adaptive penalties (**CAR-A** and both implementations of **cgSSL**), displayed higher precision in estimating the support of Ψ . In fact, at least for estimating the support of Ψ , **cgSSL-DPE** made almost no false positives.

We observed essentially the same phenomenon for Ω : although the **cgSSL** generally returned fewer non-zero estimates of $\omega_{k,k'}$, the vast majority of these estimates were true positives. In a sense, the fixed penalty methods (**cgLASSO** and **CAR**) cast a very wide net when searching for non-zero signal in Ψ and Ω , leading to large number of false positive identifications in the supports of these matrices. Adaptive penalty methods, on the other hand, are much more discerning.

In terms of estimation performance, we found that the fixed penalty methods (**cgLASSO** and **CAR**) tended to have much larger Frobenius error, reflecting the well-documented bias introduced by L_1 regularization. The one exception was in the misspecified setting where Ω was dense. Interestingly, for the four sparse Ω 's, we did not observe any method achieving high Frobenius error for Ω but low Frobenius error for Ψ . This finding helps substantiate our intuition about Corollary 1. Namely, in order to estimate Ψ well, one must estimate Ω well. Finally, like [Deshpande et al. \(2019\)](#), we found that dynamic conditional posterior exploration implementation of **cgSSL** performed slightly worse than dynamic posterior exploration implementation.

6 Real data experiments

[Claesson et al. \(2012\)](#) studied the gut microbiota of elderly individuals using data sequenced from fecal samples taken from 178 subjects. They were primarily interested in understanding differences in the gut microbiome composition across several residence types (in the community, day-hospital, rehabilitation, or in long-term residential care) and across several different types of diet. We refer the reader to the Supplementary Notes and Supplementary Table 3 of [Claesson et al. \(2012\)](#) for more details. They found that the gut microbiomes of residents in long-term care facilities were considerably less diverse than those of residents dwelling in the community. They additionally reported that diet had a large marginal effect on gut microbe diversity but they did not examine conditional or direct effects, which might align more closely with the underlying biological mechanism. In this section, we re-analyze their

data using the cgSSL to try to estimate the direct effects of each type of diet and residence type on gut microbiome composition.

We pre-processed the raw 16s-rRNA data in the MG-RAST server (Keegan et al., 2016); please see Section S4 of the Supplementary Materials for more details on the pre-processing. In all, we had $n = 178$ observations of $p = 11$ predictors and $q = 14$ taxa. Figure 3 shows the graphical model estimated by cgSSL-DPE. In the figure, edges are colored according to the sign of the effect, with blue edges corresponding to negative conditional correlation and red edges corresponding to positive conditional correlation. The edge widths correspond to the absolute value of the parameter, with wider edges indicating larger parameter values. We found a large number of edges between the different species, suggesting that there was considerable conditional dependence between their abundances after adjusting for the covariates. In fact, we found only two non-zero entries in Ψ . We estimated that percutaneous endoscopic gastronomy (PEG), in which a feeding tube is inserted into the abdomen, had a negative direct effect on the abundance of *Veillonella*, which is involved in lactose fermentation. Reassuringly for us, our finding aligns with those in Takeshita et al. (2011), which reported a negative effect of PEG on this genus. We additionally found that staying in a day hospital had a positive direct effect on *Caloramator*.

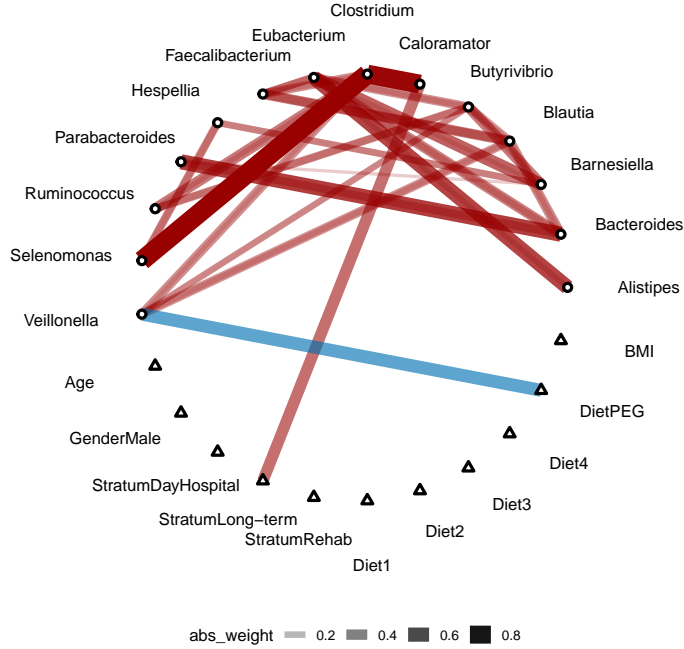


Figure 3: The estimated graphical model underlying [Claesson et al. \(2012\)](#)’s gut microbiome dataset. We annotate the edge weight by the absolute value of conditional regression coefficients and red color represents positive (conditional) dependence and blue represents negative (conditional) dependence.

Our results suggest that the large marginal effects reported by [Claesson et al. \(2012\)](#) are a by-product of only a few direct effects and substantial residual conditional dependence between species. For instance, because PEG has a direct effect on *Veillonella*, which is conditionally correlated with *Clostridium*, *Butyrivibrio*, and *Blautia*, PEG displays a marginal effect on each of these other genus. In this way, the cgSSL can provide a more nuanced understanding of the underlying biological mechanism than simply estimating the matrix of marginal effects $B = \Psi\Omega^{-1}$. We note, however, that [Claesson et al. \(2012\)](#)’s dataset does not contain an exhaustive set of environmental and patient life-style predictors. Accordingly, our re-analysis is limited in the sense that were we able to incorporate additional predictors, the estimated graphical model may be quite different.

7 Discussion

In the Gaussian chain graph model in Equation (1), Ψ is a matrix containing all of the *direct* effects of p predictors on q outcomes while Ω is the residual precision matrix that encodes the conditional dependence relationships between the outcomes that remain after adjusting for the predictors. We have introduced the cgSSL procedure for obtaining simultaneously sparse estimates of Ψ and Ω . In our procedure, we formally specify spike-and-slab LASSO priors on the free elements of Ψ and Ω and use an ECM algorithm to maximize the posterior density. Our ECM algorithm iteratively solves a penalized maximum likelihood problem with self-adaptive penalties. Across several simulated datasets, cgSSL demonstrated excellent support recovery and estimation performance, substantially out-performing competitors that deployed constant shrinkage penalties. We further characterized the asymptotic properties of cgSSL posteriors, establishing posterior concentration rates under relatively mild assumptions. To the best of our knowledge, these are the first such results for sparse Gaussian chain graph models.

Although our main theoretical result (Theorem 1) implies that a slightly modified version of the cgSSL procedure from Section 3 is asymptotically consistent, quantifying finite sample posterior uncertainty remains challenging. Several authors have proposed extensions of [Newton and Raftery \(1994\)](#)’s weighted likelihood bootstrap for quantifying posterior uncertainty. Basically, these procedures work by repeatedly maximizing a randomized objective formed by carefully re-weighting each term in the log-likelihood and the log-prior. In fact, [Nie and Ročková \(2022\)](#) recently deployed this strategy to quantify uncertainty in SSL posteriors for single-outcome regression in high dimensions. A key ingredient in [Nie and Ročková \(2022\)](#) is the introduction of an additional random location shift in the prior to offset the tendency of the SSL to return exactly sparse parameter estimates. In our Gaussian chain graph problem, introducing a similar shift is challenging due to the constraint that Ω be positive definite. Overcoming this difficulty is the subject of on-going work.

In many applications, analysts encounter multiple outcomes of mixed type (i.e. continuous and discrete). In its current form, the cgSSL is not applicable to these situations. It is possible, however, to extend the cgSSL to model outcomes of mixed type using a strategy similar to one found in [Kowal and Canale \(2020\)](#), which modeled discrete variables as truncated and transformed versions of latent Gaussian random variables.

Acknowledgements

The authors are grateful to Ray Bai for helpful comments on the theoretical results and to Gemma Moran for feedback on an early draft of the manuscript.

This work was supported by the National Institute of Food and Agriculture, United States Department of Agriculture, Hatch project 1023699. This work was also supported by the Department of Energy [DE-SC0021016 to C.S.L.]. Support for S.K.D. was provided by the University of Wisconsin–Madison, Office of the Vice Chancellor for Research and Graduate Education with funding from the Wisconsin Alumni Research Foundation.

This research was performed using the compute resources and assistance of the UW–Madison Center For High Throughput Computing (CHTC) in the Department of Computer Sciences. The CHTC is supported by UW–Madison, the Advanced Computing Initiative, the Wisconsin Alumni Research Foundation, the Wisconsin Institutes for Discovery, and the National Science Foundation, and is an active member of the OSG Consortium, which is supported by the National Science Foundation and the U.S. Department of Energy’s Office of Science.

References

- Aitchison, J. (1982). The statistical analysis of compositional data. *Journal of the Royal Statistical Society: Series B (Methodological)*, 44(2):139–160.
- Bai, R., Moran, G. E., Antonelli, J. L., Chen, Y., and Boland, M. R. (2020). Spike-and-slab group LASSOs for grouped regression and sparse generalized additive models. *Journal of the American Statistical Association*.
- Bai, R., Ročková, V., and George, E. I. (2021). Spike-and-slab meets LASSO: A review of the spike-and-slab LASSO. In Tadesse, M. and Vannucci, M., editors, *Handbook of Bayesian Variable Selection*. Routledge.
- Banerjee, O., Ghaoui, L. E., and D’Aspremont, A. (2008). Model selection through sparse maximum likelihood estimation for multivariate Gaussian or binary data. *Journal of Machine Learning Research*, 9:485–516.
- Battson, M. L., Lee, D. M., Weir, T. L., and Gentile, C. L. (2018). The gut microbiota as a novel regulator of cardiovascular function and disease. *The Journal of Nutritional Biochemistry*, 56:1–15.

- Belcheva, A., Irrazabal, T., Robertson, S. J., Streutker, C., Maughan, H., Rubino, S., Moriyama, E. H., Copeland, J. K., Surendra, A., Kumar, S., et al. (2014). Gut microbial metabolism drives transformation of MSH2-deficient colon epithelial cells. *Cell*, 158(2):288–299.
- Boucheron, S., Lugosi, G., and Massart, P. (2013). *Concentration inequalities: A nonasymptotic theory of independence*. Oxford university press.
- Boyd, S. P. and Barratt, C. H. (1991). *Linear controller design: limits of performance*. Prentice-Hall.
- Claesson, M. J., Jeffery, I. B., Conde, S., Power, S. E., O’connor, E. M., Cusack, S., Harris, H. M., Coakley, M., Lakshminarayanan, B., O’Sullivan, O., et al. (2012). Gut microbiota composition correlates with diet and health in the elderly. *Nature*, 488(7410):178–184.
- Deshpande, S. K., Ročková, V., and George, E. I. (2019). Simultaneous variable and covariance selection with the multivariate spike-and-slab LASSO. *Journal of Computational and Graphical Statistics*, 28(4):921–931.
- Friedman, J., Hastie, T., and Tibshirani, R. (2008). Sparse inverse covariance estimation with the graphical LASSO. *Biostatistics*, 9(3):432–441.
- Frydenberg, M. (1990). The chain graph Markov property. *Scandinavian Journal of Statistics*, 17(4):333–353.
- Gan, L., Narisetty, N. N., and Liang, F. (2019a). Bayesian regularization for graphical models with unequal shrinkage. *Journal of the American Statistical Association*, 114(527):1218–1231.
- Gan, L., Yang, X., Narisetty, N. N., and Liang, F. (2019b). Bayesian joint estimation of multiple graphical models. *Advances in Neural Information Processing Systems (NeurIPS)*.
- George, E. I. and McCulloch, R. E. (1993). Variable selection via Gibbs sampling. *Journal of the American Statistical Association*, 88(423):881–889.
- George, E. I. and Ročková, V. (2020). Comment: Regularization via Bayesian penalty mixing. *Technometrics*, 62(4):438 – 442.
- Ghosal, S. and van der Vaart, A. (2017). *Fundamentals of nonparametric Bayesian inference*, volume 44. Cambridge University Press.

- Guinane, C. M. and Cotter, P. D. (2013). Role of the gut microbiota in health and chronic gastrointestinal disease: understanding a hidden metabolic organ. *Therapeutic Advances in Gastroenterology*, 6(4):295–308.
- Hills Jr, R. D., Pontefract, B. A., Mishcon, H. R., Black, C. A., Sutton, S. C., and Theberge, C. R. (2019). Gut microbiome: profound implications for diet and disease. *Nutrients*, 11(7):1613.
- Hsieh, C. J., Sustik, M. A., Dhillon, I. S., and Ravikumar, P. (2011). Sparse inverse covariance matrix estimation using quadratic approximation. In *Advances in Neural Information Processing Systems (NeurIPS)*.
- Kamada, N. and Núñez, G. (2014). Regulation of the immune system by the resident intestinal bacteria. *Gastroenterology*, 146(6):1477–1488.
- Keegan, K. P., Glass, E. M., and Meyer, F. (2016). MG-RAST, a metagenomics service for analysis of microbial community structure and function. In *Microbial Environmental Genomics (MEG)*, pages 207–233. Springer.
- Kim, D., Zeng, M. Y., and Núñez, G. (2017). The interplay between host immune cells and gut microbiota in chronic inflammatory diseases. *Experimental & Molecular Medicine*, 49(5):e339–e339.
- Kowal, D. R. and Canale, A. (2020). Simultaneous transformation and rounding (STAR) models for integer-valued data. *Electronic Journal of Statistics*, 14(1):1744–1772.
- Larsbrink, J., Rogers, T. E., Hemsworth, G. R., McKee, L. S., Tauzin, A. S., Spadiut, O., Klintner, S., Pudlo, N. A., Urs, K., Koropatkin, N. M., et al. (2014). A discrete genetic locus confers xyloglucan metabolism in select human gut Bacteroidetes. *Nature*, 506(7489):498–502.
- Lauritzen, S. L. and Richardson, T. S. (2002). Chain graph models and their causal interpretations. *Journal of the Royal Statistical Society: Series B*, 64(3):321–348.
- Lauritzen, S. L. and Wermuth, N. (1989). Graphical models for associations between variables, some of which are qualitative and some quantitative. *The Annals of Statistics*, 17(1):31–57.
- Li, Z., McCormick, T., and Clark, S. (2019). Bayesian joint spike-and-slab graphical LASSO.

- In *Proceedings of the 36th International Conference on Machine Learning (ICML)*, pages 3877–3885. PMLR.
- McCarter, C. and Kim, S. (2014). On sparse Gaussian chain graph models. *Advances in Neural Information Processing Systems (NeurIPS)*.
- Meng, X.-L. and Rubin, D. B. (1993). Maximum likelihood estimation via the ECM algorithm: a general framework. *Biometrika*, 80(2):267–278.
- Mitchell, T. J. and Beauchamp, J. J. (1988). Bayesian variable selection in linear regression. *Journal of the American Statistical Association*, 83(404):1023–1032.
- Moran, G. E., Ročková, V., and George, E. I. (2019). Variance prior forms for high-dimensional Bayesian variable selection. *Bayesian Analysis*, 14(4):1091–1119.
- Moran, G. E., Ročková, V., and George, E. I. (2021). Spike-and-slab LASSO biclustering. *The Annals of Applied Statistics*, 15(1):148–173.
- Newton, M. A. and Raftery, A. E. (1994). Approximate Bayesian inference with the weighted likelihood bootstrap. *Journal of the Royal Statistical Society: Series B*, 56(1):3–26.
- Nie, L. and Ročková, V. (2022). Bayesian bootstrap spike-and-slab LASSO. *Journal of the American Statistical Association*.
- Ning, B., Jeong, S., and Ghosal, S. (2020). Bayesian linear regression for multivariate responses under group sparsity. *Bernoulli*, 26(3):2353–2382.
- R Core Team (2022). *R: A Language and Environment for Statistical Computing*. R Foundation for Statistical Consulting, Vienna, Austria.
- Ročková, V. and George, E. I. (2014). EMVS: The EM approach to Bayesian variable selection. *Journal of the American Statistical Association*, 109(506):828–846.
- Ročková, V. and George, E. I. (2018). The spike-and-slab LASSO. *Journal of the American Statistical Association*, 113(521):431–444.
- Ročková, V. and George, E. I. (2016). Fast Bayesian factor analysis via automatic rotations to sparsity. *Journal of the American Statistical Association*, 111(516):1608–1622.
- Scher, J. U., Sczesnak, A., Longman, R. S., Segata, N., Ubeda, C., Bielski, C., Rostron, T., Cerundolo, V., Pamer, E. G., Abramson, S. B., et al. (2013). Expansion of intestinal prevotella copri correlates with enhanced susceptibility to arthritis. *eLife*, 2:e01202.

- Shen, Y. and Solis-Lemus, C. (2021). Bayesian conditional auto-regressive LASSO models to learn sparse microbial networks with predictors. *arXiv preprint arXiv:2012.08397*.
- Shreiner, A. B., Kao, J. Y., and Young, V. B. (2015). The gut microbiome in health and in disease. *Current Opinion in Gastroenterology*, 31(1):69.
- Singh, R. K., Chang, H.-W., Yan, D., Lee, K. M., Ucmak, D., Wong, K., Abrouk, M., Farahnik, B., Nakamura, M., Zhu, T. H., et al. (2017). Influence of diet on the gut microbiome and implications for human health. *Journal of Translational Medicine*, 15(1):1–17.
- Takeshita, T., Yasui, M., Tomioka, M., Nakano, Y., Shimazaki, Y., and Yamashita, Y. (2011). Enteral tube feeding alters the oral indigenous microbiota in elderly adults. *Applied and Environmental Microbiology*, 77(19):6739–6745.
- Tang, Z., Shen, Y., Li, Y., Zhang, X., Wen, J., Qian, C., Zhuang, W., Shi, X., and Yi, N. (2018). Group spike-and-slab LASSO generalized linear models for disease prediction and associated genes detected by incorporating pathway information. *Bioinformatics*, 34(6):901–910.
- Tang, Z., Shen, Y., Zhang, X., and Yi, N. (2017). The spike-and-slab LASSO generalized linear models for prediction and associated genes detection. *Genetics*, 205:77–88.
- Wang, Z., Klipfell, E., Bennett, B. J., Koeth, R., Levison, B. S., DuGar, B., Feldstein, A. E., Britt, E. B., Fu, X., Chung, Y.-M., et al. (2011). Gut flora metabolism of phosphatidylcholine promotes cardiovascular disease. *Nature*, 472(7341):57–63.
- Zhang, C. H. and Zhang, T. (2012). A General theory of concave regularization for high-dimensional sparse estimation problems. *Statistical Science*, 27(4):576–593.

Supplementary Materials

In Section S1 we derive the Expectation Conditional Maximization (ECM) algorithm used to find the *maximum a posteriori* (MAP) estimates of Ψ and Ω in the cgSSL model. One of the conditional maximization steps of that algorithm involves solving a CGLASSO problem. We introduce a new algorithm, cgQUIC, to solve the general CGLASSO problem in Section S2. Specifically, we show that the problem has unique global optimum (Theorem S1) and that our cgQUIC algorithm converges to this optimum (Theorem S2). Then, we present additional results from the simulation study described in Section 5 of the main text in Section S3. In Section S4, we detail the preprocessing steps we took to prepare the gut microbiome data for analysis with the cgSSL. Finally, we state and prove our main asymptotic results in Section S5.

S1 The cgSSL algorithm

In this section, we provide full details of the Expectation Conditional Maximization (ECM) algorithm that is used in the cgSSL procedure. We describe the algorithm for a fixed set of spike-and-slab penalties $(\lambda_0, \lambda_1, \xi_0, \xi_1)$ and fixed set of hyperparameters $(a_\theta, b_\theta, a_\eta, b_\eta)$. For notational brevity, we will let $\Theta = \{\Psi, \theta, \Omega, \eta\}$ denote the set of four parameters of interest.

Recall from Section 3.3 of the main text that we wish to maximize the log posterior density

$$\begin{aligned}
 \log \pi(\Theta|\mathbf{Y}) = & -\frac{n}{2} \log |\Omega| - \frac{1}{2} \text{tr} \left((Y - X\Psi\Omega^{-1})\Omega(Y - X\Psi\Omega^{-1})^\top \right) \\
 & + \sum_{j=1}^p \sum_{k=1}^q \log \left(\theta \lambda_1 e^{-\lambda_1 |\psi_{j,k}|} + (1 - \theta) \lambda_0 e^{-\lambda_0 |\psi_{j,k}|} \right) \\
 & + \sum_{k=1}^{q-1} \sum_{k' > k}^q \log \left(\eta \xi_1 e^{-\xi_1 |\omega_{k,k'}|} + (1 - \eta) \xi_0 e^{-\xi_0 |\omega_{k,k'}|} \right) \\
 & - \sum_{k=1}^q \xi_0 \omega_{k,k} + \log \mathbb{1}(\Omega \succ 0) \\
 & + (a_\theta - 1) \log(\theta) + (b_\theta - 1) \log(1 - \theta) \\
 & + (a_\eta - 1) \log(\eta) + (b_\eta - 1) \log(1 - \eta)
 \end{aligned} \tag{S1}$$

Instead of optimizing $\log \pi(\Theta|\mathbf{Y})$ directly, we use an ECM algorithm and iteratively update

the surrogate objective

$$F(\Theta) = \mathbb{E}_{\boldsymbol{\delta}}[\log \pi(\Theta, \boldsymbol{\delta}|\mathbf{Y})|\Theta],$$

where $\log \pi(\Theta, \boldsymbol{\delta}|\mathbf{Y})$ is the log-density of the posterior in an *augmented* model involving the spike-and-slab indicators $\boldsymbol{\delta} = \{\delta_{k,k'} : 1 \leq k < k' \leq q\}$. Note that the expectation is taken with respect to the conditional posterior distribution of $\boldsymbol{\delta}$ given Θ . In our augmented model, $\delta_{k,k'}$ indicates whether $\omega_{k,k'}$ was drawn from the spike ($\delta_{k,k'} = 0$) or the slab ($\delta_{k,k'} = 1$). Given Θ and the data \mathbf{Y} , these indicators are conditionally independent with

$$\mathbb{E}[\delta_{k,k'}|\mathbf{Y}, \Theta] = \frac{\eta \xi_1 e^{-\xi_1 |\omega_{k,k'}|}}{\eta \xi_1 e^{-\xi_1 |\omega_{k,k'}|} + (1 - \eta) \xi_0 e^{-\xi_0 |\omega_{k,k'}|}}.$$

The surrogate objective $F(\Theta)$ is given by

$$\begin{aligned} F(\Theta) = & \frac{n}{2} \log(|\Omega|) + \text{tr}(Y^\top X \Psi) - \frac{1}{2} \text{tr}(Y^\top Y \Omega) - \frac{1}{2} \text{tr}((X \Psi)^\top (X \Psi) \Omega^{-1}) \\ & + \sum_{ij} \log(\theta \lambda_1 e^{-\lambda_1 |\psi_{j,k}|} + (1 - \theta) \lambda_0 e^{-\lambda_0 |\psi_{j,k}|}) - \sum_{k < k'} \xi_{k,k'}^* |\omega_{k,k'}| - \xi_1 \sum_{k=1}^q \omega_{k,k} \\ & + (a_\theta - 1) \log \theta + (b_\theta - 1) \log(1 - \theta) + (a_\eta - 1) \log \eta + (b_\eta - 1) \log(1 - \eta) \end{aligned} \quad (\text{S2})$$

where $\xi_{k,k'}^* = \xi_1 q_{k,k'}^* + \xi_0(1 - q_{k,k'}^*)$ and

$$q^*(x, \eta) = \frac{\eta \xi_1 e^{-\xi_1 |x|}}{\eta \xi_1 e^{-\xi_1 |x|} + (1 - \eta) \xi_0 e^{-\xi_0 |x|}}.$$

Our ECM algorithm iteratively computes $F(\Theta)$ based on the current value of Θ (the E-step) and then updates the value of Θ by performing two conditional maximizations (the CM-step). More specifically, for $t \geq 1$, if $\Theta^{(t-1)}$ is the value of Θ at the start of the t^{th} iteration, in the E-step we compute

$$F^{(t)}(\Theta) = \mathbb{E}_{\boldsymbol{\delta}}[\log \pi(\Theta, \boldsymbol{\delta}|\mathbf{Y})|\Theta = \Theta^{(t-1)}].$$

We then compute $\Theta^{(t)}$ by first optimizing $F^{(t)}(\Theta)$ with respect to (Ψ, θ) while fixing $(\Omega, \eta) = (\Omega^{(t-1)}, \eta^{(t-1)})$ to obtain $(\Psi^{(t)}, \theta^{(t)})$. Then we optimizing $F^{(t)}(\Theta)$ with respect to (Ω, η) while fixing $(\Psi, \theta) = (\Psi^{(t)}, \theta^{(t)})$ to obtain $(\Omega^{(t)}, \eta^{(t)})$. That is, in the CM-step we solve the following

optimization problems

$$(\Psi^{(t)}, \theta^{(t)}) = \arg \max_{\Psi, \theta} F^{(t)}(\Psi, \theta, \Omega^{(t-1)}, \eta^{(t-1)}) \quad (\text{S3})$$

$$(\Omega^{(t)}, \eta^{(t)}) = \arg \max_{\Omega, \eta} F^{(t)}(\Psi^{(t)}, \theta^{(t)}, \Omega, \eta). \quad (\text{S4})$$

Once we solve the optimization problems in Equations (S3) and (S4), we set

$$\Theta^{(t)} = (\Psi^{(t)}, \theta^{(t)}, \Omega^{(t)}, \eta^{(t)}).$$

Our ECM algorithm iterates between the E-step and CM-step until the percentage change in the estimated entries of Ψ and Ω or log posterior density is below some user-defined tolerance. In our implementation, we have found that tolerance of 10^{-3} works well. The following subsections detail how we carry out each conditional maximization step.

S1.1 Updating Ψ and θ

.

Fixing $(\Omega, \eta) = (\Omega^{(t-1)}, \eta^{(t-1)})$, observe that

$$\begin{aligned} F^{(t)}(\Psi, \theta, \Omega^{(t-1)}, \eta^{(t-1)}) &= -\frac{1}{2} \text{tr}((Y - X\Psi\Omega^{-1})\Omega(Y - X\Psi\Omega^{-1})^\top) + \log \pi(\Psi, \theta) \\ &= -\frac{1}{2} \text{tr}((Y - X\Psi\Omega^{-1})\Omega\Omega^{-1}\Omega(Y - X\Psi\Omega^{-1})^\top) + \log \pi(\Psi, \theta) \quad (\text{S5}) \\ &= -\frac{1}{2} \text{tr}((Y\Omega - X\Psi)\Omega^{-1}(Y\Omega - X\Psi)^\top) + \log \pi(\Psi, \theta) \end{aligned}$$

where

$$\begin{aligned} \log \pi(\Psi, \theta) &= \sum_{j=1}^p \sum_{k=1}^q \log(\theta \lambda_1 e^{-\lambda_1 |\psi_{j,k}|} + (1 - \theta) \lambda_0 e^{-\lambda_0 |\psi_{j,k}|}) \\ &\quad + (a_\theta - 1) \log(\theta) + (b_\theta - 1) \log(1 - \theta) \end{aligned} \quad (\text{S6})$$

We solve the optimization problem in Equation (S5) using a coordinate ascent strategy that iteratively updates Ψ (resp. θ) while holding θ (resp. Ψ) fixed. We run the coordinate ascent until all active $\psi_{j,k}$ has relative change under the user defined tolerance.

Updating θ given Ψ . Notice that the objective in Equation (S5) depends on θ only through

the $\log \pi(\Psi, \theta)$ term. Accordingly, to updating θ conditionally on Ψ , it is enough to maximize the expression in Equation (S6) as a function of θ while keeping all $\psi_{j,k}$ terms fixed. We use Newton's method for this optimization and we terminate once the Newton step has a step size less than the user defined tolerance.

Updating Ψ given θ . With θ fixed, optimizing Equation (S5) is equivalent to solving

$$\begin{aligned}\Psi^{(t)} &= \arg \max_{\Psi} \left\{ -\frac{1}{2} ((Y\Omega - X\Psi)\Omega^{-1}(Y\Omega - X\Psi)^\top) + \log \pi(\Psi|\theta) \right\} \\ &= \arg \max_{\Psi} \left\{ -\frac{1}{2} ((Y\Omega - X\Psi)\Omega^{-1}(Y\Omega - X\Psi)^\top) + \sum_{j,k} \log \left(\frac{\pi(\psi_{j,k}|\theta)}{\pi(0|\theta)} \right) \right\} \\ &= \arg \max_{\Psi} \left\{ -\frac{1}{2} ((Y\Omega - X\Psi)\Omega^{-1}(Y\Omega - X\Psi)^\top) + \sum_{j,k} \text{pen}(\psi_{j,k}|\theta) \right\}\end{aligned}\quad (\text{S7})$$

where

$$\text{pen}(\psi_{j,k}|\theta) = \log \left(\frac{\pi(\psi_{j,k}|\theta)}{\pi(0|\theta)} \right) = -\lambda_1 |\psi_{j,k}| + \log \left(\frac{p^*(\psi_{j,k}, \theta)}{p^*(0, \theta)} \right).$$

Following essentially the same arguments as those in [Deshpande et al. \(2019\)](#) and using the fact that the columns of X have norm n , the Karush-Kuhn-Tucker (KKT) condition for optimization problem in the final line of Equation (S7) tells us that the optimizer Ψ^* satisfies

$$\psi_{j,k}^* = n^{-1} [|z_{j,k}| - \lambda^*(\psi_{j,k}^*, \theta)]_+ \text{sign}(z_{j,k}), \quad (\text{S8})$$

where

$$\begin{aligned}z_{jk} &= n\psi_{j,k}^* + X_j^\top \mathbf{r}_k + \sum_{k' \neq k} \frac{(\Omega^{-1})_{k,k'}}{(\Omega^{-1})_{k,k}} X_j^\top \mathbf{r}_{k'} \\ \mathbf{r}_{k'} &= (Y\Omega - X\Psi^*)_{k'} \\ \lambda^*(\psi_{j,k}^*, \theta) &= \lambda_1 p^*(\psi_{j,k}^*, \theta) + \lambda_0 (1 - p^*(\psi_{j,k}^*, \theta)).\end{aligned}$$

The KKT condition immediately suggests a cyclical coordinate ascent strategy for solving the problem in Equation (S7) that involves soft thresholding the running estimates of $\psi_{j,k}$. Like [Ročková and George \(2018\)](#) and [Deshpande et al. \(2019\)](#), we can, however, obtain a

more refined characterization of the global model $\tilde{\Psi} = (\tilde{\psi}_{j,k})$:

$$\tilde{\psi}_{j,k} = n^{-1} \left[|z_{j,k}| - \lambda^*(\tilde{\psi}_{j,k}, \theta) \right]_+ \text{sign}(z_{j,k}) \times \mathbb{1}(|z_{j,k}| > \Delta_{j,k}),$$

where

$$\Delta_{j,k} = \inf_{t>0} \left\{ \frac{nt}{2} - \frac{\text{pen}(\tilde{\psi}_{j,k}, \theta)}{(\Omega^{-1})_{k,k}t} \right\}.$$

Though the exact thresholds $\Delta_{j,k}$ are difficult to compute, they can be bounded use an analog to Theorem 2.1 of [Ročková and George \(2018\)](#) and Proposition 2 of [Deshpande et al. \(2019\)](#). Specifically, suppose we have $(\lambda_1 - \lambda_0) > 2\sqrt{n(\Omega^{-1})_{k,k}}$ and $(\lambda^*(0, \theta) - \lambda_1)^2 > -2n(\Omega^{-1})_{k,k}p^*(0, \theta)$. Then we have $\Delta_{j,k}^L \leq \Delta_{j,k} \leq \Delta_{j,k}^U$, where:

$$\begin{aligned} \Delta_{j,k}^L &= \sqrt{-2n((\Omega^{-1})_{k,k})^{-1} \log p^*(0, \theta) - ((\Omega^{-1})_{k,k})^{-2}d + \lambda_1/(\Omega^{-1})_{k,k}} \\ \Delta_{j,k}^U &= \sqrt{-2n((\Omega^{-1})_{k,k})^{-1} \log p^*(0, \theta) + \lambda_1/(\Omega^{-1})_{k,k}} \end{aligned}$$

where $d = -(\lambda^*(\delta_{c+}, \theta) - \lambda_1)^2 - 2n(\Omega^{-1})_{k,k} \log p^*(\delta_{c+}, \theta)$ and δ_{c+} is the largest root of $\text{pen}''(x|\theta) = (\Omega^{-1})_{k,k}$.

Our refined characterization of $\tilde{\Psi}$ suggests a cyclical coordinate descent strategy that combines hard thresholding at $\Delta_{j,k}$ and soft-thresholding at $\lambda_{j,k}^*$.

Remark 1. Equation (S5) and our approach to solving the optimization problem are extremely similar to Equation 3 and the coordinate ascent strategy used in [Deshpande et al. \(2019\)](#), who fit sparse marginal multivariate linear models with spike-and-slab LASSO priors. This is because if $Y \sim \mathcal{N}(X\Psi\Omega^{-1}, \Omega^{-1})$ in our chain graph model, then $Y\Omega \sim \mathcal{N}(X\Psi, \Omega)$. Thus, if we fix the value of Ω , we can use any computational strategy for estimating marginal effects in the multivariate linear regression model to estimate Ψ by working with the transformed data $Y\Omega$.

S1.2 Updating Ω and η

Fixing $\Psi = \Psi^{(t)}$ and $\theta = \theta^{(t)}$, we compute $\Omega^{(t)}$ and $\eta^{(t)}$ by optimizing the function

$$\begin{aligned}
F^{(t)}(\Psi^{(t)}, \theta^{(t)}, \Omega, \eta) &= \frac{n}{2} [\log|\Omega| - \text{tr}(S\Omega) - \text{tr}(M\Omega^{-1})] - \sum_{k < k'} \xi_{k,k'}^* |\omega_{k,k'}| - \sum_{k=1}^q \omega_{k,k} \\
&+ \left(a_\eta - 1 + \sum_{k < k'} q_{k,k}^* \right) \times \log(\eta) \\
&+ \left(b_\eta - 1 + q(q-1)/2 - \sum_{k < k'} q_{k,k}^* \right) \times \log(1 - \eta)
\end{aligned} \tag{S9}$$

where $S = \frac{1}{n} Y^\top Y$ and $M = \frac{1}{n} (X\Psi)^\top X\Psi$.

We immediately observe that expression in Equation (S9) is separable in Ω and η , meaning that we can compute $\Omega^{(t)}$ and $\eta^{(t)}$ separately. Specifically, we have

$$\eta^{(t)} = \frac{a_\eta - 1 + \sum_{k < k'} q_{k,k'}^*}{a_\eta + b_\eta - 2 + q(q-1)/2} \tag{S10}$$

and

$$\Omega^{(t)} = \arg \max_{\Omega > 0} \left\{ \frac{n}{2} [\log(|\Omega|) - \text{tr}(S\Omega) - \text{tr}(M\Omega^{-1})] - \sum_{k < k'} \xi_{k,k'}^* |\omega_{k,k'}| - \sum_{k=1}^q \omega_{k,k} \right\}. \tag{S11}$$

The objective function in Equation (S11) is similar to a graphical LASSO (GLASSO; [Friedman et al., 2008](#)) problem insofar as both problems involve a term like $\log|\Omega| + \text{tr}(S\Omega)$ and separable $L1$ penalties on the off-diagonal elements of Ω . However, Equation (S11) includes an additional term $\text{tr}(M\Omega^{-1})$, which does not appear in the GLASSO. This term arises from through the entanglement of Ψ and Ω in the Gaussian chain graph model and we accordingly call the problem in Equation (S11) the CGLASSO problem. We solve this problem by (i) forming a quadratic approximation of the objective, (ii) computing a suitable Newton direction, and (iii) following that Newton direction for a suitable step size. We detail this solution strategy in Section S2.

S2 Chain graphical LASSO with cgQUIC

Equation (S11) is a specific instantiation of what we term the “chain graphical LASSO” (CGLASSO) problem, whose general form is

$$\arg \min_{\Omega} \left\{ -\log(|\Omega|) + \text{tr}(S\Omega) + \text{tr}(M\Omega^{-1}) + \sum_{k,k'} \xi_{k,k'} |\omega_{k,k'}| \right\} \quad (\text{S12})$$

where S and M are symmetric positive semi-definite $q \times q$ matrices; Ω is a symmetric positive definite $q \times q$ matrix; and the $\xi_{k,k'}$ ’s are symmetric non-negative penalty weights (i.e. we have $\xi_{k,k'} = \xi_{k',k}$).

Notice that when M is the 0 matrix, the CGLASSO problem reduces to a general GLASSO problem, which admits several computational solutions. One well known solution is to solve the dual problem, which involves minimization of a log determinant under L_{∞} constraint ([Banerjee et al., 2008](#)).

Unfortunately, the dual form of the CGLASSO problem does not have such a simple form. To wit, the dual of the CGLASSO problem with uniform penalty ξ is given by:

$$\min_{\|U\|_{\infty} < \xi} \max_{\Omega \succ 0} \log|\Omega| - \text{tr}[(S + U)\Omega] - \text{tr}[MX^{-1}]$$

The inner optimization about Ω can be solved by setting the derivative to 0; the optimal value of Ω solves a special case of continuous time algebraic Riccati equation (CARE) ([Boyd and Barratt, 1991](#)):

$$\Omega - \Omega(S + U)\Omega + M = 0$$

Unfortunately, this problem does not have a closed form solution and solving it numerically in every step of the cgSSL is computationally prohibitive.

We instead solve the CGLASSO problem using a suitably modified version of [Hsieh et al. \(2011\)](#)’s QUIC algorithm for solving the GLASSO problem. At a high level, instead of using the first order gradient or solving dual problem, the algorithm is based on Newton’s method and uses a quadratic approximation. Basically, we sequentially cycle over the parameters $\omega_{k,k'}$ and update each parameter by following a Newton direction for suitable step-size. The step-size is chosen to ensure that our running estimate of Ω remains positive definite while

also ensuring sufficient decrease in the overall objective. We call our solution CGQUIC, which we summarize in Algorithm 1.

To describe CGQUIC, we first define the “smooth” part of the CGLASSO objective as $g(\Omega)$ and the objective function as $f(\Omega)$:

$$\begin{aligned} g(\Omega) &= -\log(|\Omega|) + \text{tr}(S\Omega) + \text{tr}(M\Omega^{-1}), \\ f(\Omega) &= g(\Omega) + \sum_{k,k'} \lambda_{k,k'} \omega_{k,k'}. \end{aligned} \tag{S13}$$

The function $g(\Omega)$ is twice differentiable and strictly convex. To see this, observe that $g(\Omega)$ is just the log-likelihood of a Gaussian chain graph model with known Ψ . Its Hessian is just the negative Fisher information of Ω and is positive definite. The second-order Taylor expansion of the smooth part $g(\Omega)$ based on Ω and evaluated at $\Omega + \Delta$ for a symmetric Δ is

$$\begin{aligned} \bar{g}(\Delta) &= -\log(|\Omega|) + \text{tr}(S\Omega) + \text{tr}(MW) \\ &\quad + \text{tr}(S\Delta) - \text{tr}(W\Delta) - \text{tr}(WMW\Delta) \\ &\quad + \frac{1}{2} \text{tr}(W\Delta W\Delta) + \text{tr}(WMW\Delta W\Delta) \end{aligned} \tag{S14}$$

S2.1 Newton Direction

We now consider the coordinate descent update for the variable $\Omega_{k,k'}$ for $k \leq k'$. Let D denote the current approximation of the Newton direction and let D' be the updated direction. To preserve symmetry, we set $D' = D + \mu(e_k e_{k'}^\top + e_{k'} e_k^\top)$. Our goal, then, is to find the optimal μ :

$$\arg \min_{\mu} \{ \bar{g}(D + \mu(e_k e_{k'}^\top + e_{k'} e_k^\top)) + 2\xi_{k,k'} |\Omega_{k,k'} + D_{k,k'} + \mu| \} \tag{S15}$$

We begin by substituting $\Delta = D'$ into $\bar{g}(\Delta)$. Note that terms not depending on μ do not affect the line search. Compared to QUIC, we have two additional terms, $\text{tr}(WMW\Delta)$ and $\text{tr}(WMW\Delta W\Delta)$. The first term turns out to be linear μ and the second is quadratic in μ .

Algorithm 1: The CGQUIC algorithm for CGLASSO problem

Data: $S = Y^\top Y/n$, $M = (X\Psi)^\top (X\Psi)/n$, regularization parameter matrix Ξ , initial Ω_0 , inner stopping tolerance ϵ , parameters $0 < \sigma < 0.5$, $0 < \beta < 1$

Result: path of positive definite Ω_t that converge to $\arg \min_{\Omega} f$ with
 $f(\Omega) = g(\Omega) + \sum_{k,k'} \xi_{k,k'} |\omega_{k,k'}|$, where $g(\Omega) = -\log(|\Omega|) + \text{tr}(S\Omega) + \text{tr}(M\Omega^{-1})$

Initialize $W_0 = \Omega_0^{-1}$;

for $t = 1, 2, \dots$ **do**

$D = 0, U = 0$;

$Q = MW_{t-1}$;

while not converged do

 Partition the variables into fixed and free sets based on gradient¹

$S_{\text{fixed}} := \{(k, k') : |\nabla_{k,k'} g(\Omega)| < \xi_{k,k'} \text{ and } \omega_{k,k'} = 0\}$;

$S_{\text{free}} := \{(k, k') : |\nabla_{k,k'} g(\Omega)| \geq \xi_{k,k'} \text{ or } \omega_{k,k'} \neq 0\}$;

for $(k, k') \in S_{\text{free}}$ **do**

 Calculate Newton direction:

$b = S_{k,k'} - W_{k,k'} + w_k^\top D w_{k'} - w_k^\top M w_{k'} + w_{k'}^\top D W M w_k + w_k^\top D W M w_{k'}$;

$c = \Omega_{k,k'} + D_{k,k'}$;

if $i \neq j$ **then**

$a = W_{k,k'}^2 + W_{k,k} W_{k',k'} + W_{k,k} w_{k'}^\top M w_{k'} + W_{k',k'} w_k^\top M w_k + 2W_{k,k} w_k^\top M w_{k'}$;

end

else

$a = W_{k,k}^2 + 2W_{k,k} w_k^\top M w_k$;

end

$\mu = -c + [|c - b/a| - \xi_{k,k'}/a]_+ \text{sign}(c - b/a)$;

$D_{k,k'} += \mu$;

$\mathbf{u}_k += \mu \mathbf{w}_{k'}$;

$\mathbf{u}_{k'} += \mu \mathbf{w}_k$;

end

end

for $\alpha = 1, \beta, \beta^2, \dots$ **do**

 Compute the Cholesky decomposition of $\Omega_{t-1} + \alpha D$;

if Ω_t is not positive definite **then**

 continue;

end

 Compute $f(\Omega_{t-1} + \alpha D)$;

if

$f(\Omega_{t-1} + \alpha D^*) \leq f(\Omega_{t-1}) + \alpha \sigma \delta, \delta = \text{tr}[\nabla g(\Omega_{t-1})^\top D^*] + \|\Omega_{t-1} + D^*\|_{1,\Xi} - \|\Omega_{t-1}\|_{1,\Xi}$

then

 break;

end

end

$\Omega_t = \Omega_{t-1} + \alpha D$;

$W_t = \Omega_t^{-1}$ using Cholesky decomposition result;

end

return $\{\Omega_t\}$;

To see this, first observe

$$\begin{aligned}
-\text{tr}(WMW\Delta) &= -\text{tr}(WMW(D + \mu(e_k e_{k'}^\top + e_{k'} e_k^\top))) \\
&= C - \mu \text{tr}(WMW e_k e_{k'}^\top + WMW e_{k'} e_k^\top) \\
&= C - \mu \text{tr}(e_{k'}^\top WMW e_k + e_k^\top WMW e_{k'}) \\
&= C - 2\mu e_k^\top WMW e_{k'} \\
&= C - 2\mu w_k^\top M w_{k'}
\end{aligned} \tag{S16}$$

where w_k is the k^{th} column of Ω .

Furthermore, we have

$$\begin{aligned}
\text{tr}(WMW\Delta W\Delta) &= \text{tr}[WMW(D + \mu(e_k e_{k'}^\top + e_{k'} e_k^\top))W(D + \mu(e_k e_{k'}^\top + e_{k'} e_k^\top))] \\
&= \text{tr}[DWMW + 2\mu DWMW(e_k e_{k'}^\top + e_{k'} e_k^\top)W] \\
&\quad + \text{tr}[\mu^2(e_k e_{k'}^\top + e_{k'} e_k^\top)WMW(e_k e_{k'}^\top + e_{k'} e_k^\top)W] \\
&= C + \text{tr}[2\mu DWMW(e_k e_{k'}^\top + e_{k'} e_k^\top)W] \\
&\quad + \text{tr}[\mu^2(e_k e_{k'}^\top + e_{k'} e_k^\top)WMW(e_k e_{k'}^\top + e_{k'} e_k^\top)W] \\
&= C + 2\mu w_{k'}^\top DWM w_k + 2\mu w_k^\top DWM w_{k'} \\
&\quad + \mu^2 \text{tr}[(e_k e_{k'}^\top + e_{k'} e_k^\top)WMW(e_k e_{k'}^\top + e_{k'} e_k^\top)W] \\
&= C + 2\mu(w_{k'}^\top DWM w_k + w_k^\top DWM w_{k'}) \\
&\quad + \mu^2(W_{k,k} w_{k'}^\top M w_{k'} + W_{k',k'} w_k^\top M w_k + 2W_{k,k'} w_k^\top M w_{k'})
\end{aligned} \tag{S17}$$

By combining the above simplifications, we can minimize the objective with coordinate descent. The update for $\omega_{k,k'}$ is given by:

$$\begin{aligned}
&\frac{1}{2}[W_{k,k'}^2 + W_{k,k} W_{k',k'} + W_{k,k} w_{k'}^\top M w_{k'} + W_{k',k'} w_k^\top M w_k + 2W_{k,k'} w_k^\top M w_{k'}] \mu^2 \\
&+ [S_{k,k'} - W_{k,k'} + w_k D w_{k'} - w_{k'} M w_{k'} + w_{k'}^\top DWM w_k + w_k^\top DWM w_{k'}] \mu \\
&+ \xi_{k,k'} |\Omega_{k,k'} + D_{k,k'} + \mu|
\end{aligned} \tag{S18}$$

The optimal solution (for off-diagonal $\omega_{k,k'}$) is given by

$$\mu = -c + [|c - b/a| - \xi_{k,k'}/a]_+ \text{sign}(c - b/a) \quad (\text{S19})$$

where

$$\begin{aligned} a &= W_{k,k'}^2 + W_{k,k}W_{k',k'} + W_{k,k}w_{k'}^\top Mw_{k'} + W_{k',k}w_k^\top Mw_k + 2W_{k,k'}w_k^\top Mw_{k'} \\ b &= S_{k,k'} - W_{k,k'} + w_k^\top Dw_{k'} - w_k^\top Mw_{k'} + w_{k'}^\top DW Mw_k + w_{k'}^\top DW Mw_{k'} \\ c &= \omega_{k,k'} + D_{k,k'} \end{aligned}$$

For diagonal entries, we take $D' = D + \mu e_k e_k^\top$, the two terms involving D are then:

$$\begin{aligned} -\text{tr}(WMW\Delta) &= C - \mu w_k^\top Mw_k \\ \text{tr}(WMW\Delta W\Delta) &= C + 2\mu w_k^\top DW Mw_k + \mu^2 W_{k,k}w_k^\top Mw_k \end{aligned} \quad (\text{S20})$$

Then we can take

$$\begin{aligned} a &= W_{k,k}^2 + 2W_{k,k}w_k^\top Mw_k \\ b &= S_{k,k} - W_{k,k} + w_k^\top Dw_k - w_k^\top Mw_k + 2w_k^\top DW Mw_k \\ c &= \omega_{k,k} + D_{k,k} \end{aligned}$$

and use Equation (S19) to obtain the optimal μ and thus the updated Newton direction D' .

Note that computing the optimal μ requires repeated calculation of quantities like $w_k^\top Mw_{k'}$ and $w_k^\top U Mw_{k'}$. To enable rapid computation, we track and update the values of $U = DW$ and $Q = MW$ during our optimization.

S2.2 Step Size

Like [Hsieh et al. \(2011\)](#), we use Armijo's rule to set a step size α that simultaneously ensures our estimate of Ω remains positive definite and sufficient decrease of our overall objective function. We denote the Newton direction after a complete update over all active coordinates

as D^* (see Appendix S2.3 for active sets). We require our step size to satisfy the line search condition (S21).

$$f(\Omega + \alpha D^*) \leq f(\Omega) + \alpha \sigma \delta, \delta = \text{tr}[\nabla g(\Omega)^\top D^*] + \|\Omega + D^*\|_{1,\Xi} - \|\Omega\|_{1,\Xi} \quad (\text{S21})$$

Three important properties can be established following Hsieh et al. (2011):

- P1. The condition was satisfied for small enough α . This property is satisfied exactly following proposition 1 of Hsieh et al. (2011).
- P2. We have $\delta < 0$ for all $\Omega \succ 0$, which ensures that the objective function decreases. This property generally follow Lemma 2 and Proposition 2 of Hsieh et al. (2011), which requires the Hessian of the smooth part $g(\Omega)$ to be positive definite. In our case the Hessian of $g(\Omega)$ is the Fisher information of the chain graph model, ensuring its positive definiteness.
- P3. When Ω is close to the global optimum, the step size $\alpha = 1$ will satisfy the line search condition. To establish this, we follow the proof of Proposition 3 in Hsieh et al. (2011).

S2.3 Thresholding to Decide the Active Sets

Similar to the QUIC procedure, our algorithm does not need to update every $\omega_{k,k'}$ in each iteration. We instead follow Hsieh et al. (2011) and only update those parameters exceeding a certain threshold. More specifically, we can partition the parameters $\omega_{k,k'}$ into a fixed set S_{fixed} , containing those parameters falling below the threshold, and a free set S_{free} , containing those parameters exceeding the threshold. That is

$$\begin{aligned} \omega_{k,k'} &\in S_{\text{fixed}} \text{ if } |\nabla_{k,k'} g(\Omega)| \leq \xi_{k,k'} \text{ and } \omega_{k,k'} = 0 \\ \omega_{k,k'} &\in S_{\text{free}} \text{ otherwise} \end{aligned} \quad (\text{S22})$$

We can determine the free set S_{free} using the minimum-norm sub-gradient $\text{grad}_{k,k'}^S f(\Omega)$, which is defined in Definition 2 of Hsieh et al. (2011). In our case $\nabla g(\Omega) = S - \Omega^{-1} - \Omega^{-1} M \Omega^{-1}$, so the minimum-norm sub-gradient is

$$\text{grad}_{k,k'}^S f(\Omega) = \begin{cases} (S - \Omega^{-1} - \Omega^{-1}M\Omega^{-1})_{k,k'} + \xi_{k,k'} & \text{if } \omega_{k,k'} > 0 \\ (S - \Omega^{-1} - \Omega^{-1}M\Omega^{-1})_{k,k'} - \xi_{k,k'} & \text{if } \omega_{k,k'} < 0 \\ \text{sign}((S - \Omega^{-1} - \Omega^{-1}M\Omega^{-1})_{k,k'})[|(S - \Omega^{-1} - \Omega^{-1}M\Omega^{-1})_{k,k'}| - \xi_{k,k'}]_+ & \text{if } \omega_{k,k'} = 0 \end{cases} \quad (\text{S23})$$

Note that the subgradient evaluated on the fixed set is always equal to 0. Thus, following Lemma 4 in [Hsieh et al. \(2011\)](#), the elements of the fixed set do not change during our coordinate descent procedure. It suffices, then, to only compute the Newton direction on the free set and update those parameters.

S2.4 Unique minimizer

In this subsection, we show that the CGLASSO problem admits a unique minimizer. Our proof largely follows the proofs of Lemma 3 and Theorem 1 of [Hsieh et al. \(2011\)](#) but makes suitable modifications to account for the extra $\text{tr}(M\Omega^{-1})$ term in the CGLASSO objective.

Theorem S1 (Unique minimizer). *There is a unique global minimum for the CGLASSO problem (S12).*

We first show the entire sequence of iterates $\{\Omega_t\}$ lies in a particular, compact level set. To this end, let

$$U = \{\Omega | f(\Omega) \leq f(\Omega_0), \Omega \in S_{++}^p\}. \quad (\text{S24})$$

To see that all iterations lies in U , we check need to check the line search condition Equation (S21) has a $\delta < 0$. By directly applying [Hsieh et al. \(2011\)](#)'s Lemma 2 to $g(\Omega)$, we have that

$$\delta \leq -\text{vec}(D^*)^\top \nabla^2 g(\Omega) \text{vec}(D^*)$$

where D^* is the Newton direction. Since $g(\Omega)$ (Equation (S13)) is convex, $\nabla^2 g(\Omega)$ is positive definite, so the function value $f(\Omega_t)$ is always decreasing.

Now we need to check that the level set is actually contained in a compact set, by suitably adapt Lemma 3 of [Hsieh et al. \(2011\)](#).

Lemma S1. *The level set U defined in (S24) is contained in the set $\{mI \leq \Omega \leq NI\}$ for some constants $m, N > 0$, if we assume that the off-diagonal elements of Ξ and the diagonal elements of S are positive.*

Proof. We begin by showing that the largest eigenvalue of Ω is bounded by some constant that does not depend on Ω . Recall that S and M are positive semi-definite. Since Ω is positive definite, we have $\text{tr}(S\Omega) + \text{tr}(M\Omega^{-1}) > 0$ and $\|\Omega\|_{1,\Xi} + \text{tr}(M\Omega^{-1}) > 0$.

Therefore we have

$$\begin{aligned} f(\Omega_0) &> f(\Omega) \geq -\log(|\Omega|) + \|\Omega\|_{1,\Xi} \\ f(\Omega_0) &> f(\Omega) \geq -\log(|\Omega|) + \text{tr}(S\Omega) \end{aligned} \quad (\text{S25})$$

Since $\|\Omega\|_2$ is the largest eigenvalue of Ω , we have $\log(|\Omega|) \leq q \log(\|\Omega\|_2)$.

Using the assumption that off-diagonal entries of Ξ is larger than some positive number ξ , we know that

$$\xi \sum_{i \neq j} |\Omega_{k,k'}| \leq \|\Omega\|_{1,\Xi} \leq f(\Omega_0) + q \log(\|\Omega\|_2) \quad (\text{S26})$$

Similarly, we have

$$\text{tr}(S\Omega) \leq f(\Omega_0) + q \log(\|\Omega\|_2) \quad (\text{S27})$$

Let $\alpha = \min_k (S_{k,k})$ and $\beta = \max_{k \neq k'} S_{k,k'}$. We can split the $\text{tr}(S\Omega)$ into two parts, which can be further lower bounded:

$$\text{tr}(S\Omega) = \sum_k S_{k,k} \Omega_{k,k} + \sum_{k \neq k'} S_{k,k'} \Omega_{k,k'} \geq \alpha \text{tr}(\Omega) - \beta \sum_{k \neq k'} |\Omega_{k,k'}| \quad (\text{S28})$$

Since $\|\Omega\|_2 \leq \text{tr}(\Omega)$, by using Equation (S28), we have,

$$\alpha \|\Omega\|_2 \leq \alpha \text{tr}(\Omega) \leq \text{tr}(\Omega S) + \beta \sum_{k \neq k'} |\Omega_{k,k'}| \quad (\text{S29})$$

By combining Equations (S26), (S27), and (S29), we conclude that

$$\alpha \|\Omega\|_2 \leq (1 + \beta/\xi)(f(\Omega_0) + q \log(\|\Omega\|_2)) \quad (\text{S30})$$

The left hand side as a function of $\|\Omega\|_2$ grows much faster than the right hand side. Thus $\|\Omega\|_2$ can be bounded by a quantity depending only on the value of $f(\Omega_0)$, α , β and ξ .

We now consider the smallest eigenvalue denoted by a . We use the upper bound of other eigenvalues to bound the determinant. By using the fact that $f(\Omega)$ always decreases during iterations, we have

$$f(\Omega_0) > f(\Omega) > -\log(|\Omega|) \geq -\log(a) - (q-1)\log(N) \quad (\text{S31})$$

Thus we have $m = e^{-f(\Omega_0)M^{-q+1}}$ is a lower bound for smallest eigenvalue a . \square

We are now ready to prove Theorem S1, by showing the objective function is strongly convex on a compact set.

Proof. Because of Lemma S1, the level set U contains all iterates produced by cgQUIC. The set U is further contained in the compact set $\{mI \leq \Omega \leq NI\}$. By the Weierstrass extreme value theorem the continuous function $f(\Omega)$ (S13) attains its minimum on this set.

Further, the modified objective function is also strongly convex in its smooth part. This is because $\text{tr}(M\Omega^{-1})$ and $\text{tr}(S\Omega)$ are convex and $-\log(|\Omega|)$ is strongly convex. Since $\text{tr}(M\Omega^{-1})$ is convex, the Hessian of the smooth part has the same lower bound as in Theorem 1 of Hsieh et al. (2011). By following the argument of in the proof of Theorem 1 of Hsieh et al. (2011), we can show the objective function $f(\Omega)$ is strongly convex on the compact set $\{mI \leq \Omega \leq NI\}$, and thus has a unique minimizer. \square

We can further show that the cgQUIC procedure converges to the unique minimizer, using the general results on quadratic approximation methods studied in Hsieh et al. (2011).

Theorem S2 (Convergence). *The cgQUIC converge to global optimum.*

Proof. cgQUIC is an example of quadratic approximation method investigated in Section 4.1 of Hsieh et al. (2011) with a strongly convex smooth part $g(\Omega)$ in (S13). Convergence to

the global optimum follows from their Theorem 2. \square

S3 Synthetic experiment results

We now present the remaining results from our simulation experiments. These results are qualitatively similar to those from the $(n, p, q) = (100, 10, 10)$ setting presented in the main text. Generally speaking, in terms of support recovery, the methods that deployed a single fixed penalty (cgLASSO and CAR) displayed higher sensitivity but lower precision than both cgSSL-DPE and cgSSL-DCPE. The only exception was when Ω was dense. Furthermore, methods with adaptive penalties (both cgSSL procedures and CAR-A) tended to return a fewer number of non-zero estimates than the fixed penalty. Most of these non-zero estimates were in fact true positives. Across all settings of (n, p, q) , cgSSL-DPE makes virtually no false positive identifications in the support of Ψ . In terms of parameter estimation, the fixed penalty methods tended to have larger Frobenius error in estimating both Ψ and Ω than the cgSSL. Note that cgLASSO uses ten-fold cross-validation to set the two penalty levels. Even with a parallel implementation and warm-starts, the full cgLASSO procedure did not converge after 72 hours in the $n = 400$ setting.

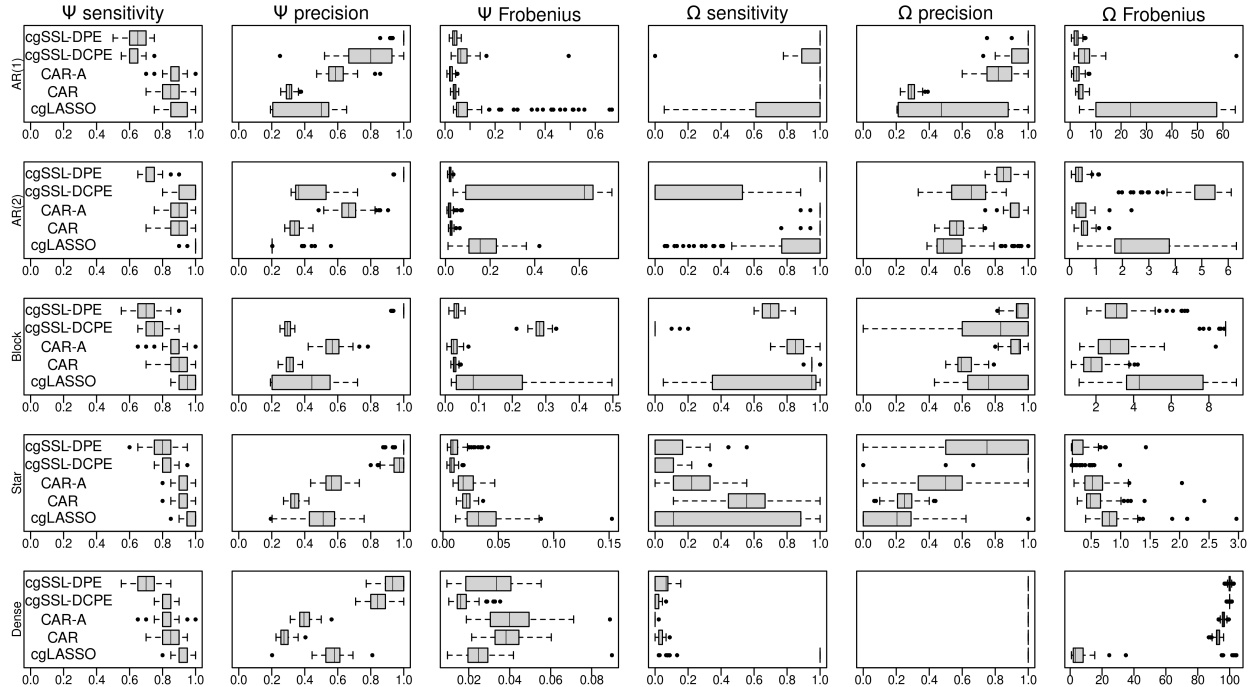


Figure S4: Sensitivity, specificity and Frobenius loss of parameter estimations when $p = 10, q = 10, n = 100$

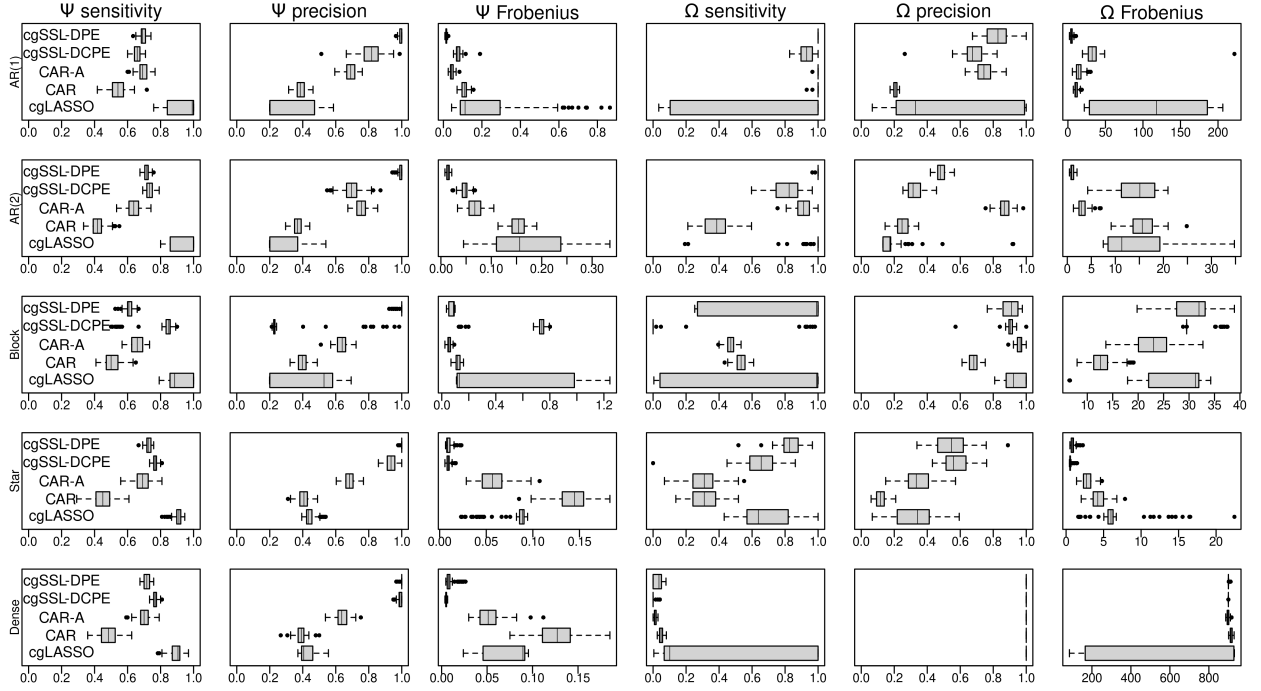


Figure S5: Sensitivity, specificity and Frobenius loss of parameter estimations when $p = 20, q = 30, n = 100$

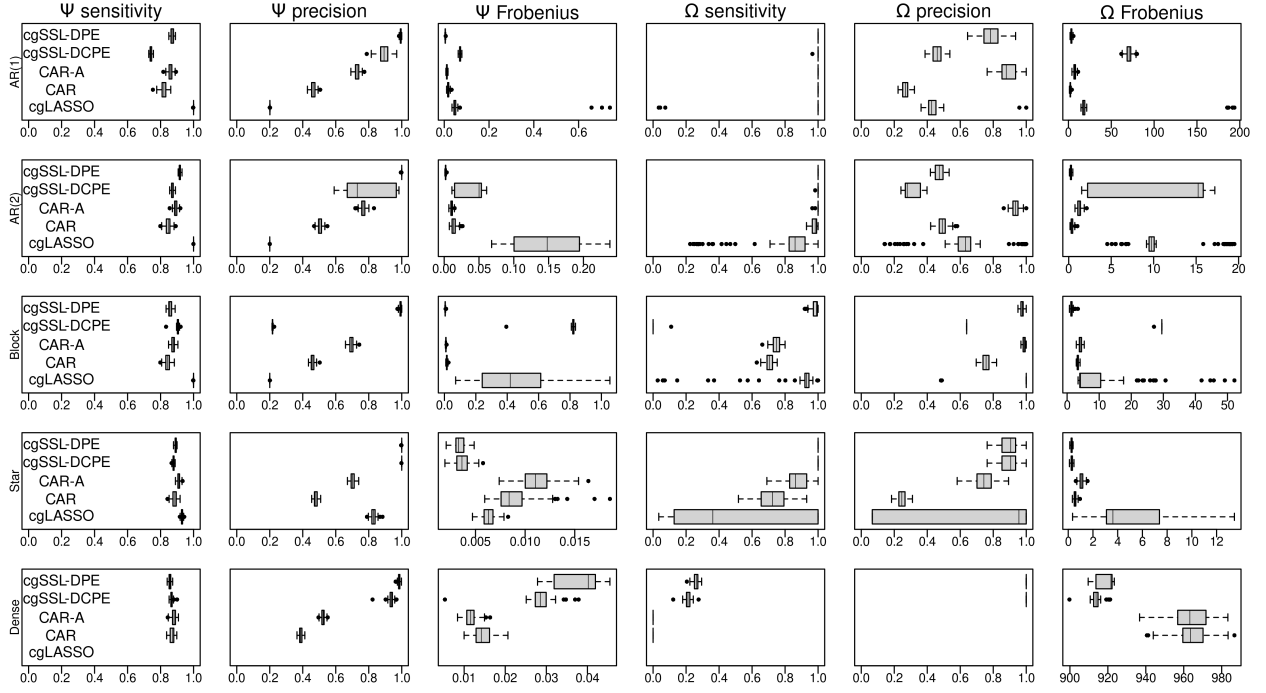


Figure S6: Sensitivity, specificity and Frobenius loss of parameter estimations when $p = 10, q = 30, n = 400$, cgLASSO was not able to finish with dense Ω within 72 hours thus we omit the result.

Table S2: Sensitivity, precision, and Frobenius error for Ψ and Ω when $(n, p, q) = (100, 20, 30)$ for each specification of Ω . For each choice of Ω , the best performance is bold-faced.

Method	SEN	Ψ recovery PREC	FROB	SEN	Ω recovery PREC	FROB
<i>AR</i> (1) model						
cgLASSO	0.94 (0.09)	0.3 (0.14)	0.21 (0.21)	0.74 (0.42)	0.48 (0.36)	111.66 (66.15)
CAR	0.54 (0.05)	0.39 (0.03)	0.11 (0.02)	1 (0.01)	0.21 (0.01)	11.15 (2.35)
CAR-A	0.69 (0.03)	0.69 (0.04)	0.04 (0.01)	1 (0)	0.74 (0.06)	15.07 (4.99)
cgSSL-dcpe	0.66 (0.02)	0.82 (0.07)	0.08 (0.02)	0.94 (0.04)	0.68 (0.07)	34.1 (19.97)
cgSSL-dpe	0.69 (0.02)	1 (0.01)	0.02 (0)	1 (0)	0.82 (0.07)	4.87 (1.73)
<i>AR</i> (2) model						
cgLASSO	0.94 (0.07)	0.3 (0.13)	0.17 (0.08)	0.98 (0.12)	0.18 (0.12)	14.44 (6.93)
CAR	0.42 (0.04)	0.37 (0.03)	0.15 (0.02)	0.38 (0.08)	0.25 (0.04)	15.8 (2.68)
CAR-A	0.64 (0.04)	0.76 (0.04)	0.07 (0.02)	0.91 (0.05)	0.87 (0.04)	3.16 (1.15)
cgSSL-dcpe	0.73 (0.02)	0.7 (0.06)	0.05 (0.01)	0.81 (0.09)	0.32 (0.05)	14.5 (4.21)
cgSSL-dpe	0.72 (0.02)	0.99 (0.01)	0.01 (0)	1 (0)	0.48 (0.03)	1.04 (0.35)
Block model						
cgLASSO	0.92 (0.07)	0.4 (0.19)	0.51 (0.46)	0.62 (0.46)	0.93 (0.06)	27.48 (6.01)
CAR	0.51 (0.05)	0.4 (0.03)	0.12 (0.02)	0.53 (0.04)	0.68 (0.03)	12.96 (2.49)
CAR-A	0.66 (0.04)	0.64 (0.04)	0.06 (0.01)	0.47 (0.03)	0.96 (0.02)	23.14 (4.16)
cgSSL-dcpe	0.82 (0.1)	0.29 (0.19)	0.68 (0.19)	0.1 (0.28)	0.88 (0.1)	30.22 (2.11)
cgSSL-dpe	0.61 (0.02)	0.99 (0.02)	0.07 (0.02)	0.66 (0.36)	0.9 (0.05)	30.39 (4.02)
Star model						
cgLASSO	0.91 (0.03)	0.45 (0.04)	0.08 (0.02)	0.7 (0.18)	0.31 (0.14)	6.45 (3.27)
CAR	0.45 (0.06)	0.41 (0.04)	0.14 (0.02)	0.32 (0.09)	0.12 (0.03)	4.36 (1.07)
CAR-A	0.69 (0.05)	0.68 (0.03)	0.06 (0.02)	0.31 (0.09)	0.35 (0.09)	2.83 (0.69)
cgSSL-dcpe	0.77 (0.02)	0.94 (0.03)	0.01 (0)	0.61 (0.21)	0.57 (0.08)	0.6 (0.21)
cgSSL-dpe	0.73 (0.02)	1 (0)	0.01 (0)	0.83 (0.08)	0.54 (0.1)	0.89 (0.32)
Dense model						
cgLASSO	0.89 (0.04)	0.43 (0.05)	0.07 (0.03)	0.34 (0.41)	1 (0)	712.46 (354.87)
CAR	0.49 (0.06)	0.39 (0.03)	0.13 (0.02)	0.05 (0.01)	1 (0)	914.47 (6.45)
CAR-A	0.7 (0.04)	0.64 (0.04)	0.05 (0.01)	0.01 (0.01)	1 (0)	897.91 (5.95)
cgSSL-dcpe	0.77 (0.01)	0.99 (0.01)	0.01 (0)	0 (0.01)	1 (0)	900 (0.01)
cgSSL-dpe	0.72 (0.02)	1 (0.01)	0.01 (0.01)	0.03 (0.03)	1 (0)	901.45 (2.97)

Table S3: Sensitivity, precision, and Frobenius error for Ψ and Ω when $(n, p, q) = (400, 100, 30)$ for each specification of Ω . For each choice of Ω , the best performance is bold-faced. The cgLASSO method was not able to finish within 72 hours.

Method	Ψ recovery			Ω recovery		
	SEN	PREC	FROB	SEN	PREC	FROB
<i>AR(1) model</i>						
cgLASSO	1 (0)	0.2 (0)	0.07 (0.11)	0.94 (0.23)	0.46 (0.14)	27.98 (40.98)
CAR	0.82 (0.02)	0.46 (0.01)	0.02 (0)	1 (0)	0.27 (0.02)	2.23 (0.51)
CAR-A	0.86 (0.01)	0.73 (0.02)	0.01 (0)	1 (0)	0.89 (0.05)	7.32 (1.48)
cgSSL-dcpe	0.74 (0.01)	0.89 (0.03)	0.07 (0)	1 (0)	0.46 (0.03)	70.84 (3.72)
cgSSL-dpe	0.87 (0.01)	0.99 (0)	0 (0)	1 (0)	0.78 (0.06)	3.42 (0.8)
<i>AR(2) model</i>						
cgLASSO	1 (0)	0.2 (0)	0.15 (0.05)	0.79 (0.23)	0.63 (0.22)	10.82 (4.04)
CAR	0.85 (0.02)	0.5 (0.01)	0.01 (0)	0.98 (0.02)	0.49 (0.03)	0.38 (0.15)
CAR-A	0.89 (0.01)	0.77 (0.02)	0.01 (0)	1 (0.01)	0.94 (0.03)	1.22 (0.24)
cgSSL-dcpe	0.87 (0.01)	0.79 (0.14)	0.04 (0.02)	1 (0)	0.31 (0.05)	10.5 (6.66)
cgSSL-dpe	0.92 (0)	1 (0)	0 (0)	1 (0)	0.47 (0.03)	0.26 (0.08)
<i>Block model</i>						
cgLASSO	1 (0)	0.2 (0)	0.44 (0.25)	0.87 (0.21)	0.97 (0.11)	10.05 (11.21)
CAR	0.84 (0.02)	0.46 (0.01)	0.02 (0)	0.71 (0.03)	0.76 (0.02)	3.36 (0.24)
CAR-A	0.88 (0.01)	0.7 (0.02)	0.01 (0)	0.75 (0.02)	0.99 (0.01)	4.13 (0.5)
cgSSL-dcpe	0.9 (0.01)	0.22 (0)	0.82 (0.04)	0 (0.01)	0.64 (NA)	29.51 (0.24)
cgSSL-dpe	0.86 (0.01)	0.99 (0.01)	0.01 (0)	0.98 (0.02)	0.98 (0.01)	1.44 (0.43)
<i>Star model</i>						
cgLASSO	0.93 (0)	0.83 (0.02)	0.01 (0)	0.53 (0.41)	0.59 (0.45)	4.68 (3.43)
CAR	0.89 (0.01)	0.48 (0.01)	0.01 (0)	0.73 (0.09)	0.25 (0.03)	0.55 (0.1)
CAR-A	0.91 (0.01)	0.7 (0.02)	0.01 (0)	0.87 (0.07)	0.74 (0.06)	1.07 (0.18)
cgSSL-dcpe	0.88 (0)	1 (0)	0 (0)	1 (0)	0.89 (0.05)	0.29 (0.08)
cgSSL-dpe	0.89 (0)	1 (0)	0 (0)	1 (0)	0.9 (0.05)	0.27 (0.06)
<i>Dense model</i>						
cgLASSO						
CAR	0.87 (0.02)	0.39 (0.01)	0.01 (0)	0 (0)	NaN (NA)	964.24 (9.25)
CAR-A	0.88 (0.01)	0.52 (0.01)	0.01 (0)	0 (0)	NaN (NA)	964.08 (9.71)
cgSSL-dcpe	0.87 (0.01)	0.94 (0.02)	0.03 (0)	0.21 (0.02)	1 (0)	913.81 (2.33)
cgSSL-dpe	0.86 (0.01)	0.98 (0.01)	0.04 (0.01)	0.26 (0.01)	1 (0)	918.35 (4.57)

S4 Preprocessing for real data experiment

To conduct our reanalysis of [Claesson et al. \(2012\)](#)’s gut microbiome data, we preprocesses the raw 16s-rRNAseq data following the workflow provided by the MG-RAST server ([Keegan et al., 2016](#)). We first “annotated” the sequences to get genus counts (i.e. number of segments belongs to one genus). The annotation process compares the rRNA segments detected during sequencing to the reference sequence of each genus of microbes, then counts the number of rRNA segments match with each genus. We used the MG-RAST server’s default tuning

parameters during the annotation process. That is, we set e-value to be 5 and annotated with 60% identity, alignment length of 15 bp, and set a minimal abundance of 10 reads.

Following standard practices of analyzing microbiome data, we transformed raw counts into relative abundance. We selected genera with more than 0.5% relative abundance in more than 50 samples as the focal genus and all other genera aggregated as the reference group. We further took the log-odds (with respect to the reference group described above) to stabilize the variances (Aitchison, 1982) in order to fit our normal model.

S5 Proofs of posterior contraction for cgSSL

This section provides detail on the posterior contraction results for the cgSSL. Our proof was inspired by Ning et al. (2020) and Bai et al. (2020). We first show the contraction in log-affinity by verifying KL condition and test conditions following Ghosal and van der Vaart (2017). Then we use the results in log-affinity to show recovery of parameters.

To establish our results, we work with a slightly modified prior on Ω that has density

$$f_{\Omega}(\Omega) \propto \prod_{k > k'} \left[\frac{(1-\eta)\xi_0}{2} \exp(-\xi_0|\omega_{k,k'}|) + \frac{\eta\xi_1}{2} \exp(\xi_1|\omega_{k,k'}|) \right] \times \prod_k \xi \exp[-\xi\omega_{k,k}] \times \mathbb{1}(\Omega \succ \tau I) \quad (\text{S32})$$

$$f_{\Psi}(\Psi) = \prod_{jk} \left[\frac{(1-\theta)\lambda_0}{2} \exp(-\lambda_0|\psi_{j,k}|) + \frac{\theta\lambda_1}{2} \exp(\lambda_1|\psi_{j,k}|) \right] \quad (\text{S33})$$

where $0 < \tau < 1/b_2$. This way τ is less than the lower bound of the smallest eigenvalue of the true precision matrix Ω_0 .

S5.1 The Kullback-Leibler condition

We need to verify that our prior places enough probability in small neighborhoods around each of the possible values of the true parameters. These neighborhoods are defined in a KL sense.

Lemma S2 (KL conditions). *Let $\epsilon_n = \sqrt{\max\{p, q, s_0^\Omega, s_0^\Psi\} \log(\max\{p, q\})/n}$. Then for all*

true parameters (Ψ_0, Ω_0) we have

$$-\log \Pi [(\Psi, \Omega) : K(f_0, f) \leq n\epsilon_n^2, V(f_0, f) \leq n\epsilon_n^2] \leq C_1 n\epsilon_n^2$$

Further, let E_n be the event

$$E_n = \{Y : \iint f/f_0 d\Pi(\Psi)\Pi d(\Omega) \geq e^{-C_1 n\epsilon_n^2}\}.$$

Then for all (Ψ_0, Ω_0) , we have $\mathbb{P}_0(E_n^c) \rightarrow 0$ as $n \rightarrow \infty$.

The last assertion that $\mathbb{P}(E_n^c) \rightarrow 0$ follows from Lemma 8.1 of [Ghosal and van der Vaart \(2017\)](#) so we now focus on establishing the first assertion of the Lemma. To verify this condition we need to bound the prior mass of certain events A . However, the truncation of the prior on Ω makes computing these masses intractable. To overcome this, we first bound the prior probability of events of the form $A \cap \{\Omega \succ \tau I\}$ by observing the prior on Ω can be viewed as a particular conditional distribution.

Specifically, let $\tilde{\Pi}$ be the untruncated spike-and-slab LASSO prior with density

$$\tilde{f}(\Omega) = \prod_{k > k'} \left[\frac{(1-\eta)\xi_0}{2} \exp(-\xi_0|\omega_{k,k'}|) + \frac{\eta\xi_1}{2} \exp(\xi_1|\omega_{k,k'}|) \right] \times \prod_k \xi \exp(-\xi\omega_{k,k}).$$

The following Lemma shows that we can bound Π probabilities using $\tilde{\Pi}$ probabilities.

Lemma S3 (Bounds of the graphical prior). *Let $\tilde{\Pi}$ be the untruncated version of the prior on Ω . Then for all events A , for large enough n there is a number R that does not depend on n such that*

$$\tilde{\Pi}(\Omega \succ \tau I | A) \tilde{\Pi}(A) \leq \Pi_\Omega(A \cap \{\Omega \succ \tau I\}) \leq \exp(2\xi Q - \log(R)) \tilde{\Pi}(A) \quad (\text{S34})$$

where $Q = q(q-1)/2$ is the total number of free off-diagonal entries in Ω .

Proof. Consider an event of form $A \cap \{\Omega \succ \tau I\} \subset \mathbb{R}^{q \times q}$. The prior mass $\Pi_\Omega(A \cap \{\Omega \succ \tau I\})$ can be viewed as a conditional probability:

$$\Pi_\Omega(A \cap \{\Omega \succ \tau I\}) = \tilde{\Pi}(A | \Omega \succ \tau I) = \frac{\tilde{\Pi}(\Omega \succ \tau I | A) \tilde{\Pi}(A)}{\tilde{\Pi}(\Omega \succ \tau I)} \quad (\text{S35})$$

The lower bound follows because the denominator is bounded from above by 1.

For the upper bound, we first observe that

$$\Pi_{\Omega}(A \cap \{\Omega \succ \tau I\}) = \tilde{\Pi}(A|\Omega \succ \tau I) = \frac{\tilde{\Pi}(\Omega \succ \tau I|A)\tilde{\Pi}(A)}{\tilde{\Pi}(\Omega \succ \tau I)} \leq (\tilde{\Pi}(\Omega \succ \tau I))^{-1}\tilde{\Pi}(A) \quad (\text{S36})$$

To upper bound the probability in Equation (S35), we find a lower bound of the denominator $\tilde{\Pi}(\Omega \succ \tau I)$. To this end, let

$$\mathcal{G} = \left\{ \Omega : \omega_{k,k} > q - 1, |\omega_{k,k'}| \leq 1 - \frac{\tau}{q-1} \text{ for } k' \neq k \right\}$$

and consider an $\Omega \in \mathcal{G}$. Since all of Ω 's eigenvalues are real, they must each be contained in at least one Gershgorin disc. Consider the k^{th} Gershgorin disc, whose intersection with the real line is an interval centered at $\omega_{k,k}$ with half-width $\sum_{k' \neq k} |\omega_{k,k'}|$. Any eigenvalue of Ω that lies in this disc must be greater than

$$\omega_{k,k} - \sum_{k' \neq k} |\omega_{k,k'}| > q - 1 - (q - 1 - \tau) = \tau$$

Thus, we have $\mathcal{G} \subset \{\Omega \succ \tau I\}$.

Since the entries of Ω are independent under $\tilde{\Pi}$, we compute

$$\begin{aligned} \tilde{\Pi}(\mathcal{G}) &\geq \prod_k \int_{q-1}^{\infty} \xi \exp(-\xi \omega_{k,k}) d\omega_{k,k'} (1-\eta)^Q \prod_{k > k'} \int_{|\omega_{k,k'}| \leq 1 - \frac{\tau}{q-1}} \frac{\xi_0}{2} \exp(-\xi_0 |\omega_{k,k'}|) d\omega_{k,k'} \\ &\geq \exp(-2\xi Q)(1-\eta)^Q \left[1 - \frac{\mathbb{E}|\omega_{k,k'}|}{1 - \frac{\tau}{q-1}} \right]^Q \\ &= \exp(-2\xi Q)(1-\eta)^Q \left[1 - \frac{1}{\xi_0(1 - \frac{\tau}{q-1})} \right]^Q \\ &\geq \exp(-2\xi Q) \left[1 - \frac{1}{1 + K_1 Q^{2+a}} \right]^Q \left[1 - \frac{1}{K_3 Q^{2+b}(1-\tau)} \right]^Q \\ &\geq \exp(-2\xi Q + \log(R)), \end{aligned} \quad (\text{S37})$$

where $R > 0$ does not depend on n . Note that the first inequality holds by ignoring the contribution to the probability from slab distribution. The second inequality is Markov's inequality and the third inequality follows from our assumptions about how ξ_0 and η are

tuned. □

Let S_0^Ψ and S_0^Ω respectively denote the supports of Ψ and Ω . Similarly, let s_0^Ψ be the number of true non-zero entries in Ψ_0 and let s_0^Ω be the true number of non-zero off-diagonal entries in Ω_0

The KL divergence between a Gaussian chain graph model with parameters (Ψ_0, Ω_0) and one with parameters (Ψ, Ω) is

$$\begin{aligned} \frac{1}{n}K(f_0, f) &= \mathbb{E}_0 \left[\log \left(\frac{f_0}{f} \right) \right] \\ &= \frac{1}{2} \left(\log \left(\frac{|\Omega_0|}{|\Omega|} \right) - q + \text{tr}(\Omega_0^{-1}\Omega) + \frac{1}{n} \sum_{i=1}^n \|\Omega^{1/2}(\Psi\Omega - \Psi_0\Omega_0)^\top X_i^\top\|_2^2 \right) \end{aligned} \quad (\text{S38})$$

The KL variance is:

$$\begin{aligned} \frac{1}{n}V(f_0, f) &= \text{Var}_0 \left[\log \left(\frac{f_0}{f} \right) \right] \\ &= \frac{1}{2} \left(\text{tr}((\Omega_0^{-1}\Omega)^2) - 2 \text{tr}(\Omega_0^{-1}\Omega) + q \right) + \frac{1}{n} \sum_{i=1}^n \|\Omega_0^{-1/2}\Omega(\Psi\Omega^{-1} - \Psi_0\Omega_0^{-1})^\top X_i^\top\|_2^2 \end{aligned} \quad (\text{S39})$$

We need to lower bound the prior probability of the event

$$\{(\Psi, \Omega) : K(f_0, f) \leq n\epsilon_n^2, V(f_0, f) \leq n\epsilon_n^2\}$$

for large enough n .

We first obtain an upper bound of the average KL divergence and variance so that the mass of such event can serve as a lower bound. To simplify the notation, we denote $(\Psi - \Psi_0) = \Delta_\Psi$ and $\Omega - \Omega_0 = \Delta_\Omega$. We observe that $\Psi\Omega^{-1} - \Psi_0\Omega_0^{-1} = (\Delta_\Psi - \Psi_0\Omega_0^{-1}\Delta_\Omega)\Omega^{-1}$.

Using the fact that $\|A - B\|_2^2 \leq (\|A\|_2 + \|B\|_2)^2 \leq 2\|A\|_2^2 + 2\|B\|_2^2$ for any two matrices A

and B , we obtain a simple upper bound:

$$\begin{aligned}
& \frac{1}{n} K(f_0, f) \\
&= \frac{1}{2} \left(\log \left(\frac{|\Omega_0|}{|\Omega|} \right) - q + \text{tr}(\Omega_0^{-1} \Omega) + \frac{1}{n} \sum_{i=1}^n \|\Omega^{-1/2} \Delta_\Psi^\top X_i^\top - \Omega^{-1/2} \Delta_\Omega \Omega_0^{-1} \Psi_0^\top X_i^\top\|_2^2 \right) \\
&\leq \frac{1}{2} \left(\log \left(\frac{|\Omega_0|}{|\Omega|} \right) - q + \text{tr}(\Omega_0^{-1} \Omega) \right) + \frac{1}{n} \sum_{i=1}^n \|\Omega^{-1/2} \Delta_\Omega \Omega_0^{-1} \Psi_0^\top X_i^\top\|_2^2 \\
&\quad + \frac{1}{n} \sum_{i=1}^n \|\Omega^{-1/2} \Delta_\Psi^\top X_i^\top\|_2^2 \\
&= \frac{1}{2} \left(\log \left(\frac{|\Omega_0|}{|\Omega|} \right) - q + \text{tr}(\Omega_0^{-1} \Omega) \right) + \frac{1}{n} \|X \Psi_0 \Omega_0^{-1} \Delta_\Omega \Omega^{-1/2}\|_F^2 \\
&\quad + \frac{1}{n} \|X \Delta_\Psi \Omega^{-1/2}\|_F^2
\end{aligned} \tag{S40}$$

The last line holds because $\Omega^{-1/2} \Delta_\Psi^\top X_i^\top$ is the i^{th} row of $X \Delta_\Psi \Omega^{-1/2}$.

Using the same inequality, we derive a similar upper bound for the average KL variance:

$$\begin{aligned}
& \frac{1}{n} V(f_0, f) \\
&= \frac{1}{2} (\text{tr}((\Omega_0^{-1} \Omega)^2) - 2 \text{tr}(\Omega_0^{-1} \Omega) + q) + \frac{1}{n} \sum_{i=1}^n \|\Omega_0^{-1/2} \Delta_\Psi^\top X_i^\top - \Omega_0^{-1/2} \Delta_\Omega \Omega_0^{-1} \Psi_0^\top X_i^\top\|_2^2 \\
&\leq \frac{1}{2} (\text{tr}((\Omega_0^{-1} \Omega)^2) - 2 \text{tr}(\Omega_0^{-1} \Omega) + q) + \frac{2}{n} \sum_{i=1}^n \|\Omega_0^{-1/2} \Delta_\Omega \Omega_0^{-1} \Psi_0^\top X_i^\top\|_2^2 \\
&\quad + \frac{2}{n} \sum_{i=1}^n \|\Omega_0^{-1/2} \Delta_\Psi^\top X_i^\top\|_2^2 \\
&= \frac{1}{2} (\text{tr}((\Omega_0^{-1} \Omega)^2) - 2 \text{tr}(\Omega_0^{-1} \Omega) + q) + \frac{2}{n} \|X \Psi_0 \Omega_0^{-1} \Delta_\Omega \Omega_0^{-1/2}\|_F^2 + \frac{2}{n} \|X \Delta_\Psi \Omega_0^{-1/2}\|_F^2
\end{aligned} \tag{S41}$$

Similar to [Ning et al. \(2020\)](#) and [Bai et al. \(2020\)](#), we find event \mathcal{A}_1 involving only Δ_Ω and event \mathcal{A}_2 involving both Δ_Ω and Δ_Ψ such that $(\mathcal{A}_1 \cap \{\Omega \succ 0\}) \cap \mathcal{A}_2$ is a subset of the event of interest $\{K/n \leq \epsilon_n^2, V/n \leq \epsilon_n^2\}$.

To this end, define

$$\begin{aligned} \mathcal{A}_1 = & \left\{ \Omega : \frac{1}{2} \left(\text{tr}((\Omega_0^{-1}\Omega)^2) - 2 \text{tr}(\Omega_0^{-1}\Omega) + q \right) + \frac{2}{n} \|X\Psi_0\Omega_0^{-1}\Delta_\Omega\Omega_0^{-1/2}\|_F^2 \leq \epsilon_n^2/2 \right\} \\ & \cap \left\{ \frac{1}{2} \left(\log \left(\frac{|\Omega_0|}{|\Omega|} \right) - q + \text{tr}(\Omega_0^{-1}\Omega) \right) + \frac{1}{n} \|X\Psi_0\Omega_0^{-1}\Delta_\Omega\Omega^{-1/2}\|_F^2 \leq \epsilon_n^2/2 \right\} \end{aligned} \quad (\text{S42})$$

and

$$\mathcal{A}_2 = \{(\Omega, \Psi) : \frac{1}{n} \|X\Delta_\Psi\Omega_0^{-1/2}\|_F^2 \leq \frac{\epsilon_n^2}{2}, \frac{2}{n} \|X\Delta_\Psi\Omega^{-1/2}\|_F^2 \leq \frac{\epsilon_n^2}{2}\} \quad (\text{S43})$$

We separately bound the prior probabilities $\Pi(\mathcal{A}_1)$ and $\Pi(\mathcal{A}_1|\mathcal{A}_2)$

S5.1.1 Bounding the prior mass $\Pi(\mathcal{A}_1)$

The goal here is to find a proper lower bound of prior mass on \mathcal{A}_1 . To do this, first consider the set

$$\mathcal{A}_1^* = \left\{ 2 \sum_{k>k'} |\omega_{0,k,k'} - \omega_{k,k'}| + \sum_k |\omega_{0,k,k} - \omega_{k,k}| \leq \frac{\epsilon_n}{c_1\sqrt{p}} \right\}$$

where $c_1 > 0$ is a constant to be specified. Since the Frobenius norm is bounded by the vectorized L1 norm, we immediately conclude that

$$\mathcal{A}_1^* \subset \left\{ \|\Omega_0 - \Omega\|_F \leq \frac{\epsilon_n}{c_1\sqrt{p}} \right\}.$$

We now show that $\left\{ \|\Omega_0 - \Omega\|_F \leq \frac{\epsilon_n}{c_1\sqrt{p}} \right\} \subset \mathcal{A}_1$.

Since the Frobenius norm bounds the L2 operator norm, if $\|\Omega_0 - \Omega\|_F \leq \frac{\epsilon_n}{c_1\sqrt{p}}$ then the absolute value of the eigenvalues of $\Omega - \Omega_0$ are bounded by $\frac{\epsilon_n}{c_1\sqrt{p}}$. Further, because we have assumed Ω_0 has bounded spectrum, the spectrum of $\Omega = \Omega_0 + \Omega - \Omega_0$ is bounded by $\lambda_{\min} - \frac{\epsilon_n}{c_1\sqrt{p}}$ and $\lambda_{\max} + \frac{\epsilon_n}{c_1\sqrt{p}}$. When n is large enough, these quantities are further bounded by $\lambda_{\min}/2$ and $2\lambda_{\max}$. Thus, for n large enough, if $\|\Omega_0 - \Omega\|_F \leq \frac{\epsilon_n}{c_1\sqrt{p}}$, then we know Ω has bounded spectrum.

Consequently, $\Omega^{-1/2}$ has bounded L2 operator norm. Using the fact that $\|AB\|_F \leq \min(\|A\|_2\|B\|_F, \|B\|_2\|A\|_F)$

we have for some constant c_2 not depending on n ,

$$\begin{aligned} \frac{2}{n} \|X \Psi_0 \Omega_0^{-1} \Delta_\Omega \Omega_0^{-1/2}\|_F^2 &\leq \frac{2}{n} \|X \Psi_0\|_2^2 \|\Omega_0^{-1} \Delta_\Omega \Omega_0^{-1/2}\|_F^2 \\ &\leq \frac{2}{n} \|X\|_F^2 \|\Psi_0\|_2^2 \|\Omega_0^{-1} \Delta_\Omega \Omega_0^{-1/2}\|_F^2 \\ &\leq p c_2^2 \|\Delta_\Omega\|_F^2, \end{aligned}$$

where we have used the fact that $\|X\|_F = \sqrt{np}$. Thus $\|\Delta_\Omega\|_F \leq \frac{\epsilon_n}{2c_2\sqrt{p}}$ implies

$$\frac{1}{n} \|X \Psi_0 \Omega_0^{-1} \Delta_\Omega \Omega_0^{-1/2}\|_F^2 \leq \epsilon_n^2/4.$$

Similarly, for some constant c_3 , we have that

$$\begin{aligned} \frac{1}{n} \|X \Psi_0 \Omega_0^{-1} \Delta_\Omega \Omega^{-1/2}\|_F^2 &\leq \frac{1}{n} \|X\|_F^2 \|\Psi_0\|_2^2 \|\Omega_0^{-1} \Delta_\Omega \Omega^{-1/2}\|_F^2 \\ &\leq p c_3^2 \|\Delta_\Omega\|_F^2 \end{aligned}$$

Thus we have $\|\Delta_\Omega\|_F \leq \frac{\epsilon_n}{2c_3\sqrt{p}}$ implies $\frac{1}{2n} \|X \Psi_0 \Omega_0^{-1} \Delta_\Omega \Omega^{-1/2}\|_F^2 \leq \epsilon_n^2/4$

Using an argument from [Ning et al. \(2020\)](#), $\|\Delta_\Omega\|_F \leq \frac{\epsilon_n}{2b_2\sqrt{p}} \leq \epsilon_n/2b_2$ implies the following two inequalities

$$\begin{aligned} \frac{1}{2} (\text{tr}((\Omega_0^{-1}\Omega)^2) - 2 \text{tr}(\Omega_0^{-1}\Omega) + q) &\leq \epsilon_n^2/4 \\ \frac{1}{2} (\log(\frac{|\Omega_0|}{|\Omega|}) - q + \text{tr}(\Omega_0^{-1}\Omega)) &\leq \epsilon_n^2/4. \end{aligned}$$

Thus by taking $c_1 = 2 \max\{c_2, c_3, b_2\}$, we can conclude $\{\|\Omega_0 - \Omega\|_F \leq \frac{\epsilon_n}{c_1\sqrt{p}}\} \subset \mathcal{A}_1$. Thus $\mathcal{A}_1^* \subset \mathcal{A}_1$

Since $\mathcal{A}_1^* \in \{\Omega : \|\Omega_0 - \Omega\|_F \leq \epsilon_n/c_1\sqrt{p}\}$, we know that $\tilde{\Pi}(\Omega \succ \tau I | \mathcal{A}_1^*) = 1$. We can therefore lower bound $\Pi(\mathcal{A}_1)$ by $\Pi(\mathcal{A}_1^* \cap \{\Omega \succ \tau I\})$. Instead of calculating the latter probability directly, we can lower bound it by observing

$$\begin{aligned} &2 \sum_{k > k'} |\omega_{0,k,k'} - \omega_{k,k'}| + \sum_k |\omega_{0,k,k} - \omega_{k,k}| \\ &= 2 \sum_{(k,k') \in S_0^\Omega} |\omega_{0,k,k'} - \omega_{k,k'}| + 2 \sum_{(k,k') \in (S_0^\Omega)^c} |\omega_{k,k'}| + \sum_k |\omega_{0,k,k} - \omega_{k,k}|. \end{aligned}$$

Consider the following events

$$\begin{aligned}\mathcal{B}_1 &= \left\{ \sum_{(k,k') \in S_0^\Omega} |\omega_{0,k,k'} - \omega_{k,k'}| \leq \frac{\epsilon_n}{6c_1\sqrt{p}} \right\} \\ \mathcal{B}_2 &= \left\{ \sum_{(k,k') \in (S_0^\Omega)^c} |\omega_{k,k'}| \leq \frac{\epsilon_n}{6c_1\sqrt{p}} \right\} \\ \mathcal{B}_3 &= \left\{ \sum_k |\omega_{0,k,k} - \omega_{k,k}| \leq \frac{\epsilon_n}{3c_1\sqrt{p}} \right\}\end{aligned}$$

Let $\mathcal{B} = \bigcap_{i=1}^3 \mathcal{B}_i \subset \mathcal{A}_1^* \subset \mathcal{A}_1$. Since the prior probability of \mathcal{B} lower bounds $\Pi(\mathcal{A}_1)$, we now focus on estimating $\tilde{\Pi}(\mathcal{B})$. Recall that the untruncated prior $\tilde{\Pi}$ is separable. Consequently,

$$\Pi(\mathcal{A}_1 \cap \{\Omega \succ \tau I\}) \geq \tilde{\Pi}(\mathcal{A}_1) \geq \tilde{\Pi}(\mathcal{B}) = \prod_{i=1}^3 \tilde{\Pi}(\mathcal{B}_i)$$

We first bound the probability of \mathcal{B}_1 . Note that we can use only the slab part of the prior to bound this probability. A similar technique was used by [Bai et al. \(2020\)](#) (specifically in their Equation D.18) and by [Ročková and George \(2018\)](#). Specifically, we have

$$\begin{aligned}\tilde{\Pi}(\mathcal{B}_1) &= \int_{\mathcal{B}_1} \prod_{(k,k') \in S_0^\Omega} \pi(\omega_{k,k'} | \eta) d\mu \\ &\geq \prod_{(k,k') \in S_0^\Omega} \int_{|\omega_{0,k,k'} - \omega_{k,k'}| \leq \frac{\epsilon_n}{6s_0^\Omega c_1 \sqrt{p}}} \pi(\omega_{k,k'} | \eta) d\omega_{k,k'} \\ &\geq \eta^{s_0^\Omega} \prod_{(k,k') \in S_0^\Omega} \int_{|\omega_{0,k,k'} - \omega_{k,k'}| \leq \frac{\epsilon_n}{6s_0^\Omega c_1 \sqrt{p}}} \frac{\xi_1}{2} \exp(-\xi_1 |\omega_{k,k'}|) d\omega_{k,k'} \\ &\geq \eta^{s_0^\Omega} \exp(-\xi_1 \sum_{(k,k') \in S_0^\Omega} |\omega_{0,k,k'}|) \prod_{(k,k') \in S_0^\Omega} \int_{|\omega_{0,k,k'} - \omega_{k,k'}| \leq \frac{\epsilon_n}{6s_0^\Omega c_1 \sqrt{p}}} \frac{\xi_1}{2} \exp(-\xi_1 |\omega_{0,k,k'} - \omega_{k,k'}|) d\omega_{k,k'} \\ &= \eta^{s_0^\Omega} \exp(-\xi_1 \|\Omega_{0,S_0^\Omega}\|_1) \prod_{(k,k') \in S_0^\Omega} \int_{|\Delta| \leq \frac{\epsilon_n}{6s_0^\Omega c_1 \sqrt{p}}} \frac{\xi_1}{2} \exp(-\xi_1 |\Delta|) d\Delta \\ &\geq \eta^{s_0^\Omega} \exp(-\xi_1 \|\Omega_{0,S_0^\Omega}\|_1) \left[e^{-\frac{\xi_1 \epsilon_n}{6c_1 s_0^\Omega \sqrt{p}}} \left(\frac{\xi_1 \epsilon_n}{6s_0^\Omega c_1 \sqrt{p}} \right) \right]^{s_0^\Omega}\end{aligned}$$

The first inequality holds because the fact that $|\omega_{0,k,k'} - \omega_{k,k'}| \leq \epsilon_n/(6s_0^\Omega c_1 \sqrt{p})$ implies that the sum less than $\epsilon_n/(6c_1 \sqrt{p})$. The last inequality is a special case of Equation D.18 of [Bai et al. \(2020\)](#).

For \mathcal{B}_2 , we derive the lower bound using the spike component of the prior. To this end, let $Q = q(q-1)/2$ denote the number of off-diagonal entries of matrix Ω . We have

$$\begin{aligned}
\tilde{\Pi}(\mathcal{B}_2) &= \int_{\mathcal{B}_2} \prod_{(k,k') \in (S_0^\Omega)^c} \pi(\omega_{k,k'}|\eta) d\mu \\
&\geq \prod_{(k,k') \in (S_0^\Omega)^c} \int_{|\omega_{k,k'}| \leq \frac{\epsilon_n}{6(Q-s_0^\Omega)c_1\sqrt{p}}} \pi(\omega_{k,k'}|\eta) d\mu \\
&\geq (1-\eta)^{Q-s_0^\Omega} \prod_{(k,k') \in (S_0^\Omega)^c} \int_{|\omega_{k,k'}| \leq \frac{\epsilon_n}{6(Q-s_0^\Omega)c_1\sqrt{p}}} \frac{\xi_0}{2} \exp(-\xi_0|\omega_{k,k'}|) d\omega_{k,k'} \\
&\geq (1-\eta)^{Q-s_0^\Omega} \prod_{(k,k') \in (S_0^\Omega)^c} \left[1 - \frac{6(Q-s_0^\Omega)c_1\sqrt{p}}{\epsilon_n} \mathbb{E}_\pi|\omega_{k,k'}| \right] \\
&= (1-\eta)^{Q-s_0^\Omega} \left[1 - \frac{6(Q-s_0^\Omega)c_1\sqrt{p}}{\epsilon_n \xi_0} \right]^{Q-s_0^\Omega} \\
&\gtrsim (1-\eta)^{Q-s_0^\Omega} \left[1 - \frac{1}{Q-s_0^\Omega} \right]^{Q-s_0^\Omega} \\
&\asymp (1-\eta)^{Q-s_0^\Omega}
\end{aligned}$$

To derive the last two lines, we used an argument similar to the one used by [Bai et al. \(2020\)](#) to derive Equation D.22. That is, we used the assumption that $\xi_0 \sim \max\{Q, n, pq\}^{4+b}$ for some $b > 0$ to conclude that $\sqrt{n}/\max\{Q, n, pq\}^{1/2+b} \leq 1$. This inequality allows us to control the Q in the numerator. Since s_0^Ω grows slower than Q , we can lower bound the above function some multiplier of the form $(1-\eta)^{Q-s_0^\Omega}$. Thus, for large enough n , we have

$$\begin{aligned}
\frac{6(Q-s_0^\Omega)c_1\sqrt{p}}{\epsilon_n \xi_0} &\leq \frac{6(Q-s_0^\Omega)c_1\sqrt{p}\sqrt{n}}{\sqrt{p \log(q)} Q^{2+b}} \\
&= \frac{6c_1}{\sqrt{\log(q)}} \frac{Q-s_0}{Q^2} \frac{\sqrt{n}}{Q^b} \\
&\leq \frac{Q-s_0}{Q^2} \\
&\leq \frac{1}{Q-s_0}
\end{aligned}$$

The event \mathcal{B}_3 only involves diagonal entries. The untruncated prior mass can be directly bounded using the exponential distribution

$$\begin{aligned}
\tilde{\Pi}(\mathcal{B}_3) &= \int_{\mathcal{B}_3} \prod_{k=1}^q \pi(\omega_{k,k}) d\mu \\
&\geq \prod_{k=1}^q \int_{|\omega_{0,k,k} - \omega_{k,k}| \leq \frac{\epsilon_n}{3qc_1\sqrt{p}}} \pi(\omega_{k,k}) d\omega_{k,k} \\
&= \prod_{k=1}^q \int_{\omega_{0,k,k} - \frac{\epsilon_n}{3qc_1\sqrt{p}}}^{\omega_{0,k,k} + \frac{\epsilon_n}{3qc_1\sqrt{p}}} \xi \exp(-\xi\omega_{k,k}) d\omega_{k,k} \\
&\geq \prod_{k=1}^q \int_{\omega_{0,k,k}}^{\omega_{0,k,k} + \frac{\epsilon_n}{3qc_1\sqrt{p}}} \xi \exp(-\xi\omega_{k,k}) d\omega_{k,k} \\
&= \exp(-\xi \sum_{i=1}^q \omega_{0,k,k}) \int_0^{\frac{\epsilon_n}{3qc_1\sqrt{p}}} \xi \exp(-\xi\omega_{k,k}) d\omega_{k,k} \\
&\geq \exp(-\xi \sum_{i=1}^q \omega_{0,k,k}) \left[e^{-\frac{\xi\epsilon_n}{3c_1q\sqrt{p}}} \left(\frac{\xi\epsilon_n}{3qc_1\sqrt{p}} \right) \right]^q
\end{aligned}$$

Now we are ready to show that the log prior mass on \mathcal{B} can be bounded by some $C_1 n \epsilon_n^2$. To this end, consider the negative log probability

$$\begin{aligned}
&-\log(\Pi(\mathcal{A}_1 \cap \{\Omega \succ \tau I\})) \\
&\leq \sum_{i=1}^3 -\log(\tilde{\Pi}(\mathcal{B}_i)) \\
&\lesssim -s_0^\Omega \log(\eta) + \xi_1 \|\Omega_{0,S_0^\Omega}\|_1 + \frac{\xi_1 \epsilon_n}{6c_1\sqrt{p}} - s_0^\Omega \log\left(\frac{\xi_1 \epsilon_n}{6s_0^\Omega c_1\sqrt{p}}\right) - (Q - s_0^\Omega) \log(1 - \eta) \\
&\quad + \xi \sum_k \omega_{0,k,k} + \frac{\xi \epsilon_n}{3c_1\sqrt{p}} - q \log\left(\frac{\xi \epsilon_n}{3qc_1\sqrt{p}}\right) \\
&= -\log\left(\eta^{s_0^\Omega} (1 - \eta)^{Q - s_0^\Omega}\right) + \xi_1 \|\Omega_{0,S_0^\Omega}\|_1 + \frac{\xi_1 \epsilon_n}{6c_1\sqrt{p}} + \xi \sum_k \omega_{0,k,k} + \frac{\xi \epsilon_n}{3c_1\sqrt{p}} \\
&\quad - s_0^\Omega \log\left(\frac{\xi_1 \epsilon_n}{6s_0^\Omega c_1\sqrt{p}}\right) - q \log\left(\frac{\xi \epsilon_n}{3qc_1\sqrt{p}}\right)
\end{aligned}$$

The $\frac{\xi_1 \epsilon_n}{6c_1\sqrt{p}}$ and $\frac{\xi \epsilon_n}{3c_1\sqrt{p}}$ terms are $O(\epsilon_n/\sqrt{p}) \lesssim n\epsilon_n^2$ which goes to infinity. The 4th term is of

order q since the diagonal entries is controlled by the largest eigenvalue of Ω , which was assumed to be bounded.

$$\xi_1 \|\Omega_{0, s_0^\Omega}\|_1 \leq \xi_1 s_0^\Omega \sup |\omega_{0, k, k'}|$$

is of order s_0^Ω as the entries of $\omega_{0, k, k'}$ is controlled.

Without tuning of η , the first term $-\log(\eta^{s_0^\Omega}(1-\eta)^{Q-s_0^\Omega})$ has order of Q . But since we assumed $\frac{1-\eta}{\eta} \sim \max\{Q, pq\}^{2+a}$ for some $a > 0$, we have $K_1 \max\{Q, pq\}^{2+a} \leq \frac{1-\eta}{\eta} \leq K_2 \max\{Q, pq\}^{2+a}$. That is, we have $1/(1+K_2 \max\{Q, pq\}^{2+a}) \leq \eta \leq 1/(1+K_1 \max\{Q, pq\}^{2+a})$. We can derive a simple lower bound as

$$\begin{aligned} \eta^{s_0^\Omega}(1-\eta)^{Q-s_0^\Omega} &\geq (1+K_2 \max\{Q, pq\}^{2+a})^{-s_0^\Omega} (1-\eta)^{Q-s_0^\Omega} \\ &\geq (1+K_2 \max\{Q, pq\}^{2+a})^{-s_0^\Omega} \left(1 - \frac{1}{1+K_1 \max\{Q, pq\}^{2+a}}\right)^{Q-s_0^\Omega} \\ &\gtrsim (1+K_2 \max\{Q, pq\}^{2+a})^{-s_0^\Omega} \end{aligned}$$

The last line is because $\max\{Q, pq\}^{2+a}$ grows faster than $Q-s_0^\Omega$. Thus $(1 - \frac{1}{1+K_1 \max\{Q, pq\}^{2+a}})^{\max\{Q, pq\}^{2+a} - s_0^\Omega}$ can be bounded below by some constant.

$$\begin{aligned} -\log(\eta^{s_0^\Omega}(1-\eta)^{Q-s_0^\Omega}) &\lesssim s_0^\Omega \log(1+K_2 \max\{Q, pq\}^{2+a}) \lesssim s_0^\Omega \log(\max\{Q, pq\}) \\ &\asymp s_0^\Omega \log(\max\{q, p\}) \leq \max(p, q, s_0^\Omega) \log(\max\{q, p\}) \end{aligned}$$

The last two terms can be treated in the same way, using the assumption $\xi_1 \asymp 1/n$ and $\xi \asymp 1/\max\{Q, n\}$.

$$\begin{aligned} -s_0^\Omega \log\left(\frac{\xi_1 \epsilon_n}{6s_0^\Omega c_1 \sqrt{p}}\right) &= s_0^\Omega \log\left(\frac{6s_0^\Omega c_1 \sqrt{p}}{\xi_1 \epsilon_n}\right) \\ &\lesssim s_0^\Omega \log\left(\frac{n^{3/2} s_0^\Omega \sqrt{p}}{\sqrt{\max\{s_0^\Omega, p, q\} \log(q)}}\right) \\ &\leq s_0^\Omega \log(n^{3/2} s_0^\Omega) \\ &\lesssim s_0^\Omega \log(q^2) \\ &\lesssim n \epsilon_n^2 \end{aligned}$$

The third line holds because $\sqrt{p} \leq \sqrt{\max\{s_0^\Omega, p, q\}}$ and $\log(q) \geq 1$, which together imply that $\sqrt{p}/\sqrt{\max\{s_0^\Omega, p, q\} \log(q)} \leq 1$. The fourth line follows from our assumption that $\log(n) \lesssim \log(q)$ because $s_0^\Omega < q^2$. The last line uses the definition of ϵ_n .

Finally, we have

$$\begin{aligned}
-q \log \left(\frac{\xi \epsilon_n}{3q c_1 \sqrt{p}} \right) &= q \log \left(\frac{3q c_1 \sqrt{p}}{\xi \epsilon_n} \right) \\
&\lesssim q \log \left(\frac{n^{1/2} \max\{Q, n\} q \sqrt{p}}{\sqrt{\max\{s_0^\Omega, p, q\} \log(q)}} \right) \\
&\leq q \log (n^{1/2} \max\{Q, n\} q) \\
&\lesssim q \log(q) \\
&\lesssim n \epsilon_n^2
\end{aligned}$$

S5.1.2 Bounding the conditional probability $\Pi(\mathcal{A}_2|\mathcal{A}_1)$

To bound $\Pi(\mathcal{A}_2|\mathcal{A}_1)$, we use a very similar strategy as the one above. The difference is that we now focus on the matrix Ψ . We show that mass on a L1 norm ball serves as a lower bound similar to that of Ω . To see that, using an argument from [Ning et al. \(2020\)](#), we show that powers of Ω and Ω_0 are bounded in operator norm. Thus the terms $\frac{1}{n} \|X \Delta_\Psi \Omega_0^{-1/2}\|_F^2$ and $\frac{2}{n} \|X \Delta_\Psi \Omega^{-1/2}\|_F^2$ that appear in the KL condition are bounded by a constant multiplier of $n^{-1} \|X \Delta_\Psi\|_F^2$. Using the fact that the columns of X have norm \sqrt{n} , we can find this norm:

$$\|X \Delta_\Psi\|_F \leq \sqrt{n} \sum_{j=1}^p \|\Delta_{\Psi, j, \cdot}\|_F \leq \sqrt{n} \sum_{j=1}^p \sum_{k=1}^q |\psi_{j,k} - \psi_{0,j,k}|$$

Thus to bound $\Pi(\mathcal{A}_2|\mathcal{A}_1)$ from below, it suffices to bound $\Pi(\sum |\psi_{j,k} - \psi_{0,j,k}| \leq c_4 \epsilon_n)$ for some fixed constant $c_4 > 0$.

We separate the sum based on whether the true value is 0, similar to our treatment on Ω :

$$\sum_{ij} |\psi_{j,k} - \psi_{0,j,k}| = \sum_{(j,k) \in S_0^\Psi} |\psi_{j,k} - \psi_{0,j,k}| + \sum_{(j,k) \in (S_0^\Psi)^c} |\psi_{j,k}|$$

Using the same argument as in Ω , we can consider the events whose intersection is a subset

of \mathcal{A}_2 :

$$\mathcal{B}_4 = \left\{ \sum_{(j,k) \in S_0^\Psi} |\psi_{j,k} - \psi_{0,j,k}| \leq \frac{c_4 \epsilon_n}{2} \right\}$$

$$\mathcal{B}_5 = \left\{ \sum_{(j,k) \in (S_0^\Psi)^c} |\psi_{j,k} - \psi_{0,j,k}| \leq \frac{c_4 \epsilon_n}{2} \right\}$$

We have $\mathcal{B}_4 \cap \mathcal{B}_5 \subset \mathcal{A}_2$. Since the elements of Ψ are *a priori* independent of each other and of Ω , we compute

$$\Pi(\mathcal{A}_2 | \mathcal{A}_1) \geq \Pi(\mathcal{B}_4 | \mathcal{A}_1) \Pi(\mathcal{B}_5 | \mathcal{A}_1) = \Pi(\mathcal{B}_4) \Pi(\mathcal{B}_5)$$

We bound each of these terms using the same argument as in the previous subsection:

$$\begin{aligned} \Pi(\mathcal{B}_4) &= \int_{\mathcal{B}_4} \prod_{(j,k) \in S_0^\Psi} \pi(\psi_{j,k} | \theta) d\mu \\ &\geq \prod_{(j,k) \in S_0^\Psi} \int_{|\psi_{j,k} - \psi_{0,j,k}| \leq \frac{c_4 \epsilon_n}{2s_0^\Psi}} \pi(\psi_{j,k} | \theta) d\psi_{j,k} \\ &\geq \theta^{s_0^\Psi} \prod_{(j,k) \in S_0^\Psi} \int_{|\psi_{j,k} - \psi_{0,j,k}| \leq \frac{c_4 \epsilon_n}{2s_0^\Psi}} \frac{\lambda_1}{2} \exp(-\lambda_1 |\psi_{j,k}|) d\psi_{j,k} \\ &\geq \theta^{s_0^\Psi} \exp(-\lambda_1 \sum_{(j,k) \in S_0^\Psi} |\psi_{0,j,k}|) \prod_{(j,k) \in S_0^\Psi} \int_{|\psi_{j,k} - \psi_{0,j,k}| \leq \frac{c_4 \epsilon_n}{2s_0^\Psi}} \frac{\lambda_1}{2} \exp(-\lambda_1 |\psi_{j,k} - \psi_{0,j,k}|) d\psi_{j,k} \\ &= \theta^{s_0^\Psi} \exp(-\lambda_1 \sum_{(j,k) \in S_0^\Psi} |\psi_{0,j,k}|) \prod_{(j,k) \in S_0^\Psi} \int_{|\Delta| \leq \frac{c_4 \epsilon_n}{2s_0^\Psi}} \frac{\lambda_1}{2} \exp(-\lambda_1 |\Delta|) d\Delta \\ &\geq \theta^{s_0^\Psi} \exp(-\lambda_1 \|\Psi_{0, S_0^\Psi}\|_1) \left[e^{-\frac{c_4 \lambda_1 \epsilon_n}{2s_0^\Psi}} \frac{c_4 \epsilon_n}{2s_0^\Psi} \right]^{s_0^\Psi} \end{aligned}$$

Similarly, we have

$$\begin{aligned} \Pi(\mathcal{B}_5) &\geq (1 - \theta)^{pq - s_0^\Psi} \left[1 - \frac{2(pq - s_0^\Psi)c_4}{\epsilon_n \lambda_0} \right]^{pq - s_0^\Psi} \\ &\gtrsim (1 - \theta)^{pq - s_0^\Psi} \end{aligned}$$

From here we have

$$\begin{aligned}
-\log(\Pi(\mathcal{A}_2|\mathcal{A}_1)) &\leq -\log(\Pi(\mathcal{B}_4)) - \log(\Pi(\mathcal{B}_5)) \\
&= -\log(\theta^{s_0^\Psi}(1-\theta)^{pq-s_0^\Psi}) + \lambda_1 \|\Psi_{0,S_0^\Psi}\|_1 + \frac{\lambda_1 c_4 \epsilon_n}{2} - s_0^\Psi \log\left(\frac{c_4 \epsilon_n}{2s_0^\Psi}\right)
\end{aligned}$$

Since Ψ_0 has bounded L2 operator norm, we know that the entries of Ψ_0 are all bounded. Thus $\lambda_1 \|\Psi_{0,S_0^\Psi}\|_1 = O(s_0^\Psi) \lesssim n\epsilon_n^2$. The last two terms are $O(\epsilon_n) \lesssim n\epsilon_n^2$.

For the first term, recall that we assumed $\frac{1-\theta}{\theta} \sim (pq)^{2+b}$ for some $b > 0$. That is, there are constants M_3 and M_4 such that $M_3(pq)^{2+b} \leq \frac{1-\theta}{\theta} \leq M_4(pq)^{2+b} \leq \frac{1-\theta}{\theta}$. Since $1/(1+M_4(pq)^{2+b}) \leq \theta \leq 1/(1+M_3(pq)^{2+b})$, we compute

$$\begin{aligned}
\theta^{s_0^\Psi}(1-\theta)^{pq-s_0^\Psi} &\geq (1+M_4(pq)^{2+b})^{-s_0^\Psi}(1-\theta)^{pq-s_0^\Psi} \\
&\geq (1+M_4(pq)^{2+b})^{-s_0^\Psi} \left(1 - 1/(1+M_3(pq)^{2+b})\right)^{pq-s_0^\Psi} \\
&\gtrsim (1+M_4(pq)^{2+b})^{-s_0^\Psi}
\end{aligned}$$

Note that the last line is due to the fact that $(pq)^{2+b}$ grows faster than $pq - s_0^\Psi$. Consequently, the term $\left(1 - 1/(1+M_3(pq)^{2+b})\right)^{pq-s_0^\Psi}$ can be bounded from below by a constant not depending on n . Thus,

$$-\log\left(\theta^{s_0^\Psi}(1-\theta)^{pq-s_0^\Psi}\right) \lesssim s_0^\Psi \log(1+M_4(pq)^{2+b}) \lesssim s_0^\Psi \log(pq) \lesssim s_0^\Psi \max\{\log(q), \log(p)\}$$

For the last term, we use the same argument as we did with Ω .

$$\begin{aligned}
-s_0^\Psi \log\left(\frac{c_4 \epsilon_n}{2s_0^\Psi}\right) &= s_0^\Psi \log\left(\frac{2s_0^\Psi}{c_4 \epsilon_n}\right) \\
&\lesssim s_0^\Psi \log\left(\frac{\sqrt{n}}{\sqrt{\log(pq)}}\right) \\
&\leq s_0^\Psi \log(\sqrt{n}) \\
&\lesssim n\epsilon_n^2
\end{aligned}$$

S5.2 Test condition

To simplify the parameter space to be concerned in the test condition, we first show the dimension recovery result by bounding the prior probability, with our effective dimension defined as number of entries whose absolute value is larger than the intersection of spike and slab components. Then we find the proper vectorized L1 norm sieve in the “lower-dimensional” parameter space. We construct tests based on the supremum of a collection of single-alternative Neyman-Pearson likelihood ratio tests in the subsets of the sieve that are norm balls, then we show that the number of such subsets needed to cover the sieve can be bounded properly.

S5.2.1 Dimension recovery

Unlike [Ning et al. \(2020\)](#), our prior assigns no mass on exactly sparse solutions. Nevertheless, similar to [Ročková and George \(2018\)](#), we can define a notion of “effective sparsity” and generalized dimension. Intuitively the generalized dimension can be defined as how many coefficients are drawn from the slab rather than the spike part of the prior. Formally the generalized inclusion functions ν_ψ and ν_ω for Ψ and Ω can be defined as:

$$\begin{aligned}\nu_\psi(\psi_{j,k}) &= \mathbb{1}(|\psi_{j,k}| > \delta_\psi) \\ \nu_\omega(\omega_{k,k'}) &= \mathbb{1}(|\omega_{k,k'}| > \delta_\omega)\end{aligned}$$

where δ_ψ and δ_ω is the threshold where the spike and slab part has the same density.

$$\begin{aligned}\delta_\psi &= \frac{1}{\lambda_0 - \lambda_1} \log \left[\frac{1 - \theta}{\theta} \frac{\lambda_0}{\lambda_1} \right] \\ \delta_\omega &= \frac{1}{\xi_0 - \xi_1} \log \left[\frac{1 - \eta}{\eta} \frac{\xi_0}{\xi_1} \right]\end{aligned}$$

Then the generalized dimension can be defined as number of entries are included:

$$\begin{aligned}|\nu(\psi)| &= \sum_{jk} \nu_\psi(\psi_{j,k}) \\ |\nu(\Omega)| &= \sum_{k > k'} \nu_\omega(\omega_{k,k'})\end{aligned}\tag{S44}$$

Note that we only count the off-diagonal entries in Ω .

We are now ready to prove Lemma 1 from the main text. The main idea is to check the posterior probability directly. Let $\mathcal{B}_n^\Psi = \{\Psi : |\nu(\Psi)| < r_n^\Psi\}$ for some $r_n^\Psi = C'_3 \max\{p, q, s_0^\Psi, s_0^\Omega\}$ with $C'_3 > C_1$ in the KL condition. For Ω , let $\mathcal{B}_n^\Omega = \{\Omega \succ \tau I : |\nu(\Omega)| < r_n^\Omega\}$ for $r_n^\Omega = C'_3 \max\{p, q, s_0^\Psi, s_0^\Omega\}$ with some $C'_3 > C_1$ in the KL condition. We aim to show that $\mathbb{E}_0 \Pi(\Omega \in (\mathcal{B}_n^\Omega)^c | Y_1, \dots, Y_n) \rightarrow 0$ and $\mathbb{E}_0 \Pi(\Psi \in (\mathcal{B}_n^\Psi)^c | Y_1, \dots, Y_n) \rightarrow 0$.

The marginal posterior can be expressed using log-likelihood ℓ_n :

$$\begin{aligned} \Pi(\Psi \in \mathcal{B}_n^\Psi | Y_1, \dots, Y_n) &= \frac{\iint_{\mathcal{B}_n^\Psi} \exp(\ell_n(\Psi, \Omega) - \ell_n(\Psi_0, \Omega_0)) d\Pi(\Psi) d\Pi(\Omega)}{\iint \exp(\ell_n(\Psi, \Omega) - \ell_n(\Psi_0, \Omega_0)) d\Pi(\Psi) d\Pi(\Omega)} \\ \Pi(\Omega \in \mathcal{B}_n^\Omega | Y_1, \dots, Y_n) &= \frac{\iint_{\mathcal{B}_n^\Omega} \exp(\ell_n(\Psi, \Omega) - \ell_n(\Psi_0, \Omega_0)) d\Pi(\Psi) d\Pi(\Omega)}{\iint \exp(\ell_n(\Psi, \Omega) - \ell_n(\Psi_0, \Omega_0)) d\Pi(\Psi) d\Pi(\Omega)} \end{aligned} \quad (\text{S45})$$

By using the result of KL condition (Lemma S2), we know the denominators are bounded from below by $e^{-C_1 n \epsilon_n^2}$ with large probability. Thus, we focus now on upper bounding the numerators beginning with Ψ .

Consider the numerator:

$$\begin{aligned} \mathbb{E}_0 \left(\iint_{(\mathcal{B}_n^\Psi)^c} f / f_0 d\Pi(\Psi) d\Pi(\Omega) \right) &= \int \iint_{(\mathcal{B}_n^\Psi)^c} f / f_0 d\Pi(\Psi) d\Pi(\Omega) f_0 dy \\ &= \iint_{(\mathcal{B}_n^\Psi)^c} \int f dy d\Pi(\Psi) d\Pi(\Omega) \\ &\leq \int_{(\mathcal{B}_n^\Psi)^c} d\Pi(\Psi) = \Pi(|\nu(\Psi)| \geq r_n^\Psi) \end{aligned}$$

We can bound the above display using the fact that when $|\psi_{j,k}| > \delta_\psi$ we have $\pi(\psi_{j,k}) < 2\theta \frac{\lambda_1}{2} \exp(-\lambda_1 |\psi_{j,k}|)$, this is by definition of the effective dimension:

$$\begin{aligned} \Pi(|\nu(\Psi)| \geq r_n^\Psi) &\leq \sum_{|S| > r_n^\Psi} (2\theta)^{|S|} \prod_{(j,k) \in S} \int_{|\psi_{j,k}| > \delta_\psi} \frac{\lambda_1}{2} \exp(-\lambda_1 |\psi_{j,k}|) d\psi_{j,k} \prod_{(j,k) \notin S} \int_{|\psi_{j,k}| < \delta_\psi} \pi(\psi_{j,k}) d\psi_{j,k} \\ &\leq \sum_{|S| > r_n^\Psi} (2\theta)^{|S|} \end{aligned}$$

Using the assumption on θ , and the fact $\binom{pq}{k} \leq (epq/k)^k$ (similar to Bai et al. (2020)'s equation D.32), we can further upper bound the probability

$$\begin{aligned}
\Pi(|\nu(\Psi)| \geq r_n^\Psi) &\leq \sum_{|S| > r_n^\Psi} (2\theta)^{|S|} \leq \sum_{|S| > r_n^\Psi} \left(\frac{2}{1 + M_4(pq)^{2+b}} \right)^{|S|} \\
&\leq \sum_{k=\lfloor r_n^\Psi \rfloor + 1}^{pq} \binom{pq}{k} \left(\frac{2}{M_4(pq)^2} \right)^k \leq \sum_{k=\lfloor r_n^\Psi \rfloor + 1}^{pq} \left(\frac{2e}{M_4 k pq} \right)^k \\
&< \sum_{k=\lfloor r_n^\Psi \rfloor + 1}^{pq} \left(\frac{2e}{M_4(\lfloor r_n^\Psi \rfloor + 1)pq} \right)^k \\
&\lesssim (pq)^{-(\lfloor r_n^\Psi \rfloor + 1)} \\
&\leq \exp(-(\lfloor r_n^\Psi \rfloor) \log(pq)).
\end{aligned}$$

Taking $r_n^\Psi = C'_3 \max\{p, q, s_0^\Psi, s_0^\Omega\}$ for some $C'_3 > C_1$, we have:

$$\Pi(|\nu(\Psi)| \geq r_n^\Psi) \leq \exp(-C'_3 \max\{p, q, s_0^\Psi, s_0^\Omega\} \log(pq))$$

Therefore,

$$\mathbb{E}_0 \Pi((\mathcal{B}_n^\Psi)^c | Y_1, \dots, Y_n) \leq \mathbb{E}_0 \Pi((\mathcal{B}_n^\Psi)^c | Y_1, \dots, Y_n) I_{E_n} + P_0(E_n^c),$$

where E_n is the event in the KL condition. On E_n , the KL condition ensures that the denominator in Equation (S45) is lower bounded by $\exp(-C_1 n \epsilon_n^2)$ while the denominator is upper bounded by $\exp(-C'_3 \max\{p, q, s_0^\Psi, s_0^\Omega\} \log(pq))$. Since $\mathbb{P}_0(E_n^c)$ is $o(1)$ per KL condition, we have the upper bound

$$\mathbb{E}_0 \Pi((\mathcal{B}_n^\Psi)^c | Y_1, \dots, Y_n) \leq \exp(C_1 n \epsilon_n^2 - C'_3 \max\{p, q, s_0^\Psi, s_0^\Omega\} \log(pq)) + o(1) \rightarrow 0$$

This completes the proof of the dimension recovery result of Ψ .

The workflow for Ω is very similar, except we need to use the upper bound of the graphical prior in Equation (S34) to properly bound the prior mass.

We upper bound the numerator:

$$\mathbb{E}_0 \left(\iint_{(\mathcal{B}_n^\Omega)^c} f/f_0 d\Pi(\Psi) d\Pi(\Omega) \right) \leq \int_{(\mathcal{B}_n^\Omega)^c} d\Pi(\Omega) = \Pi(|\nu(\Omega)| \geq r_n^\Omega) \leq \exp(2\xi Q - \log(R)) \tilde{\Pi}(|\nu(\Omega)| \geq r_n^\Omega)$$

We bound the above display using the fact that when $|\omega_{k,k'}| > \delta_\omega$ we have $\pi(\omega_{k,k'}) < 2\eta \frac{\xi_1}{2} \exp(-\xi_1 |\omega_{k,k'}|)$. Note that this follows from the definition of the effective dimension. We have

$$\begin{aligned} \tilde{\Pi}(|\nu(\Omega)| \geq r_n^\Omega) &\leq \sum_{|S| > r_n^\Omega} (2\eta)^{|S|} \prod_{(k,k') \in S} \int_{|\omega_{k,k'}| > \delta_\omega} \frac{\xi_1}{2} \exp(-\xi_1 |\omega_{k,k'}|) d\omega_{k,k'} \prod_{(k,k') \notin S} \int_{|\omega_{k,k'}| < \delta_\omega} \pi(\omega_{k,k'}) d\omega_{k,k'} \\ &\leq \sum_{|S| > r_n^\Omega} (2\eta)^{|S|} \end{aligned}$$

By using the assumption on η , and the fact $\binom{Q}{k} \leq (eQ/k)^k$, we can further upper bound the probability:

$$\begin{aligned} \tilde{\Pi}(|\nu(\Omega)| \geq r_n^\Omega) &\leq \sum_{|S| > r_n^\Omega} (2\eta)^{|S|} \leq \sum_{|S| > r_n^\Omega} \left(\frac{2}{1 + K_4 \max\{pq, Q\}^{2+b}} \right)^{|S|} \\ &\leq \sum_{k=\lfloor r_n^\Omega \rfloor + 1}^Q \binom{Q}{k} \left(\frac{2}{K_4 \max\{pq, Q\}^2} \right)^k \leq \sum_{k=\lfloor r_n^\Omega \rfloor + 1}^{\max\{pq, Q\}} \binom{\max\{pq, Q\}}{k} \left(\frac{2}{K_4 \max\{pq, Q\}^2} \right)^k \\ &\leq \sum_{k=\lfloor r_n^\Omega \rfloor + 1}^{\max\{pq, Q\}} \left(\frac{2e}{K_4 k \max\{pq, Q\}} \right)^k < \sum_{k=\lfloor r_n^\Omega \rfloor + 1}^{\max\{pq, Q\}} \left(\frac{2e}{K_4 (\lfloor r_n^\Omega \rfloor + 1) \max\{pq, Q\}} \right)^k \\ &\lesssim \max\{pq, Q\}^{-(\lfloor r_n^\Omega \rfloor + 1)} \\ &\leq \exp(-(\lfloor r_n^\Omega \rfloor) \log(\max\{pq, Q\})) \end{aligned}$$

Taking $r_n^\Omega = C'_3 \max\{p, q, s_0^\Psi, s_0^\Omega\}$ and $C'_3 > C_1$, we have

$$\tilde{\Pi}(|\nu(\Omega)| \geq r_n^\Omega) \leq \exp(-C'_3 \max\{p, q, s_0^\Psi, s_0^\Omega\} \log(\max\{pq, Q\})) \leq \exp(-C_3 n \epsilon_n^2)$$

Thus, using the assumption $\xi \asymp 1/\max\{Q, n\}$, for some R' not depending on n , we have

$$\Pi(|\nu(\Omega)| \geq r_n^\Omega) \leq \exp(-C_3 n \epsilon_n^2 + 2\xi Q - \log(R)) \leq \exp(-C_3 n \epsilon_n^2 + \log(R'))$$

We therefore conclude that

$$\mathbb{E}_0 \Pi((\mathcal{B}_n^\Omega)^c | Y_1, \dots, Y_n) \leq \mathbb{E}_0 \Pi((\mathcal{B}_n^\Omega)^c | Y_1, \dots, Y_n) I_{E_n} + P_0(E_n^c)$$

where E_n is the event in KL condition. On E_n , the KL condition ensures that the denominator in Equation (S45) is lower bounded by $\exp(-C_1 n \epsilon_n^2)$ while the denominator is upper bounded by $\exp(-C_3 n \epsilon_n^2 + \log(R'))$. Since $\mathbb{P}_0(E_n^c)$ is $o(1)$ per KL condition, we conclude

$$\mathbb{E}_0 \Pi((\mathcal{B}_n^\Omega)^c | Y_1, \dots, Y_n) \leq \exp(C_1 n \epsilon_n^2 - C_3 n \epsilon_n^2 + \log(R')) + o(1) \rightarrow 0$$

We pause now to reflect on how dimension recovery can help us establish contraction. Our end goal is to show the posterior distribution contract to the true value by first showing that event with log-affinity difference larger than any given $\epsilon > 0$ has an $o(1)$ posterior mass. For any such event, we can take a partition based on whether it intersects with $\mathcal{B}_n^\Psi, \mathcal{B}_n^\Omega$ or their complements. Because the complements $(\mathcal{B}_n^\Psi)^c$ and $(\mathcal{B}_n^\Omega)^c$ have $o(1)$ posterior mass, we have the partition that intersects with any of these two complements also has $o(1)$ posterior mass. Thus, we only need to show that events with log-affinity difference larger than any given $\epsilon > 0$ and recovered the low dimension structure have an $o(1)$ posterior mass. The recovery condition reduces the complexity of the events (on the parameter space) that we need to deal with by reducing the effective dimension of such events. We will make use of this low dimension structure during checking the test condition.

Formally for every $\epsilon > 0$, we have

$$\begin{aligned} & \mathbb{E}_0 \Pi(\Psi, \Omega \succ \tau I : \frac{1}{n} \sum \rho(f_i, f_{0,i}) > \epsilon | Y_1, \dots, Y_n) \\ & \leq \mathbb{E}_0 \Pi(\Psi \in \mathcal{B}_n^\Psi, \Omega \succ \tau I : \frac{1}{n} \sum \rho(f_i, f_{0,i}) > \epsilon | Y_1, \dots, Y_n) + \mathbb{E}_0 \Pi((\mathcal{B}_n^\Psi)^c | Y_1, \dots, Y_n) \\ & \leq \mathbb{E}_0 \Pi(\Psi \in \mathcal{B}_n^\Psi, \Omega \in \mathcal{B}_n^\Omega : \frac{1}{n} \sum \rho(f_i, f_{0,i}) > \epsilon | Y_1, \dots, Y_n) \\ & \quad + \mathbb{E}_0 \Pi((\mathcal{B}_n^\Psi)^c | Y_1, \dots, Y_n) + \mathbb{E}_0 \Pi((\mathcal{B}_n^\Omega)^c | Y_1, \dots, Y_n) \end{aligned}$$

The last two terms are $o(1)$, as proved above.

S5.2.2 Sieve

As shown in the previous section, we can concentrate on the events with proper dimension recovery, i.e. $\{\Psi \in \mathcal{B}_n^\Psi, \Omega \in \mathcal{B}_n^\Omega\}$. To apply [Ghosal and van der Vaart \(2017\)](#)'s general theory of posterior contraction, to establish contraction on the event of proper dimension recovery (i.e. $\mathbb{E}_0 \Pi(\Psi \in \mathcal{B}_n^\Psi, \Omega \in \mathcal{B}_n^\Omega : \frac{1}{n} \sum \rho(f_i, f_{0,i}) > \epsilon | Y_1, \dots, Y_n) \rightarrow 0$), we need to find a sieve that covers enough of the support of the prior. We will show that an L1 norm sieve is sufficient. Formally we will show that there exist a sieve \mathcal{F}_n such that for some constants $C_2 > C_1 + 2$:

$$\Pi(\mathcal{F}_n^c) \leq \exp(-C_2 n \epsilon_n^2) \quad (\text{S46})$$

Consider the sieve:

$$\mathcal{F}_n = \{\Psi \in \mathcal{B}_n^\Psi, \Omega \in \mathcal{B}_n^\Omega : \|\Psi\|_1 \leq 2C_3 p, \|\Omega\|_1 \leq 8C_3 q\} \quad (\text{S47})$$

for some large $C_3 > C_1 + 2 + \log(3)$ where C_1 is the constant in KL condition. We have

$$\Pi(\mathcal{F}_n^c) \leq \Pi(\|\Psi\|_1 > 2C_3 p) + \Pi((\|\Omega\|_1 > 8C_3 q) \cap \{\Omega \succ \tau I\})$$

We upper bound each term similar to [Bai et al. \(2020\)](#). By using the bound in Equation (S34), we know that

$$\Pi((\|\Omega\|_1 > 8C_3 q) \cap \{\Omega \succ \tau I\}) \leq \exp(2\xi Q - \log(R)) \tilde{\Pi}(\|\Omega\|_1 > 8C_3 q).$$

Since $\|\Omega\|_1 = 2 \sum_{k > k'} |\omega_{k,k'}| + \sum_k |\omega_{k,k}|$, at least one of these two sums exceeds $8C_3 q/2$. Thus, we can form an upper bound on the L1 norm probability

$$\tilde{\Pi}(\|\Omega\|_1 > 8C_3 q) \leq \tilde{\Pi} \left(\sum_{k > k'} |\omega_{k,k'}| > \frac{8C_3 q}{4} \right) + \tilde{\Pi} \left(\sum_k |\omega_{k,k}| > \frac{8C_3 q}{2} \right).$$

To get an upper bound under $\tilde{\Pi}$, we can act as if all $\omega_{k,k'}$'s were drawn from the slab distribution. In that setting, $\sum_{k > k'} |\omega_{k,k'}|$ is Gamma distributed with shape parameter Q and rate parameter ξ_1 . By using an appropriate tail probability for the Gamma distribution

(Boucheron et al. (2013), pp.29) and the fact $1 + x - \sqrt{1 + 2x} \geq (x - 1)/2$, we compute

$$\begin{aligned} \exp(2\xi Q - \log(R)) \tilde{\Pi}(\sum_{k > k'} |\omega_{k,k'}| > 8C_3 q/4) &\leq \exp \left[-Q \left(1 - \sqrt{1 + 2\frac{8C_3 q}{4Q\xi_1} + \frac{8C_3 q}{4Q\xi_1}} \right) + 2Q - \log(R) \right] \\ &\leq \exp \left[-\frac{8C_3 q}{8\xi_1} + \left(\frac{5}{2}Q - \log(R) \right) \right] \end{aligned}$$

Since we have assumed $\xi_1 \asymp 1/n$, for sufficiently large n , we have $n\epsilon_n^2 \geq q \log(q)$. Consequently, $qn\epsilon_n^2 \geq Q \log(q)$, $Q = o(qn\epsilon_n^2)$, and we see that

$$\begin{aligned} \frac{8C_3 q}{8\xi_1} - \left(\frac{5}{2}Q - \log(R) \right) &\asymp C_3(nq) - \left(\frac{5}{2}Q - \log(R) \right) \\ &\geq C_3(qn\epsilon_n^2) - \left(\frac{5}{2}Q - \log(R) \right) \\ &= C_3(qn\epsilon_n^2) - o(qn\epsilon_n^2) \\ &\geq C_3 n\epsilon_n^2 \end{aligned}$$

The first order term of Q on the left hand side can be ignored when n large as the left hand side is dominated by the $Q \log(q)$ term. Note that we used the assumption that $\epsilon_n \rightarrow 0$. We further have

$$\exp(2\xi Q - \log(R)) \tilde{\Pi}(\sum_{k > k'} |\omega_{k,k'}| > 8C_3 q/4) \leq \exp(-C_3 n\epsilon_n^2)$$

For the diagonal, the sum follows a gamma distribution with shape q and rate ξ . We obtain a similar bound

$$\begin{aligned} \exp(2\xi Q - \log(R)) \tilde{\Pi}(\sum_k |\omega_{k,k}| > 8C_3 q/2) &\leq \exp(2Q - \log(R)) \exp \left[-q \left(1 - \sqrt{1 + 2\frac{8C_3 q}{2q\xi} + \frac{8C_3 q}{2q\xi}} \right) \right] \\ &\leq \exp \left[-\frac{8C_3 q}{4\xi} + Q \left(2 + \frac{q}{2Q} \right) - \log(R) \right] \end{aligned}$$

Using the same argument as before and the fact that $\xi \asymp 1/\max\{Q, n\}$, we have

$$\begin{aligned} \frac{8C_3q}{4\xi} - Q \left(2 + \frac{q}{2Q} \right) + \log(R) &\asymp 2C_3(\max\{Q, n\}q) - Q \left(2 + \frac{q}{2Q} \right) + \log(R) \\ &\geq C_3qn\epsilon_n^2 - o(qn\epsilon_n^2) \\ &\geq C_3n\epsilon_n^2 \end{aligned}$$

The first order term of Q on the left hand side can be ignored when n large as the left hand side is dominated by the $Q \log(q)$ term and $q/Q \rightarrow 0$.

By combining the above results, we have:

$$\begin{aligned} \Pi((\|\Omega\|_1 > 8C_3q) \cap \{\Omega \succ \tau I\}) &\leq \exp(2Q - \log(R)) \tilde{\Pi}(\|\Omega\|_1 > 8C_3q) \\ &\leq \exp(2Q - \log(R)) \tilde{\Pi}\left(\sum_{k>k'} |\omega_{k,k'}| > \frac{8C_3q}{4}\right) \\ &\quad + \exp(2Q - \log(R)) \tilde{\Pi}\left(\sum_k |\omega_{k,k}| > \frac{8C_3q}{2}\right) \\ &\leq 2 \exp(-C_3n\epsilon_n^2) \end{aligned} \tag{S48}$$

The probability $\|\Psi\|_1 > 2C_3p$ can be bounded by tail probability of Gamma distribution with shape parameter pq and rate parameter λ_1 :

$$\begin{aligned} \Pi(\|\Psi\|_1 > 2C_3p) &\leq \exp \left[-pq \left(1 - \sqrt{1 + 2\frac{2C_3p}{pq\lambda_1}} + \frac{2C_3p}{pq\lambda_1} \right) \right] \\ &\leq \exp \left[-pq \left(\frac{2C_3p}{2pq\lambda_1} - \frac{1}{2} \right) \right] \\ &\leq \exp \left(-\frac{2C_3p}{2\lambda_1} + \frac{pq}{2} \right) \end{aligned}$$

Using the same argument, we have $pn \geq pn\epsilon_n^2 \geq pq \log(q)$ and thus, $pq = o(pn\epsilon_n^2)$ for large n . Consequently,

$$\exp \left(-\frac{2C_3p}{2\lambda_1} + \frac{pq}{2} \right) \leq \exp(-C_3pn\epsilon_n^2 + o(pn\epsilon_n^2)) \leq \exp(-C_3n\epsilon_n^2)$$

and

$$\Pi(\|\Psi\|_1 > 2C_3p) \leq \exp(-C_3n\epsilon_n^2) \quad (\text{S49})$$

By combining the result from Equations (S48) and (S49), we conclude

$$\Pi(\mathcal{F}_n^c) \leq 3 \exp(-C_3n\epsilon_n^2) = \exp(-C_3n\epsilon_n^2 + \log(3)).$$

With our choice of C_3 , the above probability is asymptotically bounded from above by $\exp(-C_2n\epsilon_n^2)$ with some $C_2 \geq C_1 + 2$.

S5.2.3 Tests around a representative point

To apply the general theory, we need to construct test φ_n , such that for some $M_2 > C_1 + 1$:

$$\begin{aligned} \mathbb{E}_{f_0} \varphi_n &\lesssim e^{-M_2n\epsilon^2/2} \\ \sup_{f \in \mathcal{F}_n: \rho(f_0, f) > M_2n\epsilon_n^2} \mathbb{E}_f(1 - \varphi_n) &\lesssim e^{-M_2n\epsilon_n^2} \end{aligned} \quad (\text{S50})$$

where $f = \prod_{i=1}^n \mathcal{N}(X_i \Psi \Omega^{-1}, \Omega^{-1})$ while $f_0 = \prod_{i=1}^n \mathcal{N}(X_i \Psi_0 \Omega_0^{-1}, \Omega_0^{-1})$

Instead of directly constructing the φ_n on the whole sieve, we use the method similar to [Ning et al. \(2020\)](#). That is, we construct tests versus a representative point and show that these tests works well in the neighborhood of the representative points. We then take the supremum of these tests and show that the number of pieces needed to cover the entire sieve can be appropriately bounded.

For a representative point f_1 , consider the Neyman-Pearson test for a single point alternative $H_0 : f = f_0, H_1 : f = f_1, \phi_n = I\{f_1/f_0 \geq 1\}$. If the average half order Rényi divergence $-n^{-1} \log(\int \sqrt{f_0 f_1} d\mu) \geq \epsilon^2$, we will have:

$$\begin{aligned} \mathbb{E}_{f_0}(\phi_n) &\leq \int_{f_1 > f_0} \sqrt{f_1/f_0} f_0 d\mu \leq \int \sqrt{f_1 f_0} d\mu \leq e^{-n\epsilon^2} \\ \mathbb{E}_{f_1}(1 - \phi_n) &\leq \int_{f_0 > f_1} \sqrt{f_0/f_1} f_1 d\mu \leq \int \sqrt{f_0 f_1} d\mu \leq e^{-n\epsilon^2} \end{aligned}$$

By Cauchy-Schwarz, for any alternative f we can control the Type II error rate:

$$\mathbb{E}_f(1 - \phi_n) \leq \{\mathbb{E}_{f_1}(1 - \phi_n)\}^{1/2} \{\mathbb{E}_{f_1}(f/f_1)^2\}^{1/2}$$

So long as the second factor grows at most like e^{cne^2} for some properly chosen small c , the full expression can be controlled. Thus we can consider the neighborhood around the representative point small enough so that the second factor can be actually bounded.

Consider every density with parameters satisfying

$$\begin{aligned} |||\Omega|||_2 &\leq |||\Omega|||_1 \leq 8C_3q, \\ ||\Psi_1 - \Psi||_2 &\leq ||\Psi_1 - \Psi||_1 \leq \frac{1}{\sqrt{2C_3np}}, \\ |||\Omega_1 - \Omega|||_2 &\leq |||\Omega_1 - \Omega|||_1 \leq \frac{1}{8C_3n \max\{p, q\}^{3/2}} \leq \frac{1}{8C_3nq^{3/2}} \end{aligned} \tag{S51}$$

We show that $\mathbb{E}_{f_1}(f/f_1)^2$ is bounded on the above set when parameters are from the sieve \mathcal{F}_n .

Similar to [Ning et al. \(2020\)](#), denote $\Sigma_1 = \Omega_1^{-1}$, $\Sigma = \Omega^{-1}$ as well as $\Sigma_1^* = \Omega^{1/2}\Sigma_1\Omega^{1/2}$, and $\Delta_\Psi = \Psi - \Psi_1$ while $\Delta_\Omega = \Omega - \Omega_1$. Using the observation $\Psi\Omega^{-1} - \Psi_1\Omega_1^{-1} = (\Delta_\Psi - \Psi_1\Omega^{-1}\Delta_\Omega)\Omega^{-1}$, we have

$$\begin{aligned} \mathbb{E}_{f_1}(f/f_1)^2 &= |\Sigma_1^*|^{n/2} |2I - \Sigma_1^{*-1}|^{-n/2} \\ &\quad \times \exp \left(\sum_{i=1}^n X_i (\Psi\Omega^{-1} - \Psi_1\Omega_1^{-1}) \Omega^{1/2} (2\Sigma_1^* - I)^{-1} \Omega^{1/2} (\Psi\Omega^{-1} - \Psi_1\Omega_1^{-1})^\top X_i^\top \right) \\ &= |\Sigma_1^*|^{n/2} |2I - \Sigma_1^{*-1}|^{-n/2} \\ &\quad \times \exp \left(\sum_{i=1}^n X_i (\Delta_\Psi - \Psi_1\Omega^{-1}\Delta_\Omega) \Omega^{-1/2} (2\Sigma_1^* - I)^{-1} \Omega^{-1/2} (\Delta_\Psi - \Psi_1\Omega^{-1}\Delta_\Omega)^\top X_i^\top \right) \end{aligned} \tag{S52}$$

For the first factor we use a similar argument as in [Ning et al. \(2020\)](#) (after Equation 5.9). Since $\Omega \in \mathcal{F}_n$, we have $|||\Omega^{-1}|||_2 \leq 1/\tau$. The fact $|||\Omega_1 - \Omega|||_2 \leq \delta'_n = 1/8C_3nq^{3/2}$ implies

$$|||\Sigma_1^* - I|||_2 \leq |||\Omega^{-1}|||_2 |||\Omega_1 - \Omega|||_2 \leq \delta'_n/\tau$$

and thus we can bound the spectrum of Σ_1^* , i.e. $1 - \delta'_n/\tau \leq \text{eig}_1(\Sigma_1^*) \leq \text{eig}_q(\Sigma_1^*) \leq 1 + \delta'_n/\tau$.

Thus

$$\begin{aligned}
\left(\frac{|\Sigma_1^*|}{|2I - \Sigma_1^{*-1}|} \right)^{n/2} &= \exp \left(\frac{n}{2} \sum_{i=1}^q \log(\text{eig}_i(\Sigma_1^*)) - \frac{n}{2} \sum_{i=1}^q \log \left(2 - \frac{1}{\text{eig}_i(\Sigma_1^*)} \right) \right) \\
&\leq \exp \left(\frac{nq}{2} \log(1 + \delta'_n/\tau) - \frac{nq}{2} \log \left(1 - \frac{\delta'_n/\tau}{1 - \delta'_n/\tau} \right) \right) \\
&\leq \exp \left(\frac{nq^2}{2} \delta'_n + \frac{nq}{2} \left(\frac{\delta'_n/\tau}{1 - 2\delta'_n/\tau} \right) \right) \\
&\leq \exp(nq\delta'_n/\tau) \\
&\leq e
\end{aligned}$$

The third inequality is due to the fact $1 - x^{-1} \leq \log(x) \leq x - 1$.

We can bound the log of the second factor of Equation (S52).

$$|||\Omega^{-1}|||_2 |||(2\Sigma_1^* - I)^{-1}|||_2 \sum_{i=1}^n \|X_i(\Delta_\Psi - \Psi_1 \Omega^{-1} \Delta_\Omega)\|_2^2 \leq 2/\tau \sum_{i=1}^n \|X_i(\Delta_\Psi - \Psi_1 \Omega^{-1} \Delta_\Omega)\|_2^2$$

We can further bound the sum on the sieve.

$$\begin{aligned}
\sum_{i=1}^n \|X_i(\Delta_\Psi - \Psi_1 \Omega^{-1} \Delta_\Omega)\|_2^2 &\leq 2 \sum_{i=1}^n \|X_i \Delta_\Psi\|_2^2 + 2 \sum_{i=1}^n \|X_i \Psi_1 \Omega^{-1} \Delta_\Omega\|_2^2 \\
&\leq 2np |||\Delta_\Psi|||_2^2 + 2np |||\Psi_1|||_2^2 |||\Omega^{-1}|||_2^2 |||\Delta_\Omega|||_F^2 \\
&\leq 2np \frac{1}{2C_3 np} + 2np \left(2C_3 p + \frac{1}{\sqrt{2C_3 np}} \right)^2 \frac{1}{\tau^2} \frac{1}{(8C_3 n \max\{p, q\}^{3/2})^2} \\
&\leq 2np \frac{1}{2C_3 np} + 2np 16C_3^2 p^2 \frac{1}{\tau^2} \frac{1}{(8C_3 n \max\{p, q\}^{3/2})^2} \\
&\lesssim 1
\end{aligned}$$

We bound the norm of Ψ_1 using triangle inequality, $|||\Psi_1||| \leq |||\Psi||| + |||\Psi_1 - \Psi||| \leq 2C_3 p + 1/\sqrt{2C_3 np}$. The first term is $O(1)$ and second term is $O(1/q)$, by combining the result we conclude the second factor of Equation (S52) is bounded.

Thus, following the argument of Ning et al. (2020), the desired test φ_n in Equation (S50) can be obtained as the maximum of all tests ϕ_n described above.

S5.2.4 Pieces needed to cover the sieve

From here we show the contraction in log-affinity $\rho(f, f_0)$. To finish up the proof, we check that number of sets described in Equation (S51) needed to cover sieve \mathcal{F}_n , denoted by N_* , can be bounded by $\exp(Cn\epsilon_n^2)$ for some suitable constant C .

The number N_* is called a covering number of \mathcal{F}_n . A closely related quantity is the packing number, which is defined as the maximum number of disjoint balls centered in a set and upper bounds the covering number. Both the covering number and packing number can be used as a measure of complexity of a given set (Ghosal and van der Vaart, 2017).

The packing number of a set usually depends exponentially on the sets dimensions. Because Ning et al. (2020) studied posteriors which place positive probability on exactly sparse parameters, they were able to directly bound the packing number of suitable low-dimensional sets. In our case, which uses an absolutely continuous prior, we need to instead control the packing number of “effectively low dimensional” spaces.

Lemma S4 provides a sufficient condition for bounding the complexity (evaluated by packing number) of an set of “effectively sparse” vectors can be bounded by the complexity of a set of actually sparse vectors.

Lemma S4 (packing a shallow cylinder in L_p). *For a set of form $E = A \times [-\delta, \delta]^{Q-s} \subset \mathbb{R}^Q$ where $A \subset \mathbb{R}^s$, (with $s > 0$ and $Q \geq s + 1$ are integers) for $1 \leq p < \infty$ and a given $T > 1$, if $\delta < \frac{\epsilon}{2[T(Q-s)]^{1/p}}$, we have the packing number:*

$$D(\epsilon, A, \|\cdot\|_p) \leq D(\epsilon, E, \|\cdot\|_p) \leq D((1 - T^{-1})^{1/p}\epsilon, A, \|\cdot\|_p)$$

Proof. The lower bound is trivial by observing $A \times \{0\}^{Q-s} \subset E$ and the packing number of $A \times \{0\}^{Q-s}$ is exactly the packing number of A . For the upper bound, we show that for each packing on E , we can slice that packing with the 0-plane to form a packing on A with the same number of balls but smaller radius (see Figure S7 for an illustration).

We first show any L_p $\epsilon/2$ -ball $B_\theta(\epsilon/2)$ centered in the set E intersects the plane $\mathbb{R}^s \times \{0\}^{Q-s}$. Assume the center is $\theta = (x_1, \dots, x_Q)$. It suffices to show the center’s distance to the plane is less than the radius of the ball. Since the center is in E , we have $|x_i| \leq \delta$ for the last $Q - s$ coordinates. Denote the projection of the center on the plane as $\theta_A = (x_1, \dots, x_s, 0) \in$

$A \times \{0\}^{Q-s}$. Then the Lp distance from the center to the plane is

$$\|\theta_A - \theta\|_p^p = \sum_{i=s+1}^Q |x_i|^p \leq (Q-s)\delta^p < T^{-1}(\epsilon/2)^p$$

Next we show the slice $B_\theta(\epsilon) \cap \mathbb{R}^s \times \{0\}^{Q-s}$ is also a ball centered at θ_A in the lower dimensional plane. It suffice to show the boundary is a sphere. Suppose we take a point a from the intersection of boundary of $B_\theta(\epsilon) \cap \mathbb{R}^s \times \{0\}^{Q-s}$, the vector from center to the point can be decomposed to sum of two orthogonal component, namely the vector from θ_A to a and from θ_A to θ , we have in this case

$$\|a - \theta_A\|_p^p + \|\theta_A - \theta\|_p^p = \|a - \theta\|_p^p = \epsilon^p/2^p$$

because $a - \theta_A$ has all 0 entries on the last $Q - s$ axis and $\theta_A - \theta$ has all 0 entries on the first s entries. Thus any such point has a fixed distance to θ_A , the projection of the center θ on the plane of A . Notice that

$$\|a - \theta_A\|_p^p = \epsilon^p/2^p - \|\theta_A - \theta\|_p^p,$$

which is fixed. Thus the collection of a forms a sphere on A 's plane.

From here, we can also lower bound the radius of slice by $(1 - T^{-1})^{1/p}\epsilon/2$ since $\|\theta_A - \theta\|_p^p < T^{-1}(\epsilon/2)^p$, thus we have the radius $\|a - \theta_A\|_p > (1 - T^{-1})^{1/p}\epsilon/2$. Thus, we have the smaller ball must lie within the slice, i.e.

$$B_{\theta_A}((1 - T^{-1})^{1/p}\epsilon/2) \times \{0\}^{Q-s} \subset (B_\theta(\epsilon/2) \cap (\mathbb{R}^s \times \{0\}^{Q-s})) \subset B_\theta(\epsilon/2) \quad (\text{S53})$$

That is, any $\epsilon/2$ -ball centered in E has a corresponding $(1 - T^{-1})^{1/p}\epsilon/2$ lower dimension ball centered in A . With the above observations in hand, we can now prove the inequality by contradiction.

Suppose we have a packing on E $\{\theta_1, \dots, \theta_D\}$, where D is larger than the packing number of A in the main result. By Equation (S53), the lower dimension balls $B_{\theta_{iA}}((1 - T^{-1})^{1/p}\epsilon/2)$ must also be disjoint. Since the centers of the balls $\theta_{iA} \in A$, these balls form a packing of A with radius $\epsilon' = (1 - T^{-1})^{1/p}\epsilon$. That is, we can find a packing with more balls than the

packing number, yielding the desired contradiction. Thus we must have

$$D \leq D((1 - T^{-1})^{1/p} \epsilon, A, \|\cdot\|_p)$$

□

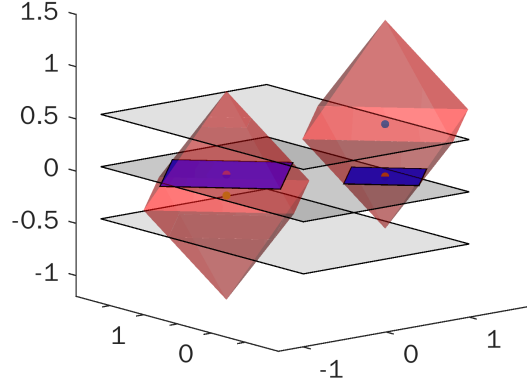


Figure S7: A schematic of argument used in the packing number lemma proof. We showed two disjoint unit L1 balls (red) centered in $(0.8, 0, 0.5)$ and $(-.3, 1, -.2)$, all within $A \times [-0.5, 0.5]$ (with $A = [-1, 1] \times [-1, 1]$ shown in the middle plane), their slice in the $z = 0$ plane (in blue) also forms L1 balls in \mathbb{R}^2 whose radius are lower bounded and centered within A , thus induced a packing of the lower dimensional set.

Now we can bound the logarithm of the covering number $\log(N_*)$ similar to [Ning et al. \(2020\)](#).

$$\begin{aligned} \log(N_*) \leq & \log \left[N \left(\frac{1}{\sqrt{2C_3np}}, \{\Psi \in \mathcal{B}_n^\Psi : \|\Psi\|_1 \leq 2C_3p\}, \|\cdot\|_1 \right) \right] \\ & + \log \left[N \left(\frac{1}{8C_3n \max\{p, q\}^{3/2}}, \{\Omega \in \mathcal{B}_n^\Omega, \|\Omega\|_1 \leq 8C_3q\}, \|\cdot\|_1 \right) \right] \end{aligned}$$

The two terms above can be treated in a similar way. Denote $\max\{p, q, s_0^B, s_0^\Omega\} = s^*$. There are multiple ways to allocate the effective 0's, which introduces the binomial coefficient

below:

$$\begin{aligned}
& N \left(\frac{1}{8C_3 n \max\{p, q\}^{3/2}}, \{\Omega \in \mathcal{B}_n^\Omega, \|\Omega\|_1 \leq 8C_3 q\}, \|\cdot\|_1 \right) \\
& \leq \left(\frac{Q}{C'_3 s^*} \right) N \left(\frac{1}{8C_3 n \max\{p, q\}^{3/2}}, \{V \in \mathbb{R}^{Q+q} : |v_i| < \delta_\omega \text{ for } 1 \leq i \leq Q+q-C'_3 s^*, \|V\|_1 \leq 8C_3 q\}, \|\cdot\|_1 \right) \\
& \quad N \left(\frac{1}{\sqrt{2C_3 np}}, \{\Psi \in \mathcal{B}_n^\Psi : \|\Psi\|_1 \leq 2C_3 p\}, \|\cdot\|_1 \right) \\
& \leq \left(\frac{pq}{C'_3 s^*} \right) N \left(\frac{1}{\sqrt{2C_3 np}}, \{V \in \mathbb{R}^{pq} : |v_i| < \delta_\psi \text{ for } 1 \leq i \leq pq-C'_3 s^*, \|V\|_1 \leq 2C_3 p\}, \|\cdot\|_1 \right)
\end{aligned}$$

Note that Ω has $Q+q < 2Q$ free parameters. We have first

$$\begin{aligned}
\log \left(\frac{Q}{C'_3 s^*} \right) & \lesssim s^* \log(Q) \lesssim n\epsilon_n^2 \\
\log \left(\frac{pq}{C'_3 s^*} \right) & \lesssim s^* \log(pq) \lesssim n\epsilon_n^2
\end{aligned}$$

We further bound the covering number using the result in Lemma S4. Observe that $\|V\|_1 \cap \{|v_i| < \delta_\omega \text{ for } 1 \leq i \leq Q+q-C'_3 s^*\} \subset \{\|V'\| \leq 8C_3 q\} \times [-\delta_\omega, \delta_\omega]^{Q+q-C'_3 s^*}$ where $V' \in \mathbb{R}^{C'_3 s^*}$ we have

$$\begin{aligned}
& N \left(\frac{1}{8C_3 n \max\{p, q\}^{3/2}}, \{V : |v_i| < \delta_\omega \text{ for } 1 \leq i \leq Q+q-C'_3 s^*, \|V\|_1 \leq 8C_3 q\}, \|\cdot\|_1 \right) \\
& \leq N \left(\frac{1}{8C_3 n \max\{p, q\}^{3/2}}, \{V \in \mathbb{R}^{C'_3 s^*} : \|V'\|_1 \leq 8C_3 q \times [-\delta_\omega, \delta_\omega]^{Q+q-C'_3 s^*}\}, \|\cdot\|_1 \right)
\end{aligned}$$

We check the condition of Lemma S4 (with $p = 1$ and $T = 2$), by our assumption on ξ_0 , we have:

$$\begin{aligned}
(Q+q-C'_3 s^*)\delta_\omega & \leq 2Q\delta_\omega = 2Q \frac{1}{\xi_0 - \xi_1} \log \left[\frac{1-\eta}{\eta} \frac{\xi_0}{\xi_1} \right] \lesssim \frac{Q \log(\max\{p, q, n\})}{\max\{Q, pq, n\}^{4+b/2+b/2}} \\
& \leq \frac{1}{\max\{Q, pq, n\}^{3+b/2}}
\end{aligned}$$

The denominator dominates $C_3 n \max\{p, q\}^{3/2}$ thus for large enough n , we have $(Q + q - C'_3 s^*)\delta_\omega \leq \frac{1}{32C_3 n \max\{p, q\}^{3/2}}$ thus by Lemma S4, we can control the covering number by the packing number:

$$\begin{aligned}
& \log N \left(\frac{1}{8C_3 n \max\{p, q\}^{3/2}}, \{V : |v_i| < \delta_\omega \text{ for } 1 \leq i \leq Q + q - C'_3 s^*, \|V\|_1 \leq 8C_3 q\}, \|\cdot\|_1 \right) \\
& \leq \log D \left(\frac{1}{16C_3 n \max\{p, q\}^{3/2}}, \{V' \in \mathbb{R}^{C'_3 s^*}, \|V'\|_1 \leq 8C_3 q\}, \|\cdot\|_1 \right) \\
& \lesssim s^* \log(128C_3^2 q n \max\{p, q\}^{3/2}) \\
& \lesssim n\epsilon_n^2
\end{aligned}$$

Similarly for Ψ ,

$$\begin{aligned}
& N \left(\frac{1}{\sqrt{2C_3 np}}, \{V : |v_i| < \delta_\psi \text{ for } 1 \leq i \leq pq - C'_3 s^*, \|V\|_1 \leq 2C_3 p\}, \|\cdot\|_1 \right) \\
& \leq N \left(\frac{1}{\sqrt{2C_3 np}}, \{V' \in \mathbb{R}^{C'_3 s^*} : \|V'\|_1 \leq 2C_3 p \times [-\delta_\psi, \delta_\psi]\}, \|\cdot\|_1 \right)
\end{aligned}$$

We again check the condition of Lemma S4 (again with $p = 1$ and $T = 2$):

$$\begin{aligned}
(pq - C'_3 s^*)\delta_\psi & \leq pq\delta_\psi = \frac{pq}{\lambda_0 - \lambda_1} \log \left[\frac{1 - \theta \lambda_0}{\theta \lambda_1} \right] \lesssim \frac{pq \log(\max\{p, q, n\})}{\max\{pq, n\}^{5/2+b/2+b/2}} \\
& \leq \frac{1}{\max\{pq, n\}^{3/2+b/2}}
\end{aligned}$$

The denominator dominates $\sqrt{2C_3 np}$, Thus for enough large n , we have $(pq - C'_3 s^*)\delta_\psi \leq 1/4\sqrt{2C_3 np}$. Thus similar to Ω , we have:

$$\begin{aligned}
& \log N \left(\frac{1}{\sqrt{2C_3 np}}, \{V : |v_i| < \delta_\omega \text{ for } 1 \leq i \leq pq - C'_3 s^*, \|V\|_1 \leq 2C_3 p\}, \|\cdot\|_1 \right) \\
& \leq \log D \left(\frac{1}{2\sqrt{2C_3 np}}, \{V' \in \mathbb{R}^{C'_3 s^*}, \|V'\|_1 \leq 2C_3 p\}, \|\cdot\|_1 \right) \\
& \lesssim s^* \log(4C_3 p \sqrt{2C_3 np}) \\
& \lesssim n\epsilon_n^2
\end{aligned}$$

Thus we finally get the contraction under log-affinity.

S5.3 From log-affinity to Ω and $X\Psi\Omega^{-1}$

In this section we show the main result Theorem 1 using the contraction under log-affinity.

Denoting $\Psi - \Psi_0 = \Delta_\Psi$ and $\Omega - \Omega_0 = \Delta_\Omega$ we have the log-affinity $\frac{1}{n} \sum \rho(f_i, f_{0i})$ is

$$\begin{aligned} \frac{1}{n} \sum \rho(f_i, f_{0i}) &= -\log \left(\frac{|\Omega^{-1}|^{1/4} |\Omega_0^{-1}|^{1/4}}{|(\Omega^{-1} + \Omega_0^{-1})/2|^{1/2}} \right) \\ &\quad + \frac{1}{8n} \sum X_i (\Psi\Omega^{-1} - \Psi_0\Omega_0^{-1}) \left(\frac{\Omega^{-1} + \Omega_0^{-1}}{2} \right)^{-1} (\Psi\Omega^{-1} - \Psi_0\Omega_0^{-1})^\top X_i^\top \end{aligned}$$

Thus $\sum \rho(f_i - f_{0i}) \lesssim n\epsilon_n^2$ implies

$$\begin{aligned} &-\log \left(\frac{|\Omega^{-1}|^{1/4} |\Omega_0^{-1}|^{1/4}}{|(\Omega^{-1} + \Omega_0^{-1})/2|^{1/2}} \right) \lesssim \epsilon_n^2 \\ \frac{1}{8n} \sum X_i (\Psi\Omega^{-1} - \Psi_0\Omega_0^{-1}) \left(\frac{\Omega^{-1} + \Omega_0^{-1}}{2} \right)^{-1} (\Psi\Omega^{-1} - \Psi_0\Omega_0^{-1})^\top X_i^\top &\lesssim \epsilon_n^2 \end{aligned} \tag{S54}$$

This is almost the same as Ning et al. (2020)'s Equations 5.11-5.12. We can directly apply the result from Ning et al. (2020)'s Equation 5.11 as it is the same as the first equation in Equation (S54). Because Ψ_0 and Ω^{-1} have bounded operator norms and because Δ_Ω can be controlled, the cross-term is also controlled by ϵ_n . The first part of Equation (S54) implies $\|\Omega^{-1} - \Omega_0^{-1}\|_F^2 \lesssim \epsilon_n^2$.

Meanwhile $\|\Omega^{-1} - \Omega_0^{-1}\|_F^2 \lesssim \epsilon_n^2$ implies for large enough n Ω 's L2 operator norm is bounded (since we assume bounds on Ω_0^{-1} 's operator norm and the difference cannot have very large eigenvalues which make the sum has 0 eigenvalue), using the result $\|AB\|_F \leq \|A\|_2 \|B\|_F$, while also observe $\Omega_0 - \Omega = \Omega(\Omega^{-1} - \Omega_0^{-1})\Omega_0$, and by assumption that Ω_0 has bounded L2 operator norm, we conclude (S54) implies $\|\Omega - \Omega_0\|_F \lesssim \epsilon_n$.

Since $\|[\Omega^{-1}]\|_2$ is bounded for large enough n , we can directly apply an argument from Ning et al. (2020) (specifically the argument around their Equation 5.12) to conclude (S54)'s

second part implies:

$$\begin{aligned}
\epsilon_n^2 &\gtrsim \frac{1}{8n} \sum \|X_i(\Psi\Omega^{-1} - \Psi_0\Omega_0^{-1})\|_2^2 \left\| \frac{\Omega^{-1} + \Omega_0^{-1}}{2} \right\|_2^{-1} \\
&\gtrsim \frac{1}{8n} \sum \|X_i(\Psi\Omega^{-1} - \Psi_0\Omega_0^{-1})\|_2^2 \left\| \frac{\Omega^{-1} + \Omega_0^{-1}}{2} \right\|_2^{-1} \\
&\gtrsim \frac{1}{n} \sum \|X_i(\Psi\Omega^{-1} - \Psi_0\Omega_0^{-1})\|_2^2 / \sqrt{\epsilon_n^2 + 1}
\end{aligned}$$

Combining all of these results yields the desired result.

S5.4 Contraction of Ψ

Contraction of Ψ requires more assumptions on the design matrix X . Similar to [Ročková and George \(2018\)](#) and [Ning et al. \(2020\)](#), we introduce the restricted eigenvalue

$$\phi^2(\tilde{s}) = \inf \left\{ \frac{\|XA\|_F^2}{n\|A\|_F^2} : 0 \leq |\nu(A)| \leq \tilde{s} \right\}$$

With this definition,

$$\begin{aligned}
\|X(\Psi\Omega^{-1} - \Psi_0\Omega_0^{-1})\|_F^2 &\lesssim n\epsilon_n^2 \\
\|\Omega - \Omega_0\|_F^2 &\lesssim \epsilon_n^2
\end{aligned}$$

implies the result in Equation (15) of the main text. Namely,

$$\|\Psi\Omega^{-1} - \Psi_0\Omega_0^{-1}\|_F^2 = \|(\Delta_\Psi - \Psi_0\Omega^{-1}\Delta_\Omega)\Omega^{-1}\|_F^2 \lesssim \epsilon_n^2 / \phi^2(s_0^\Psi + C'_3 s^*)$$

Since both Ω and Ω^{-1} have bounded operator norm when $\|\Omega - \Omega_0\|_F^2 \lesssim \epsilon_n^2$, for large enough n , we must have:

$$\|\Delta_\Psi\|_F - \|\Psi_0\Omega^{-1}\Delta_\Omega\|_F \leq \|\Delta_\Psi - \Psi_0\Omega^{-1}\Delta_\Omega\|_F \lesssim \epsilon_n / \sqrt{\phi^2(s_0^\Psi + C'_3 s^*)}$$

Since Ψ_0 and Ω^{-1} have bounded operator norm, $\|\Psi_0\Omega^{-1}\Delta_\Omega\|_F \lesssim \epsilon_n$, and we must have:

$$\|\Delta_\Psi\|_F \lesssim \epsilon_n / \sqrt{\min\{\phi^2(s_0^\Psi + C'_3 s^*), 1\}}$$

Thus we can conclude

$$\sup_{\Psi \in \mathcal{T}_0, \Omega \in \mathcal{H}_0} \mathbb{E}_0 \Pi \left(\|\Psi - \Psi_0\|_F^2 \geq \frac{M' \epsilon_n^2}{\min\{\phi^2(s_0^\Psi + C'_3 s^\star), 1\}} \right) \rightarrow 0$$